THE EFFECTS OF SOLAR RADIATION PRESSURE

ON THE MOTION OF AN ARTIFICIAL SATELLITE

F. C. E. RYLAND.

Thesis submitted for the Degree of Ph.D.

University of Aston
in Birmingham.

November, 1978.

THE EFFECTS OF SOLAR RADIATION PRESSURE ON THE MOTION OF AN ARTIFICIAL SATELLITE

Frederick Charles Edward Ryland

Ph.D., 1978

SUMMARY

This thesis documents an investigation of the effect of solar radiation pressure on the motion of an artificial satellite. Consideration is given to the methods required for the inclusion of the discontinuous effect of the Earth's shadow.

The analysis resulting from the description of a deformed diffusely reflecting balloon satellite and an algorithm describing the effects of Earth reflected solar radiation pressure are developed, culminating in the application of the derived theory to the orbital data of the balloon satellite, Explorer 19.

SATELLITE
ORBIT
PERTURBATION
SOLAR RADIATION

CONTENTS

Acknowledgements

The author wishes to express his appreciation to all who have assisted towards this thesis. In particular I would like to thank my supervisor Dr. C.J. Brookes, for his guidance and encouragement. I am indebted to the University of Aston in Birmingham for providing the financial support for my research.

1.

INTRODUCTION

The theory of artificial satellites was first propounded by Sir Isaac Newton (1642-1727) in his "Philosophiae Naturalis Principia Mathematica". The pattern of research developed from the orbit of satellites about the Earth, is mainly concerned with the composition, temperature and density of the atmosphere above a height of about 180 km. Further developments are, a geodetic study of the Earth's shape by building up an accurate picture of the gravity potential over the Earth, the physical studies of the Earth's magnetic field, the concentration of positive ions in the atmosphere, the prevalence of micro-meteorites and the measurement and analysis of solar radiation.

Originally it was hoped that balloon satellites could act as passive reflectors of radio waves at a relatively low cost compared with active communications satellites. Trial radio links were established between the U.S.S.R. and the United States via Jodrell Bank using the Echo balloons as orbiting reflectors. The quality of reception, however, was not always good, as passive satellites suffer from the fact that the signal received is already weak, and it is this signal that is returned to Earth. Use must therefore be made of an amplifier and retransmitter with a permanent energy source in the form of solar cells.

Balloon satellites really constitute a method of determining atmospheric densities and their variations at very high altitudes. Before this was possible it was noted that such satellites with large surface area to mass ratios,

(Echo 1 was of the order of 100 sq. cm. per gm.) are particularly sensitive to the effects of solar radiation while the converse is true of active satellites.

In general, during a complete orbital period, solar radiation pressure (SRP) causes a first order perturbation of all six orbital elements. However the most conspicuous effect for a near circular orbit, is a displacement of its geometric centre. This displacement will be parallel to the Earth-Sun line for a spherical satellite and can be almost perpendicular to this direction for a specularly reflecting flat plate. If it is assumed that the satellite is orbiting in a plane parallel to the Sun's rays, the light received at a point A (fig. 1) in the form of photons, will give it a small supplementary amount of energy. The satellite will have extra kinetic energy, and instead of describing a circular orbit an increase in the major axis will take the satellite to B, and not B'. At this point the satellite, still in

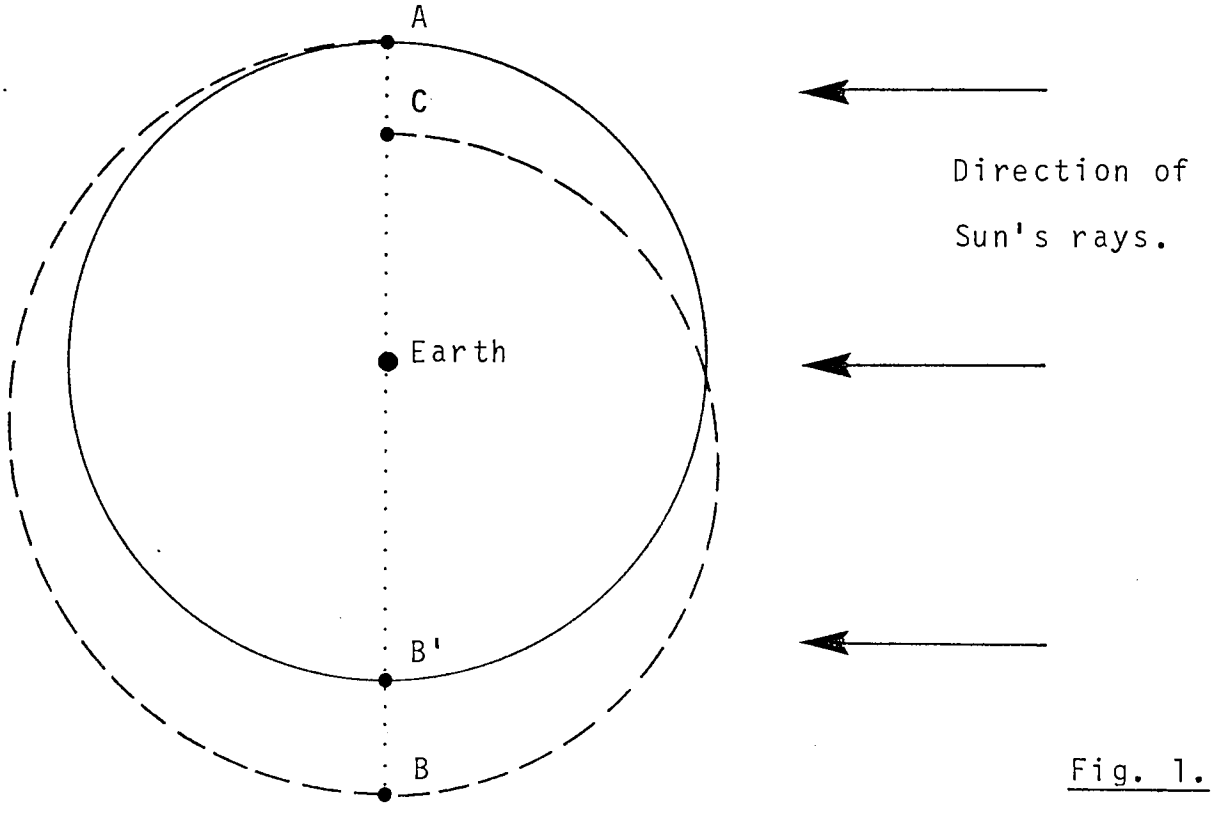

Fig. 1.

sunlight, is subjected to the same force as at A, but now this force acts so as to oppose the satellite's motion and the orbit is modified, bringing the satellite to C. After six months the Sun's rays approach the orbit from the opposite direction and the effect described is reversed. If a balloon satellite is placed into an orbit with the plane and major axis selected in such a way that the precessionary movement needs exactly six months to bring the plane back to its original position, there will be an inversion of the above situation, and the satellite's trajectory will be perturbed continuously in one direction only. That is, A will continue to move closer to the Earth and B will continue to move away. This example of a resonant orbit may occur when a balloon satellite has a near circular polar orbit, and in the absence of other forces this orbit would rapidly decay. In reality the force of SRP is generally just distinguishable from the other forces to which a satellite is subjected. To illustrate this a simple comparison is now made with the effect of atmospheric drag by calculating the ratio of the perturbing accelerations caused by solar radiation (F) and by air drag (D) for a spherical satellite in circular orbit. It is known that,

$$F = P_0 \frac{As}{m}(a_0/r_0)^2 \qquad \text{(Aksnes, 1976)}$$

$$D = \frac{1}{2} \frac{A}{m} C_D \rho v^2 \qquad \text{(King-Hele, 1964)}$$

where

A= cross-sectional area,

s= constant depending on the reflection characteristics of the

satellite's surface,

m= satellite mass,

P_0 = 4.65 x 10^{-5} dyne per sq. cm., is the force per unit area exerted at the Earth by the Sun, when $r_\odot$, the geocentric distance from the Sun is equal to its mean distance $a_\odot$,

ρ= atmospheric density (Jacchia, 1971),

ν= satellite velocity relative to the Earth centre,

C_D = drag coefficient (Cook, 1965),

so that,

$$\frac{F}{D} \simeq \frac{2sP_o}{C_D \rho \nu^2} \quad .$$

As an example suppose that the constants s and C_D are taken as 1.105 and 2.2 respectively.

Height of circular orbit h km.	200	300	400	500	600	700	800	900	1000
F/D	.0003	.002	.01	.04	.2	.8	2.1	4.3	12.4

It can be seen from the above table that for heights less than about 600 km., radiation pressure has much less effect than air drag, and therefore SRP effects at such heights are generally ignored. To illustrate these effects when they become significant, consider the orbit of Echo 1. For this satellite, at a mean height of 1600 km., a reduction of up to 6 km. per day was found in its perigee height, due in the main to radiation pressure. It was noted that at launch in 1960, this satellite had an almost circular orbit. However, due to the presence of this force the orbit tended markedly to that of an ellipse during the first few months of its life. Subsequently,

this increase in eccentricity ceased and by mid-1961 the orbit attained a perfect circle. This cycle of events was repeated and with each increase of eccentricity Echo 1's perigee entered a denser atmosphere, thus increasing the effect of air drag, which in turn caused the reduction in perigee height.

Now the force, $\underline{F}$, exerted by sunlight pressure is proportional to the area of a satellite as projected on a plane perpendicular to the direction of the flux, and is dependent on the characteristics of reflection of the satellite itself. These forces can be said to contribute a conservative field of force, unless the orbital plane is such that the satellite passes into the Earth's shadow. Here the force due to SRP will naturally be zero until emergence from the shadow.

Several authors in early treatments of SRP acting on balloon satellites, applied trial and error methods by using different values for the area to mass ratios, to derive results that fitted the previously unexplained residuals from the observed perturbations. These methods were fashioned to apply to the satellite Echo 1 in order that the analysis of the semi-major axis might lead to improved values of air density, (Shapiro and Jones, 1960). Papers by Musen, Bryant and Bailie (1960) and Parkinson, Jones and Shapiro(1960) also discuss SRP perturbations, although they do not give general results, but rather the effects on particular satellites. This has also been the case more recently with papers by Fea (1970), Slowey (1974i) and Slowey (1974ii).

The time rate of change for orbital elements has been

found by employing a vectorial method (Musen, 1960), when the Earth's shadow is neglected. A similar method was utilised by Bryant (1961) to include the effects of this eclipsing of the satellite by the Earth using an iterative technique. This paper required the derived equations to be numerically integrated, and was only concerned with long-period perturbations.

A simplified demonstration of how certain resonant conditions of orbital altitudes and inclinations can cause the monotonic build up of effects of SRP was given by Parkinson, Jones and Shapiro (1960), while citing Echo 1.

A paper by Fea and Smith (1970) gives the results for the satellite 1963-30D, Dash 2, but again there is no formal presentation of general results. It is of interest, though, to note that after attempting to assign suitable values for the area to mass ratio and the reflection coefficient, in order that the best fit could be obtained between the observed and predicted values of eccentricity, a discrepancy was still found. Fea and Smith explained this as a result of Earth reflected radiation pressure effects. It is possible to conceal this small effect by careful choice of $^{s}\frac{A}{m}$, but when this value for $^{s}\frac{A}{m}$ was used in the development of orbital elements other than eccentricity, the variations between observed and predicted data were rather large. On inspection of the periods where parts of the orbits were in shadow this discrepancy was very marked relative to the periods when the orbit was fully sunlit. It is therefore necessary to evaluate and distinguish between the differing effects of Earth reflected radiation and the variation in $^{s}\frac{A}{m}$ due to rotation of the deformed spheroidal

balloon. This conclusion was also arrived at by Aksnes (1976), who found similar discrepancies with Dash 2 while including short period perturbations.

Another question raised by Aksnes that needs to be answered is that of the method used for finding the positions of the shadow entry and exit points. Some early authors did not take this into account while Lála (1970) applied a continuous series expansion in order to simulate the discontinuous effects of the Earth's shadow. Kozai (1961) suggested that the solution of a quartic in the eccentric anomaly is required for each revolution in order to discover when the orbit passes through the shadow, if indeed it does. Then the exact points of intersection need to be determined, bearing in mind that modelling the Earth's shadow by a right circular cylinder is an approximation that excludes the vagaries caused by the penumbral shadow, refraction through the Earth's atmosphere and any cloud cover that might be present.

The development that follows attempts to answer these questions, and concludes with a practical application of the derived theory, to the satellite 1963-53A, Explorer 19.

2.

DIRECT SOLAR RADIATION PRESSURE

In the subsequent discussion the perturbation method is applied to the orbits of Earth satellites that are affected by the external force of direct solar radiation pressure. The main concern of this text is with the consequences that this disturbing acceleration has on the shape and orientation of the orbit, and therefore the prediction of satellite orbits.

The forces considered are small compared to that of the central force field, and thus the orbits are described in terms of the elements of the osculating ellipse. The notation incorporated herein is shown in Figure 2.

The Gaussian form of Lagrange's planetary equations express the rate of change of the osculating elements in terms of the components of the perturbing force. These equations, from Smart (1953), are

$$\frac{da}{dt} = \frac{2na^3F}{\sqrt{(1-e^2)}} \{T(e + \cos\theta) - S(\sin\theta)\} \quad , \tag{2.1}$$

$$\frac{de}{dt} = \frac{na^2\sqrt{(1-e^2)}F}{(1 + e\cos\theta)} \{T(\frac{3}{2} + 2e\cos\theta + \frac{1}{2}\cos2\theta) - S(e\sin\theta + \frac{1}{2}\sin2\theta)\} \quad , \tag{2.2}$$

$$\frac{di}{dt} = \frac{na^2\sqrt{(1-e^2)}FW}{(1 + e\cos\theta)} \cos(\omega + \theta) \quad , \tag{2.3}$$

$$\frac{d\Omega}{dt} = \frac{na^2\sqrt{(1-e^2)}FW}{(1 + e\cos\theta)} \operatorname{cosec} i \sin(\omega + \theta) \quad , \tag{2.4}$$

$$\frac{d\omega}{dt} = \frac{na^2\sqrt{(1-e^2)}F}{e(1 + e\cos\theta)} \{S(\frac{3}{2} + e\cos\theta - \frac{1}{2}\cos2\theta)$$

$$+T(\frac{1}{2}\sin 2\theta)\} - \cos i \frac{d\Omega}{dt} \quad , \qquad (2.5)$$

$$\frac{dM}{dt} = n - \frac{2na^2(1-e^2)F}{(1 + e\cos\theta)} (S\cos\theta + T\sin\theta)$$

$$- \sqrt{(1-e^2)}\left(\frac{d\omega}{dt} + \cos i \frac{d\Omega}{dt} \right) \quad . \qquad (2.6)$$

$S(\theta)$, $T(\theta)$ and W are the direction cosines of the perturbatory force vector, acting along the satellite's radius vector, $\underline{r}$, perpendicular to $\underline{r}$ in the orbital plane and normal to this plane respectively. These expressions can be written in a more manageable form, for

$$S(\theta) = S\cos\theta + T\sin\theta \quad ,$$

$$T(\theta) = T\cos\theta - S\sin\theta \quad ,$$

where $S=S(0)$ and $T=T(0)$, so that

$$\begin{Bmatrix} S \\ T \end{Bmatrix} = \begin{Bmatrix} - \\ + \end{Bmatrix} \sum_{i=1}^{6} \alpha_i \begin{Bmatrix} \cos \\ \sin \end{Bmatrix} \beta_i \quad , \qquad (2.7)$$

where

$\underline{i}$	$\underline{\alpha_i}$	$\underline{\gamma_i}$
1	$si\ s\varepsilon$	-1
2	$si\ c\varepsilon$	-1
3	$ci\ c\varepsilon$	+1
4	$ci\ s\varepsilon$	+1
5	$\frac{1}{2}sini\ sin\varepsilon$	0
6	$\frac{1}{2}sini\ sin\varepsilon$	0

with

$$\beta_i = \omega + \gamma_i\Omega + (-1)^i\lambda \quad , \qquad (2.8)$$

and

$$si = \sin^2(i/2) \qquad s\varepsilon = \sin^2(\varepsilon/2)$$

$$ci = \cos^2(i/2) \qquad c\varepsilon = \cos^2(\varepsilon/2) \quad ,$$

and also,

$$W = \sin i \{c\varepsilon \sin(\lambda-\Omega) - s\varepsilon \sin(\lambda+\Omega)\} - \cos i \sin\varepsilon \sin\lambda \quad . \qquad (2.9)$$

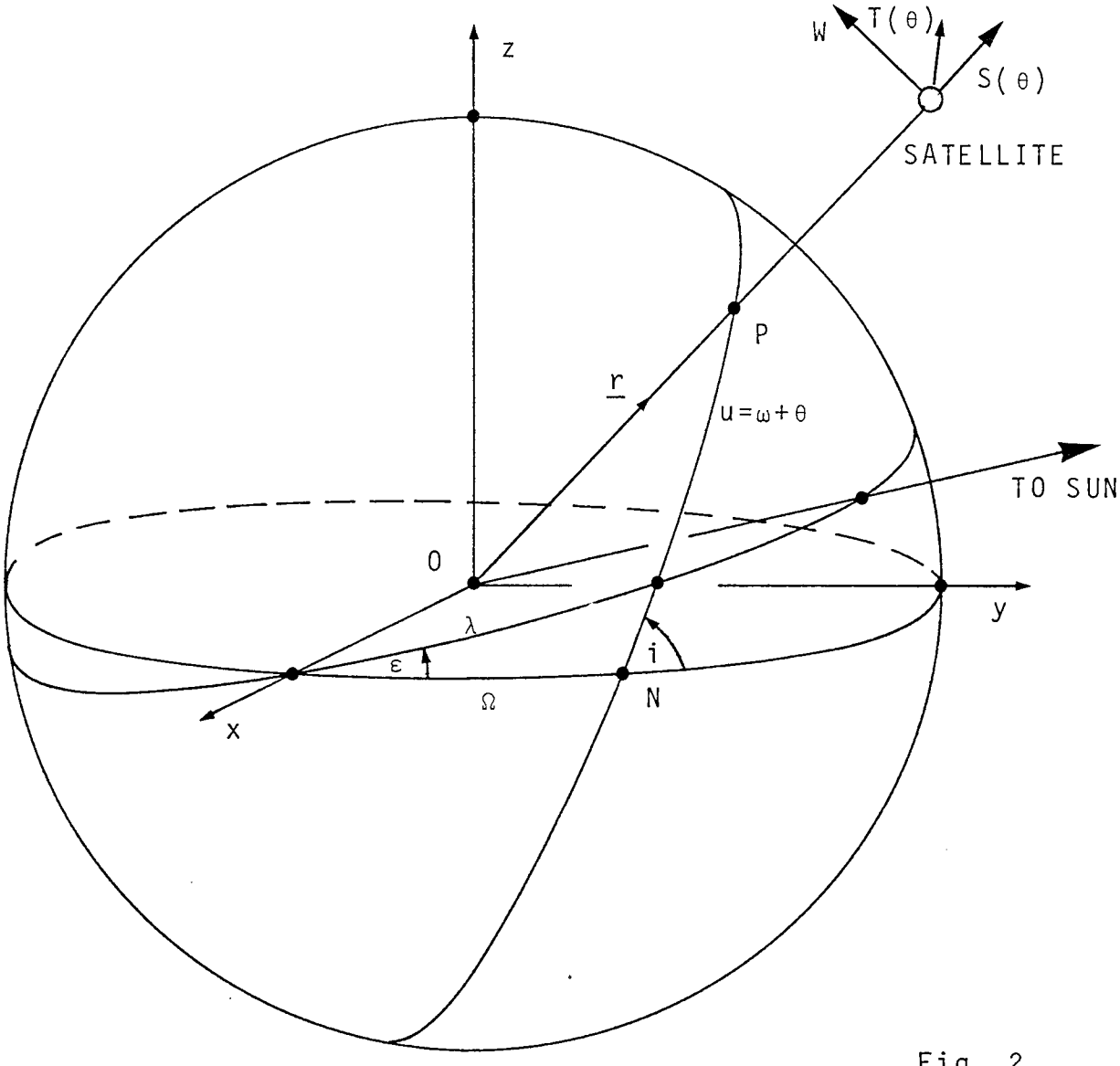

Fig. 2.

The following discourse arises as a result of the deviation, found in the example given by Aksnes (1976), of the computed theoretical data from the observed values of the perturbations to 'a', the semi-major axis, of the satellite 1963-30D. This unexplained perturbation was particularly evident during the periods when the satellite orbits were continuously sunlit. It has been shown by several authors, e.g. Kozai and Aksnes, that under certain assumptions the perturbation for 'a', due to direct solar radiation pressure, can be expressed by

$$\delta a = 2a^3F \left[S \cos E + T \sqrt{(1-e^2)} \sin E \right]_{E_1}^{E_2} , \qquad (2.10)$$

μF being the magnitude of the radiation pressure force per unit mass of satellite, $\mu = n^2a^3$ = gravitational constant multiplied by the Earth's mass, acting in the direction of, and parallel to, the Sun-Earth line. E is the eccentric anomaly and in the present example E_1 and E_2 are taken as zero and 2π respectively, for a fully sunlit orbit. This leads to the result that there are no secular or long-period perturbations of the semi-major axis in a complete revolution that does not pass through the Earth's shadow. The situation has however, been simplified by several assumptions. The integration of the planetary equations has been carried out by holding all variables on the right hand side of (2.1) constant, except those explicitly dependent on the eccentric anomaly, also the force vector was assumed to act along the Sun-Earth line, parallel to the Sun-satellite line. The first simplification can be removed by allowing S and T to vary secularly. This is performed by approximating linearly the variation of the perigee ω, the orbital node Ω and the long itude of the ecliptic λ with time. This will be a reasonable approximation to the secular motion of ω and Ω due to the Earth's flattening, and the near linear variation of λ. S and T can therefore be written as,

$$\begin{Bmatrix} S \\ T \end{Bmatrix} = \begin{Bmatrix} - \\ + \end{Bmatrix} \sum_{i=1}^{6} \alpha_i \begin{Bmatrix} \cos \\ \sin \end{Bmatrix} (\beta_{i0} + \beta_{i1}t) , \qquad (2.11)$$

where

$$\beta_{ij} = \omega_j + \gamma_i\Omega_j + (-1)^i \lambda_j \qquad j=0,1,$$

$j=0$ represents initial values and $\omega_1 \simeq \dot{\omega}$, $\Omega_1 \simeq \dot{\Omega}$ and $\lambda_1 \simeq \dot{\lambda}$. This will lead to long periodic terms not found in equation (2.10). This was adequately approximated to by Aksnes, by

evaluating S,T,W and ω at times $t(E_1)$ and $t(E_2)$, and does not explain the deviation at present discussed. E_1 and E_2 define the points of intersection of the satellite's orbit with the Earth's shadow.

Consideration will now be given to the effects of removing the second assumption by taking the vector $\underline{F}$ to act along the Sun-satellite line, as shown by Figure 3.

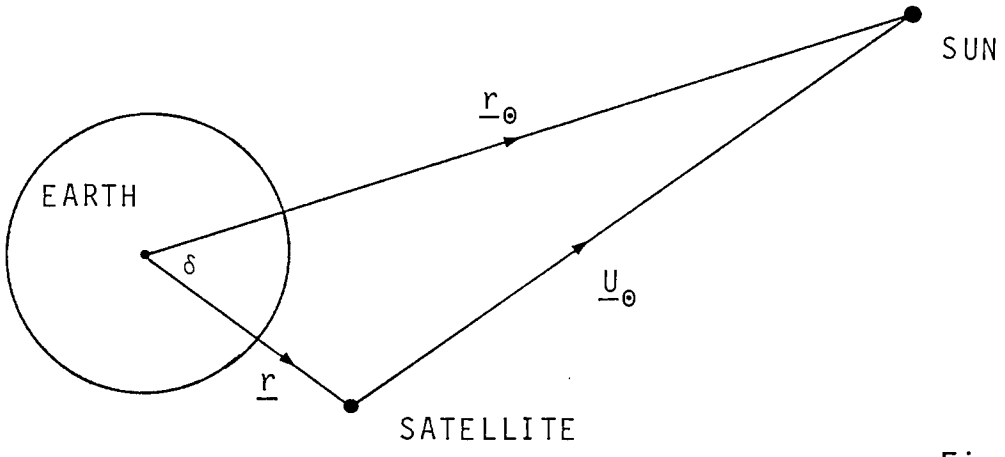

Fig. 3.

$(\underline{i},\underline{j},\underline{k})$ are a right hand set of unit vectors with respect to the geocentric coordinate axes defined in Figure 2. The satellite position and Sun position are defined by (x,y,z) and (X,Y,Z) respectively, so that

$$\left.\begin{aligned} \underline{r} &= x\underline{i} + y\underline{j} + z\underline{k} \\ \underline{r}_\odot &= X\underline{i} + Y\underline{j} + Z\underline{k} \end{aligned}\right\} \quad \underline{U}_\odot = \underline{r}_\odot - \underline{r} \ .$$

Therefore,

$$\begin{aligned} \underline{U}_\odot &= (X-x)\underline{i} + (Y-y)\underline{j} + (Z-z)\underline{k} \\ &= (r_\odot \cos\lambda - r\ell_1)\underline{i} + (r_\odot \sin\lambda \cos\varepsilon - rm_1)\underline{j} \\ &\quad + (r_\odot \sin\lambda \sin\varepsilon - rn_1)\underline{k} \ , \end{aligned}$$

where

$$\begin{aligned} U_\odot &= \sqrt{(r_\odot^2 + r^2 - 2rr_\odot \cos\delta)} \\ &= r_\odot \sqrt{\{1 + (r/r_\odot)^2 - 2(r/r_\odot)\cos\delta\}} \ , \end{aligned}$$

$$\cos\delta = \ell_1 \cos\lambda + m_1 \sin\lambda \cos\varepsilon + n_1 \sin\lambda \sin\varepsilon \ ,$$

and ℓ_1, m_1 and n_1 are the direction cosines of $\hat{\underline{r}}$. The force vector is now given in full viz.,

$$\underline{F} = -\frac{\sigma A}{m} P_0 \, (a_\odot/U_\odot)^2 \, \hat{\underline{U}}_\odot$$

$$= -\frac{F_0}{U_\odot^3} \underline{U}_\odot \quad ,$$

where σ is a constant, less than 2, to allow for the fraction of incident radiation absorbed by the satellite. If R is taken as the disturbing potential resulting from the radiation pressure force, and $\hat{\underline{S}}$,$\hat{\underline{T}}$ and $\hat{\underline{W}}$ are unit vectors in the directions of the components of force of $\underline{F}$, then

$$\underline{F} = F_0 \frac{[\{r + r_\odot \, S(\theta)\} \, \hat{\underline{S}} + r_\odot \, T(\theta) \, \hat{\underline{T}} + r_\odot \, W \, \hat{\underline{W}} \,]}{r_\odot^3 \{1 + (r/r_\odot)^2 - 2(r/r_\odot) \cos\delta \}^{3/2}}$$

$$= \nabla R$$

$$= (\ell_1 \hat{\underline{S}} + \ell_2 \hat{\underline{T}} + \ell_3 \hat{\underline{W}}) \frac{\partial R}{\partial x} + (m_1 \hat{\underline{S}} + m_2 \hat{\underline{T}} + m_3 \hat{\underline{W}}) \frac{\partial R}{\partial y} +$$

$$+ (n_1 \hat{\underline{S}} + n_2 \hat{\underline{T}} + n_3 \hat{\underline{W}}) \frac{\partial R}{\partial z} \quad ,$$

(ℓ_2, m_2, n_2) and (ℓ_3, m_3, n_3) being the direction cosines of $\hat{\underline{T}}$ and $\hat{\underline{W}}$. On equating coefficients of $\hat{\underline{S}}$, $\hat{\underline{T}}$ and $\hat{\underline{W}}$ and after some manipulation, it is found that

$$\frac{\partial R}{\partial x} = \frac{F_0 \, [\ell_1 \{ \frac{r}{r_\odot} + S(\theta) \} + \ell_2 T(\theta) + \ell_3 W]}{r_\odot^2 \{1 + (r/r_\odot)^2 - 2(r/r_\odot) \cos\delta\}^{3/2}} \quad ,$$

$$\frac{\partial R}{\partial y} = \frac{F_0 \, [m_1 \{ \frac{r}{r_\odot} + S(\theta) \} + m_2 T(\theta) + m_3 W]}{r_\odot^2 \{1 + (r/r_\odot)^2 - 2(r/r_\odot) \cos\delta\}^{3/2}} \quad ,$$

and

$$\frac{\partial R}{\partial z} = \frac{F_o \left[n_1 \left\{ \frac{r}{r_\Theta} + S(\theta) \right\} + n_2 T(\theta) + n_3 W\right]}{r_\Theta^2 \left\{1 + (r/r_\Theta)^2 - 2(r/r_\Theta) \cos\delta\right\}^{3/2}} \quad .$$

Now $x = r\ell_1$, $y = rm_1$, $z = rn_1$ so that for a general element ϕ,

$$\frac{\partial R}{\partial \phi} = \frac{F_o}{r_\Theta^2 \left\{1 + (r/r_\Theta)^2 - 2(r/r_\Theta) \cos\delta\right\}^{3/2}} \left[\left\{ \frac{r}{r_\Theta} + S(\theta) \right\} \frac{\partial r}{\partial \phi}\right.$$

$$+ rT(\theta) \left(\ell_2 \frac{\partial \ell_1}{\partial \phi} + m_2 \frac{\partial m_1}{\partial \phi} + n_2 \frac{\partial n_1}{\partial \phi}\right)$$

$$\left. + rW \left(\ell_3 \frac{\partial \ell_1}{\partial \phi} + m_3 \frac{\partial m_1}{\partial \phi} + n_3 \frac{\partial n_1}{\partial \phi}\right)\right] \quad . \qquad (2.12)$$

Noting that

$$R \equiv R(a, e, i, \omega, \Omega, \chi)$$

where the mean anomaly M is given by

$$M = n(t - t_o) = nt + \chi \quad ,$$

and using the equations

$$\frac{\partial \ell_1}{\partial \phi} = -m_1 \frac{\partial \Omega}{\partial \phi} + \ell_2 \frac{\partial u}{\partial \phi} + \ell_3 \sin u \frac{\partial i}{\partial \phi} \quad ,$$

$$\frac{\partial m_1}{\partial \phi} = \ell_1 \frac{\partial \Omega}{\partial \phi} + m_2 \frac{\partial u}{\partial \phi} + m_3 \sin u \frac{\partial i}{\partial \phi} \quad ,$$

$$\frac{\partial n_1}{\partial \phi} = n_2 \frac{\partial u}{\partial \phi} + n_3 \sin u \frac{\partial i}{\partial \phi} \quad ,$$

$$\frac{\partial r}{\partial \phi} = \frac{\partial}{\partial \phi} \{a(1 - e \cos E)\}$$

$$= \frac{r}{a} \frac{\partial a}{\partial \phi} - a \cos\theta \frac{\partial e}{\partial \phi} + \frac{a^2 e}{r} \sin E \frac{\partial \chi}{\partial \phi} \quad ,$$

substitution of the relevant elements for ϕ, gives

$$\frac{\partial R}{\partial a} = K \left[\{ S(\theta) + \frac{r}{r_\Theta} \} \frac{r}{a} \right] \quad , \tag{2.13}$$

$$\frac{\partial R}{\partial e} = K \left[\left[-\{ S(\theta) + \frac{r}{r_\Theta} \} a \cos\theta \right. \right.$$

$$\left. \left. + rT(\theta) \left[\frac{\sin\theta}{1-e^2} (2 + e \cos\theta) \right] \right] \right] \quad , \tag{2.14}$$

$$\frac{\partial R}{\partial i} = KrW \sin u \quad , \tag{2.15}$$

$$\frac{\partial R}{\partial \omega} = KrT(\theta) \quad , \tag{2.16}$$

$$\frac{\partial R}{\partial \Omega} = K \left[rT(\theta) \cos i - rW \cos u \sin i \right] \quad , \tag{2.17}$$

$$\frac{\partial R}{\partial \chi} = K \left[\left[\{ S(\theta) + \frac{r}{r_\Theta} \} \frac{a^2 e}{r} \sin E + \frac{a^2 \sqrt{(1-e^2)}}{r} T(\theta) \right] \right] \quad , \tag{2.18}$$

$$K = \frac{F_o}{r_\Theta^2 \{ 1 + (r/r_\Theta)^2 - 2(r/r_\Theta) \cos\delta \}^{3/2}} \quad .$$

These equations, (2.13) to (2.18), may now be substituted into the planetary equations, viz.,

$$\frac{da}{dt} = \frac{2}{n a} \frac{\partial R}{\partial \chi} \quad , \tag{2.19}$$

$$\frac{de}{dt} = \frac{\sqrt{(1-e^2)}}{n a^2 e} \left[\sqrt{(1-e^2)} \frac{\partial R}{\partial \chi} - \frac{\partial R}{\partial \omega} \right] \quad , \tag{2.20}$$

$$\frac{di}{dt} = \frac{1}{n a^2 \sqrt{(1-e^2)} \sin i} \left[\frac{\partial R}{\partial \omega} \cos i - \frac{\partial R}{\partial \Omega} \right] \quad , \tag{2.21}$$

$$\frac{d\omega}{dt} = \frac{\sqrt{(1-e^2)}}{na^2e}\frac{\partial R}{\partial e} - \frac{\cot i}{na^2\sqrt{(1-e^2)}}\frac{\partial R}{\partial i} \quad , \tag{2.22}$$

$$\frac{d\Omega}{dt} = \frac{1}{na^2\sqrt{(1-e^2)}\,\sin i}\frac{\partial R}{\partial i} \quad , \tag{2.23}$$

$$\frac{d\chi}{dt} = -\frac{2}{na}\frac{\partial R}{\partial a} - \frac{1-e^2}{na^2e}\frac{\partial R}{\partial e} \quad .$$

In the above χ may be replaced by M and

$$\dot{M} = \dot{\chi} + n$$

so that

$$\frac{dM}{dt} = n - \frac{2}{na}\frac{\partial R}{\partial a} - \frac{1-e^2}{na^2e}\frac{\partial R}{\partial e} \tag{2.24}$$

and,

$$\dot{a} = \frac{2}{na}\frac{\partial R}{\partial M} = \frac{2K}{na}\left[\{S(\theta) + \frac{r}{r_\odot}\}\frac{a^2e}{r}\sin E + rT(\theta)\{\frac{a^2}{r^2}\sqrt{(1-e^2)}\}\right]$$

$$= \frac{2F_0}{r_\odot^2}\frac{1}{n\sqrt{(1-e^2)}}\left[\{S(\theta) + \frac{r}{r_\odot}\}e\sin\theta + T(\theta)(1 + e\cos\theta)\right]$$

$$\times\left[1 - 2(r/r_\odot)S(\theta) + (r/r_\odot)^2\right]^{-3/2}$$

from equations (2.18) and (2.19).

As a first approximation, terms $O(r/r_\odot)$ are neglected so that

$$\dot{a} = \left(\frac{da}{dt}\right)_{\text{Aksnes, 1976}} \quad .$$

Now neglecting only terms $O\left(\frac{r^2}{r_\odot^2}\right)$ leads to,

$$\frac{da}{dE} = \frac{\dot{a}r}{na} = 2F'a^3\left[T\sqrt{(1-e^2)}\cos E - S\sin E\right.$$

$$+ 3\left(\frac{a}{r_\odot}\right)\{ST\sqrt{(1-e^2)}(\cos 2E - e\cos E)$$

$$\left. - S^2(\sin E\cos E - e\sin E)\right.$$

$$+ T^2 (1-e^2) \sin E \cos E\}\Big]$$

$$+ \frac{2F'a^4e}{r_0} \sin E (1 - e \cos E) \quad ,$$

where $\mu F' = \frac{\sigma A}{m} P_0 (a_0/r_0)^2$.

Then on integration, holding all terms constant except those explicitly dependent on E,

$$\delta a = 2F'a^3 \Big[S \cos E + T\sqrt{(1-e^2)} \sin E$$

$$+ 3(a/r_0) \{ST \sqrt{(1-e^2)}(\frac{\sin 2E}{2} - e \sin E)$$

$$- S^2 (e \cos E - \frac{\cos 2E}{4}) - T^2 (1-e^2) \frac{\cos 2E}{4}\}\Big]_{E_1}^{E_2}$$

$$- \Big[\frac{2F'a^4e}{r_0} (\cos E - \frac{e}{4} \cos 2E)\Big]_{E_1}^{E_2} \quad .$$

Similar derivatives have been found for the remaining five orbital elements and programmed in such a way as to compare the results given by Aksnes for Dash 2 (1963-30D). No other alterations were made to the theory at this stage, and the method described by Aksnes was used to sum the perturbations over complete orbits. These equations are seen to contain long and short period, first and second order terms in S, T and W. There were no measurable differences found between the two sets of perturbations for the elements over the period of 200 days analysed by Aksnes, other than in the case of δa. Here the mean long period effect was found to be of the order of about one metre per day, and would not lead to a satisfactory explanation, for what would appear to be a secular discrepancy between the observed and theoretical

changes in 'a'. It does however strengthen the assumption that the force acting along the Sun-Earth line can be taken as parallel to the Sun-satellite line.

3.

METHODS OF ANALYSIS FOR SATELLITES ECLIPSED BY THE EARTH'S SHADOW

The shadow phase is defined as that time during which the satellite's orbit includes part of the Earth's shadow. Musen (1960) and several early authors neglected to take into account the discontinuous effect of the shadow phase. Kozai (1961), however, provided a basic relationship for the derivation of the shadow boundary, assuming that the Earth's equatorial radius, R_E, is constant and $\omega,\Omega,\lambda,S,T$ and e are taken as constant for each revolution considered. Kozai, though, did not apply this in the numerical example that he gave as he assumed that the satellite in question, namely Echo 1, did not enter the Earth's shadow, when in fact this was known to be untrue.

If the shadow phase is simplified by considering a circular orbit so that r=a, with the Sun in the orbital plane, then some idea of the time spent by the satellite in shadow can be obtained. The fraction of the orbital path in shadow for this situation is given approximately by,

$$0.2 < \frac{1}{\pi} \sin^{-1} \left(\frac{R_E}{a}\right) < 0.4 \quad ,$$

for the average balloon satellite. This suggests that whenever the orbital inclination, i, takes a value close to that of ε, the inclination of the ecliptic to the equatorial plane, and Ω is small, neglect of the effects of the shadow phase can introduce quite appreciable errors in the magnitudes of the perturbations

so obtained. In fact the fractional change in the amplitude of the relevant element, due to the inclusion of the shadow phase, can be approximately equal to the fraction of the orbit in shadow. For example, the balloon satellite Explorer 19 was in shadow during about 3/10 of the revolution that started on the MJD 42822.0 . The amplitude of δa, while neglecting the shadow phase, was 32 m. and when the shadow was taken into account this amplitude was found to be 25 m.

The general expression defining the shadow boundary, assuming that the shadow cast by the Earth is a right circular cylinder, is now given.

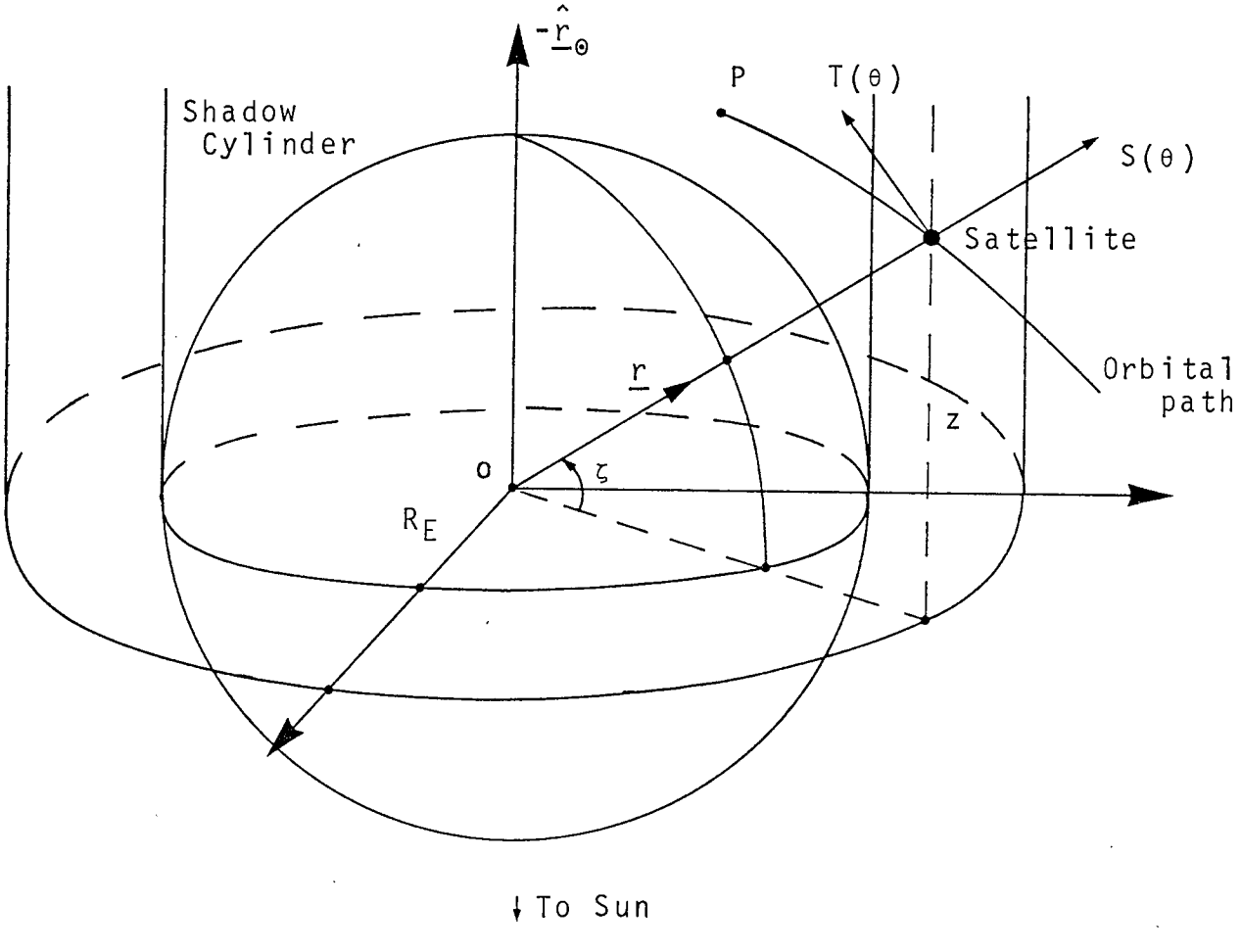

Fig. 4.

From Figure 4,

$$\cos \zeta = \sqrt{(1 - z^2/r^2)} \quad ,$$

and

$$\underline{r}.\hat{\underline{r}}_{\odot} = -rS(\theta) = -z \quad ,$$

therefore

$$\cos \zeta = \sqrt{\{1 - S^2(\theta)\}} \quad .$$

If $S(\theta)>0$ then it is ensured that the satellite is not over the sunlit hemisphere of the Earth and also from Figure 4, if

$$r \cos \zeta \leq R_E$$

then the satellite is in or on the surface of the shadow cylinder. The conditions for the satellite to be in shadow, are therefore,

$$S(\theta) > 0 \qquad (3.1)$$

and

$$R_E - r\sqrt{\{1 - S^2(\theta)\}} > 0 \qquad (3.2)$$

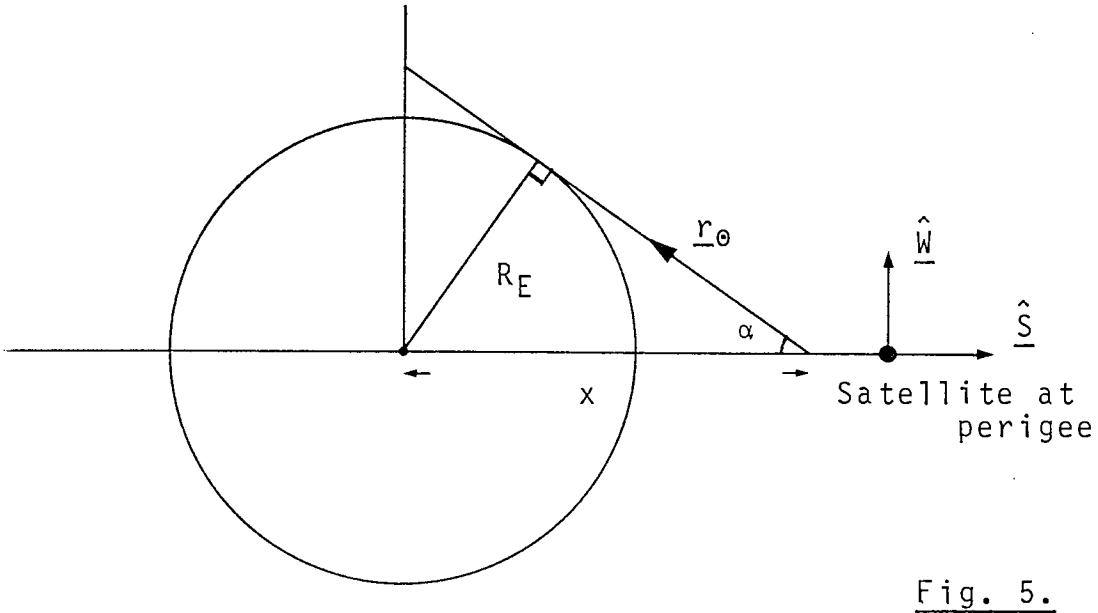

Fig. 5.

A useful property for the shadow phase is given by Figure 5, that is from,

$$\sin \alpha = \frac{R_E}{X} \quad ,$$

and

$$W = \pm \sin \alpha \quad .$$

Then the satellite will be fully sunlit throughout its orbit if,

$$a(1-e) > X \quad ,$$

or

$$a(1-e) > \frac{R_E}{|W|} \quad . \tag{3.3}$$

The condition given by equation (3.2) is now expanded in terms of the eccentric anomaly, E, so that

$$\left[(1 - e \cos E)^2 - (\frac{R_E}{a})^2\right] = S^2(\cos E - e)^2 + T^2(1-e^2) \sin^2 E + 2ST\sqrt{(1-e^2)} \sin E (\cos E - e)$$

gives the boundary value of E for the shadow. After some manipulation this can be written as a quartic in cosE, viz.,

$$A \cos^4 E + B \cos^3 E + C \cos^2 E + D \cos E + G = 0 \quad , \tag{3.4}$$

where

$$A = e^4(T^2-1)^2 + 2e^2(T^2-S^2-S^2T^2-T^4) + (T^2+S^2)^2 \quad ,$$

$$B = 4e^3(S^2+T^2+S^2T^2-1) + 4e(S^2-T^2-S^2T^2-S^4) \quad ,$$

$$C = 2e^4(T^2 - S^2 - S^2T^2 - T^4)$$

$$+ 2e^2\{2T^4 + 3S^4 + 2S^2T^2 - 2T^2 - 4S^2 + (T^2-1)(R_E/a)^2 + 3\}$$

$$+ 2\{T^2 - T^4 - S^2 - S^2T^2 + (S^2 - T^2)(R_E/a)^2\} \quad ,$$

$$D = 4e^3(S^2 - T^2 - S^2T^2 - S^4) + 4e\{S^2 + T^2 + S^2T^2 - 1 + (1-S^2)(R_E/a)^2\} \quad ,$$

and

$$G = e^4(S^4 + T^4 + 2S^2T^2) + 2e^2\{T^2 - S^2 - S^2T^2 - T^4 + (S^2 - T^2)(R_E/a)^2$$

$$+ [1 - 2T^2 + T^4 + (R_E/a)^2\{2T^2 - 2 + (R_E/a)^2\}] \quad .$$

During one revolution S,T,W,a and R_E are taken as constant in order to evaluate the coefficients of equation (3.4). This quartic can be solved numerically noting that there will be no real solutions when the orbit considered does not enter the shadow cylinder. Two distinct roots are found when the satellite enters and leaves the Earth's shadow together with a pair of complex conjugate roots. There are several numerical approaches that readily lend themselves for computational evaluation of the quartic. The iterative process of Bairstow (Buckingham, 1962) is particularly suitable for the quartic involved here, as there will be at least one pair of complex roots, and Bairstow's method is one that separates the quartic into two quadratics which can be individually tested for real solutions, and thus the eccentric anomalies of the shadow entry and exit points may be evaluated. In theory, once these solutions have been found the computational process should require only a few iterative steps to find the shadow phase for the next revolution. It will be necessary to re-evaluate the coefficients of equation

(3.4) for each orbit and this involves quite lengthy computational time.

Naturally the required accuracy can be obtained by this method, but the solutions so found will be for the approximation of the shadow cylinder, which does not take into account the penumbra and refraction due to the Earth's atmosphere. Any improvement in accuracy that might result from the solution of the quartic will be lost by the neglect of the penumbra and refraction effects.

In a paper by Lála and Sehnal (1969), an attempt was made to include the effects of the penumbral region in the shadow model. This was carried out by introducing a discontinuous function that is zero while the satellite is in shadow, and equal to unity while in sunlight. This function was expanded as a series and its product was formed with Lagrange's planetary equations.

The shadow function introduced by Lála and Sehnal was

$$F(x) = \tfrac{1}{2}\{1 + \sin x \sum_{r=0}^{\infty} (-1)^r \binom{-\frac{1}{2}}{r} \cos^{2r} x\} \quad , \quad (3.5)$$

where x is the geocentric angle between the satellite's position and the exit or entry position of the shadow, assuming a spherical Earth and an ideal shadow cylinder dependent on the position of the Sun and the orbital elements. In equation (3.5),

$$(-1)^r \binom{-\frac{1}{2}}{r} = \frac{(2r)!}{2^{2r}\,(r!)^2} \quad .$$

The number of terms chosen for the summation of the above series should be selected so as to optimise the simulation of the penumbral and umbral regions.

There are several expansions of functions that can fulfil the required conditions. For example

$$\Gamma(x) = \tfrac{1}{2}\{1+\mathrm{sgn}(x)\} \quad , \tag{3.6}$$

where

$$\mathrm{sgn}(x) = \frac{4}{\pi} \sum_{r=0}^{\infty} \frac{(-1)^r}{2r+1} T_{2r+1}(x) \quad ,$$

and T_{2r+1} are the odd Chebyshev polynomials given by,

$$T_{2r+1}(x) = \cos\{(2r+1)\cos^{-1}x\} \quad .$$

When functions such as equation (3.6) are employed, and the products with the Lagrange Planetary Equations are formed, it is necessary to express x in terms of the orbital elements for the satellite.

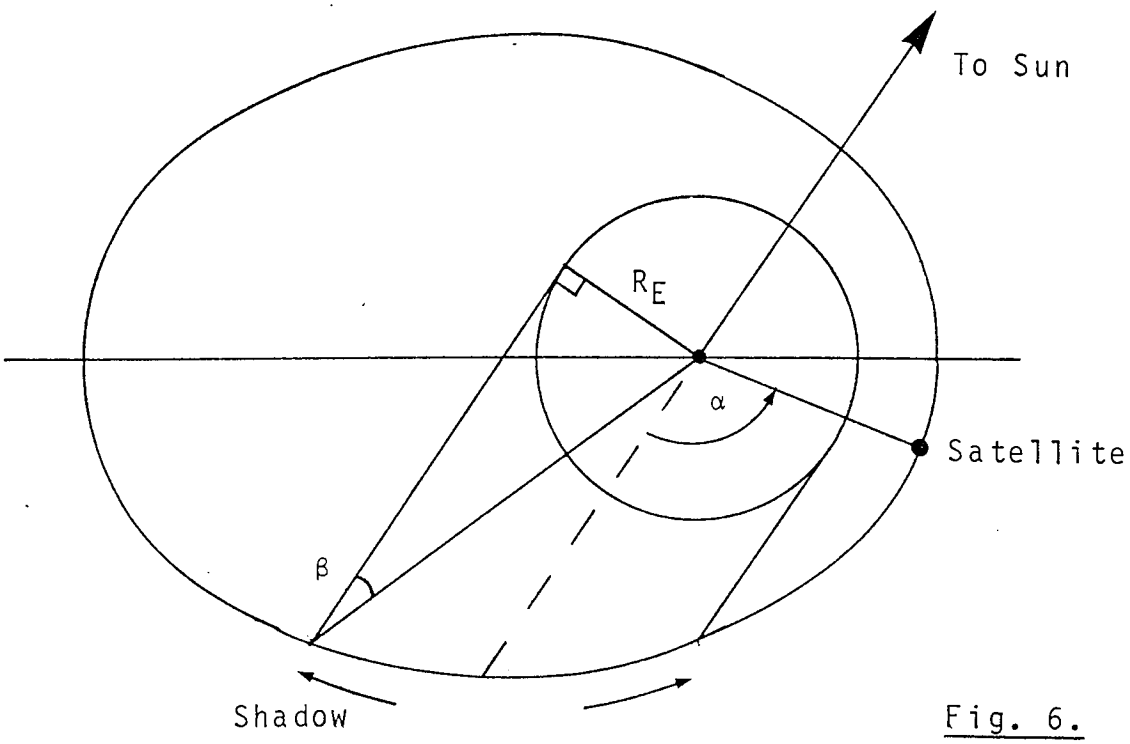

Fig. 6.

From Figure 6, if $x=\alpha-\beta < 0$ then the satellite is in shadow, where α and β are given by,

$$\cos \alpha = S(\theta) = S \cos \theta + T \sin \theta \quad , \tag{3.7}$$

and

$$\sin \beta = \frac{R_E}{p} (1 + e \cos \theta) \quad , \tag{3.8}$$

p being the semi-latus rectum of the orbit. In the example using the function given by equation (3.6), it is not possible to separate the argument θ from the inverse trig function once x has been substituted. This leads to unmanageable equations that require integration.

Lála and Sehnal expressed equation (3.5) in terms of orbital elements by employing equations (3.7) and (3.8), but neglected to give the coefficients of the ensuing series. The development of these coefficients is now briefly outlined. The series from equation (3.5) is truncated to m_1 terms and written as,

$$\Gamma_{m1}(x) = \tfrac{1}{2}(1 + \sum_{s=0}^{m1} A_s \sin^{2s+1} x) \tag{3.9}$$

where

$$A_s = (-1)^s \sum_{r=s}^{m1} (-1)^r \binom{-\frac{1}{2}}{r} \binom{r}{s} \quad . \tag{3.10}$$

Now

$$\sin^{2s+1} x = \sum_{i=0}^{2s+1} (-1)^i \binom{2s+1}{i} (\sin \alpha \cos \beta)^{2s+1-i} (\cos \alpha \sin \beta)^i$$

which may be re-written as a sum of even and odd multiples of $(\cos \alpha \sin \beta)$,

so that

$$\sin^{2s+1}x = \sum_{i=0}^{s} \binom{2s+1}{2i} \sum_{p=0}^{\infty} \sum_{q=0}^{\infty} (-1)^{p+q} \binom{s-i+\frac{1}{2}}{p} \binom{s-i+\frac{1}{2}}{q}$$

$$\times \cos^{2p+2i}\alpha \sin^{2q+2i}\beta$$

$$- \sum_{i=0}^{s} \binom{2s+1}{2i+1} \sum_{p=0}^{s-i} \sum_{q=0}^{s-i} (-1)^{p+q} \binom{s-i}{p} \binom{s-i}{q}$$

$$\times \cos^{2p+2i+1}\alpha \sin^{2q+2i+1}\beta \quad .$$

The accuracy of the series for Γ, while depending on m_1 , will also depend on how many terms (m_2 say) that are taken for the double summation to infinity, above. The odd multiples of ($\cos\alpha \sin\beta$) are summed over i,p and q . For uniformity one may consider the double summation over p and q to (s-i) as being infinite. This is feasible as the notation $\binom{s-i}{p}$ is zero by definition when $p > s-i$, so that p may exist as $p=0,1,2,\ldots\infty$. Γ_{m_1} is now written as

$$\Gamma_{m_1 m_2}(x) = \tfrac{1}{2}\Big[1 + \sum_{s=0}^{m_1} \sum_{i=0}^{s} \sum_{p=0}^{m_2} \sum_{q=0}^{m_2} A_s (-1)^{p+q}$$

$$\times \{\binom{2s+1}{2i}\binom{s-i+\frac{1}{2}}{p}\binom{s-i+\frac{1}{2}}{q} \cos^{2p+2i}\alpha \sin^{2q+2i}\beta$$

$$- \binom{2s+1}{2i+1}\binom{s-i}{p}\binom{s-i}{q} \cos^{2p+2i+1}\alpha \sin^{2q+2i+1}\beta\}\Big] \quad ,$$

which may be re-arranged in the form

$$\Gamma_{m_1 m_2}(x) = \tfrac{1}{2}\Big[1 + \sum_{a=0}^{m_2} \sum_{b=0}^{m_2} C_{ab} \cos^a\alpha \sin^b\beta\Big] \quad , \qquad (3.11)$$

where

$$C_{ab} = 0 \quad , \text{ for } a+b \text{ odd}, \tag{3.12}$$

$$= \sum_{s=0}^{m_1} A_s \sum_{i=0}^{\nu/4} \left[(-1)^{\frac{a+b}{2} - 2i} \binom{2s+1}{2i} \binom{s-i+\frac{1}{2}}{a'} \binom{s-i+\frac{1}{2}}{b'} \right] , \tag{3.13}$$

for a,b both even,

$$= -\sum_{s=0}^{m_1} A_s \sum_{i=0}^{\frac{\nu-2}{4}} \left[(-1)^{\frac{a+b}{2} - (2i+1)} \binom{2s+1}{2i+1} \binom{s-i}{a''} \binom{s-i}{b''} \right] , \tag{3.14}$$

for a,b both odd.

In the above ν is given by,

$$\nu = 2a \quad \text{when } b > a$$

or

$$\nu = 2b \quad \text{when } a \geq b \quad ,$$

and

$$a' = \frac{a-2i}{2} \quad , \qquad b' = \frac{b-2i}{2} \quad ,$$

$$a'' = \frac{a-2i-1}{2} \quad , \quad b'' = \frac{b-2i-1}{2} \quad .$$

$\Gamma_{m_1 m_2}$ can now be written in terms of the orbital elements of the satellite, the inclination of the ecliptic and the ecliptic longtitude of the Sun. On substituting for $\cos \alpha$ and $\sin \beta$ from equations (3.7) and (3.8), equation (3.11), can be further manipulated to give

$$\Gamma_{m_1 m_2}(x) = \tfrac{1}{2} \sum_{i=0}^{m_2} \sum_{j=i}^{m_2} A_{ij} \cos^{j-i}\theta \sin^{i}\theta \quad . \tag{3.16}$$

For $i+j > 0$

$$A_{ij} = A'_{ij} \quad ,$$

and when $i+j = 0$

$$A_{00} = A'_{00} + 1 \quad ,$$

where

$$A'_{ij} = \sum_{a=0}^{m_2} \sum_{b=0}^{m_2} C_{ab} \; (R_E/p)^b \; e^{j-a} \; S^{a-i} \; T^i \; \binom{a}{i} \binom{b}{j-a} \quad .$$

At this point Lála and Sehnal formed the product of $\Gamma_{m_1 m_2}(x)$ with a generalised form of equations (2.1)-(2.6), after expanding $(1 + e \cos \theta)^{-1}$, which occurs in all these equations apart from equation (2.1). The resulting formula is in terms of integer powers of $\cos \theta$ and $\sin \theta$ which are converted into multiples of the argument. This equation can then be integrated with respect to the true anomaly, or with respect to the mean anomaly if Hansen coefficients are used.

It should be noted that, while this method does not require the external evaluation of the shadow boundaries, the computational time for the evaluation of the coefficients A_{ij} is rather excessive. There is an advantage in the method, in that it is possible to simulate the penumbral region of the shadow, but this must be compared with the disadvantage resulting from the termination of the series approximation to the original planetary equations, required to facilitate integration.

Returning, then, to the function given by Lála and Sehnal, it is of value to discuss another form that the expansion could take. When Lála developed the shadow function by employing Fourier analysis, it was possible to take the summation to a relatively large number of terms without an excessive increase in the computational time, but this did not give the necessary improvement in accuracy required to simulate the shadow phase. This was due to the resulting Gibb's oscillations that allowed Γ to take values greater than unity and less than zero. The use of Fourier series here would greatly reduce the time involved on the numerical evaluation of the series coefficients. Now the Fourier series for Γ is given by

$$\Gamma(x) = \sum_{k=-\infty}^{\infty} C_k \exp(jkx) \quad ,$$

where $j^2 = -1$. Truncating the resulting series to N terms gives,

$$\Gamma_N(x) = \frac{1}{2} + \frac{2}{\pi} \sum_{k=1}^{N} \frac{\sin(2k-1)x}{2k-1} \qquad \text{for} \quad -\pi \leq x \leq \pi \quad . \quad (3.17)$$

The rate of convergence of this Fourier series can be increased by reducing the amplitudes of the Gibb's oscillations. This may be performed by finding a suitable series of coefficients, σ_k, that will have a smoothing effect on these extraneous variations. Let the smoothed, truncated series of equation (3.17), be given by

$$\Gamma_\sigma(x) = \sum_{k=-N}^{N} \sigma_k C_k \exp(jkx)$$

$$= \frac{N}{2\pi} \sum_{k=-N}^{N} \int_{-\pi/N}^{\pi/N} \Gamma_N(x+t)\, dt$$

$$= \frac{N}{\pi} \sum_{k=-N}^{N} \frac{C_k}{k} \exp(jkx)\, \sin\left(\frac{k\pi}{N}\right) \quad .$$

Then,

$$\sigma_k = \frac{N}{k\pi} \sin\left(\frac{k\pi}{N}\right)$$

so that

$$\Gamma_\sigma(x) = \frac{1}{2} + \frac{2}{\pi}\left[\sin x + \sum_{k=1}^{N} \frac{\sin\left(\frac{k\pi}{N}\right)}{\left(\frac{k\pi}{N}\right)} \frac{\sin(2k+1)x}{2k+1} \right] \quad . \qquad (3.18)$$

Figures 7 and 8 show the comparison of the three series expansions of the shadow function for two values of N. Here it may be seen that fewer terms than the Taylor's series are required to arrive at a suitable approximation to the shadow phase.

The substitution for x, in equation (3.18), for terms in the true anomaly is carried out in the manner suggested by Lála and Sehnal for their shadow function. The product is then formed with the general expression for the planetary equations that arises in equation (7) in their paper.

An attempt to reduce the computational time was made by introducing equations (3.1)-(3.3) to the program. This allowed a step by step search along the orbit to find a point 5^o from the distinct boundary defined by the shadow cylinder. During this time the function Γ was taken as

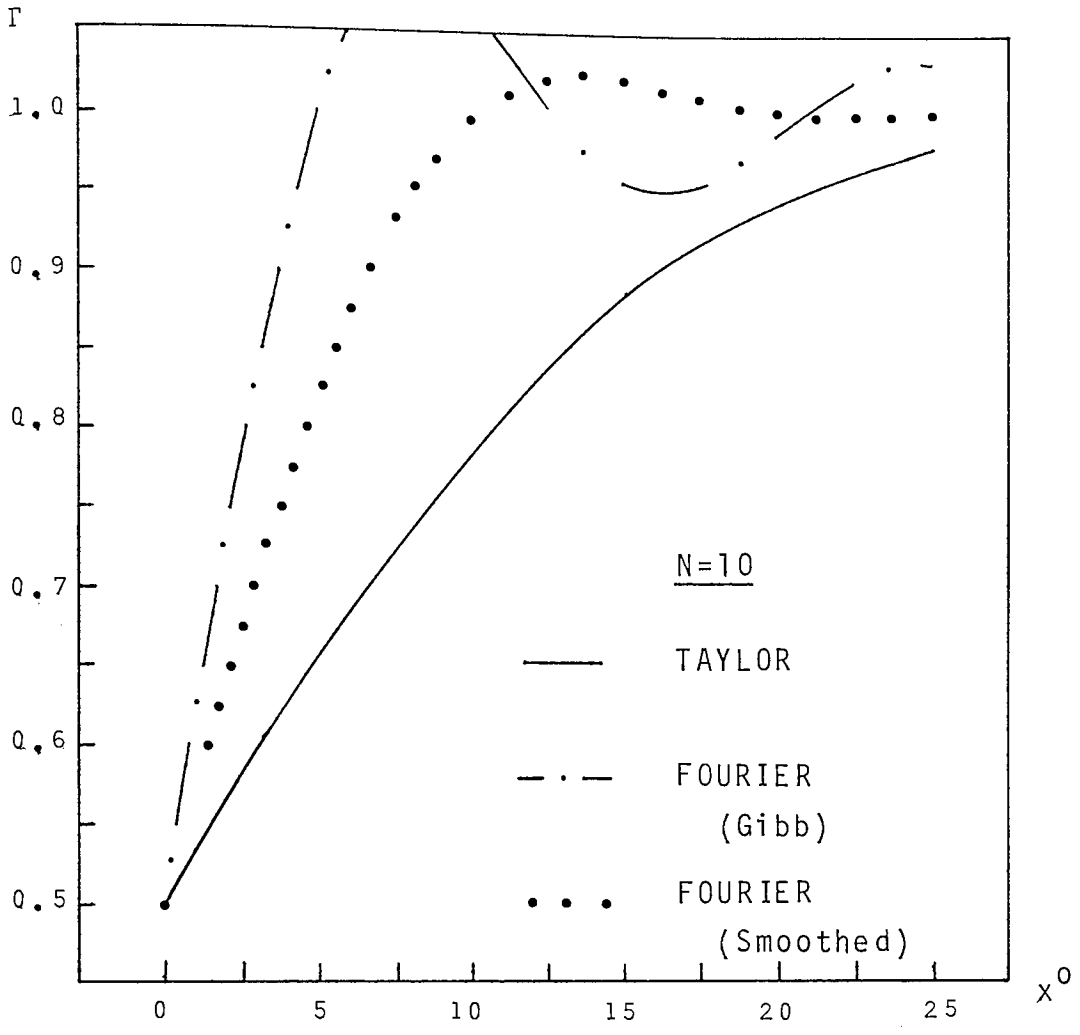
Γ
1.0
0.9
0.8
0.7
0.6
0.5
N=10
TAYLOR
FOURIER
(Gibb)
FOURIER
(Smoothed)
0
5
10
15
20
25
x°

Fig. 7.

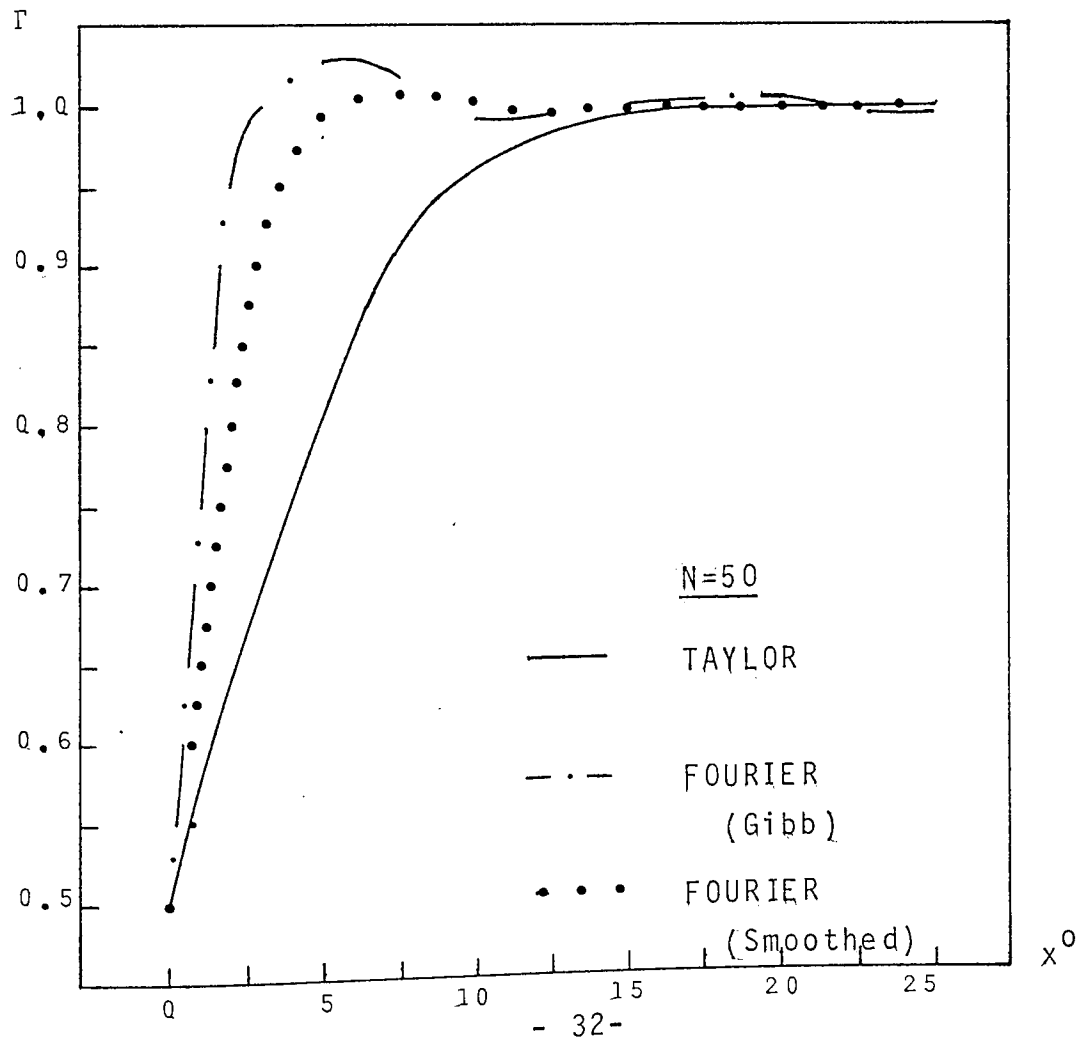
Γ
1.0
0.9
0.8
0.7
0.6
0.5
N=50
TAYLOR
FOURIER
(Gibb)
FOURIER
(Smoothed)
0
5
10
15
20
25
x°

Fig. 8.

equal to unity. When the shadow boundary had been found, the theory developed from equation (3.18) was used. This removed the unnecessary evaluation of the lengthy coefficients needed to define Γ, when a complete orbit is sunlit. The number of terms, N, chosen for the summation for Γ_σ was selected so that Γ_σ would equal unity at the point 5^0 from the boundary of the cylindrical shadow.

This process was applied to the satellite 1963-30D using the same initial data as Aksnes (1976) to predict the changes in semi-major axis and eccentricity over a period of 200 days. It is necessary to increase the value of N until δa and δe are zero during the shadow phase of an orbit that intersects the Earth's shadow. The residual differences between the results found in this way and those computed by Aksnes were found to be relatively large. This was felt to be due, in part, to the effect of neglecting the change of orientation of the orbit with respect to the Sun. It is not possible to allow for this motion in the continuous theory of the shadow function, Γ. The variation in S,T and W due to the Earth's orbital motion can be approximated by assuming their variation to be linear between shadow exit and entry. This may be done by taking the linear rates of change of S,T and W during the orbit previous to the one considered, and applying these rates to evaluate the new values of S,T and W at the next shadow intersection. This can only be applied when a discrete method is employed to evaluate the changes in orbital elements.

It should be noted that it is difficult to ascertain to what degree the choice of N, (m_1 and m_2 for Lála's function)

simulates the penumbral region when the main criterion for this choice is that N should be as large as the computational time will allow, in order that the regions where the orbits do not enter the shadow, do not lead to spurious results for δa.

The step by step method that is employed in the analysis of Section 6, is the utilisation of equations (3.1), (3.2) and (3.3). If the condition represented by the third of these is not met then a step length of $\frac{2\pi}{100}$ is used until both the first two conditions are satisfied. Then the step length is progressively halved until the shadow entry angle is found to within a limit of 0.001^{o} (2×10^{-5} rads). The process is then applied to find the exit point of the shadow.

The effect of the Earth's flattening can be readily included in this algorithm, but it has not been possible to model the effect of the refraction of light by the Earth's atmosphere. This, and the effect of the penumbral region of the shadow can only be accurately included when visual timings or photometric observations are available for the shadow boundaries.

4.

DEFORMATION OF A SPHERICAL SATELLITE INCLUDING THE EFFECTS OF DIFFUSE RADIATION

An effect related to direct SRP that was not included by Aksnes was that of a component of radiation pressure force acting normally to the Sun-satellite line. This is a consequence of the departure of the satellite's shape from that of a sphere. Aksnes suggested that the inclusion of this effect might be feasible and possibly valuable. This is now investigated along the lines of the exact development provided by Lucas (1974).

The components of force due to direct SRP on a prolate spheroid have been defined in terms of satellite orientated coordinates.

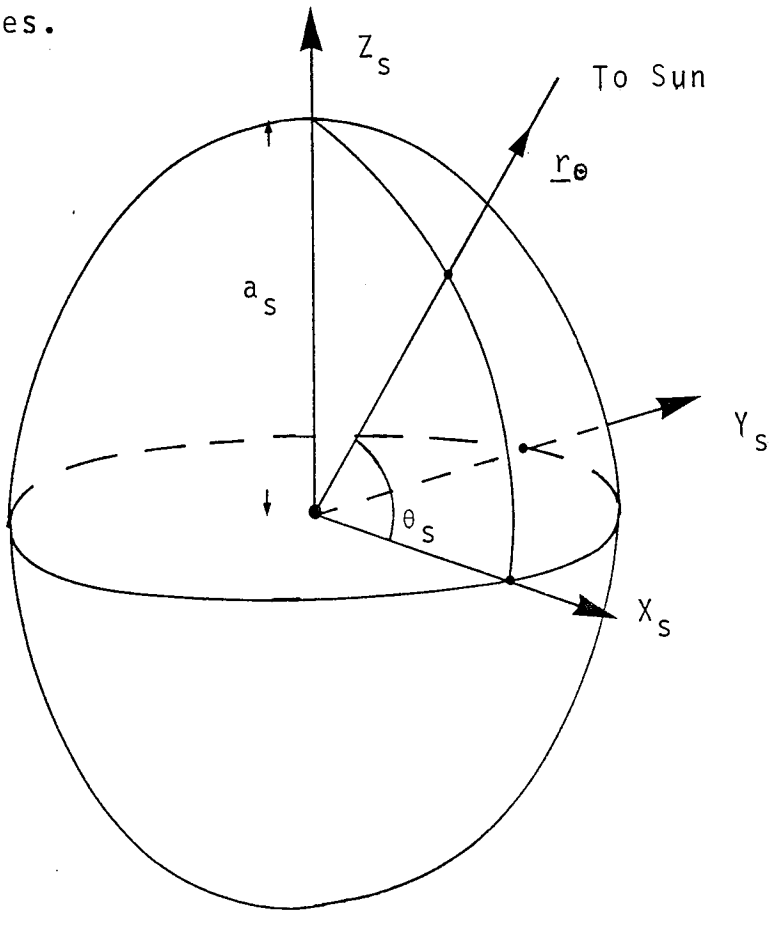

NON-ROTATING PROLATE SPHEROIDAL SATELLITE. FIG. 9.

The Sun-satellite line is taken to be in the $X_s Z_s$ -plane, defined in Figure 9.

In order to apply these components to Gauss' form of Lagrange's planetary equations, it is necessary to define this force in terms of the direction cosines, along the Earth-satellite radius vector, $\underline{r}$, perpendicular to $\underline{r}$ in the orbital plane and along the orbit normal, i.e. along $\hat{\underline{S}}$, $\hat{\underline{T}}$ and $\hat{\underline{W}}$ defined previously. Suppose, therefore, that

$$\begin{pmatrix} \hat{\underline{S}} \\ \hat{\underline{T}} \\ \hat{\underline{W}} \end{pmatrix} = R_{s,E} \begin{pmatrix} \hat{\underline{X}}_s \\ \hat{\underline{Y}}_s \\ \hat{\underline{Z}}_s \end{pmatrix}$$

where $R_{s,E}$ is a rotation matrix defining the rotation of axes from the satellite centred system, to the geocentric set of coordinate axes. $R_{s,E}$ can be defined in terms of the direction cosines of $\hat{\underline{r}}_\Theta$. Thus,

$$\begin{pmatrix} \hat{\underline{S}} \\ \hat{\underline{T}} \\ \hat{\underline{W}} \end{pmatrix} = R_3(u)\, R_1(i)\, R_3(\Omega)\, R_1(-\varepsilon)\, R_3(-\lambda)\, R_2(-\theta_s) \begin{pmatrix} \hat{\underline{X}}_s \\ \hat{\underline{Y}}_s \\ \hat{\underline{Z}}_s \end{pmatrix}$$

$$= \begin{pmatrix} l_1 & m_1 & n_1 \\ l_2 & m_2 & n_2 \\ l_3 & m_3 & n_3 \end{pmatrix} \begin{pmatrix} \cos\lambda, & -\sin\lambda, & 0 \\ \sin\lambda\cos\varepsilon, & \cos\lambda\cos\varepsilon, & -\sin\varepsilon \\ \sin\lambda\sin\varepsilon, & \cos\lambda\sin\varepsilon, & \cos\varepsilon \end{pmatrix}$$

$$\times R_2(-\theta_s) \begin{pmatrix} \hat{\underline{X}}_s \\ \hat{\underline{Y}}_s \\ \hat{\underline{Z}}_s \end{pmatrix}$$

where

$$
\begin{aligned}
l_1 &= \cos\Omega\cos u - \cos i \sin\Omega \sin u \quad , \\
m_1 &= \sin\Omega\cos u + \cos i \cos\Omega \sin u \quad , \\
n_1 &= \sin i \sin u \quad , \\
l_2 &= -\cos\Omega \sin u - \cos i \sin\Omega \cos u \quad , \\
m_2 &= -\sin\Omega \sin u + \cos i \cos\Omega \cos u \quad , \\
n_2 &= \sin i \cos u \quad , \\
l_3 &= \sin i \sin\Omega \quad , \\
m_3 &= -\sin i \cos\Omega \quad , \\
n_3 &= \cos i \quad .
\end{aligned}
$$

After some manipulation, this reduces to

$$
\begin{pmatrix} \hat{\underline{S}} \\ \hat{\underline{T}} \\ \hat{\underline{W}} \end{pmatrix} = \begin{pmatrix} A_{11} & A_{12} & A_{13} \\ A_{21} & A_{22} & A_{23} \\ A_{31} & A_{32} & A_{33} \end{pmatrix} \begin{pmatrix} \hat{\underline{X}}_S \\ \hat{\underline{Y}}_S \\ \hat{\underline{Z}}_S \end{pmatrix}
$$

Here the matrix elements are given by,

$$
\begin{aligned}
A_{11} &= -S(\theta)\cos\theta_S + (m_1 \sin\varepsilon - n_1 \cos\varepsilon)\sin\theta_S \quad , \\
A_{12} &= -l_1 \sin\lambda + m_1 \cos\lambda \cos\varepsilon + n_1 \cos\lambda \sin\varepsilon \quad , \\
A_{13} &= -S(\theta)\sin\theta_S - (m_1 \sin\varepsilon - n_1 \cos\varepsilon)\cos\theta_S \quad , \\
A_{21} &= -T(\theta)\cos\theta_S + (m_2 \sin\varepsilon - n_2 \cos\varepsilon)\sin\theta_S \quad , \\
A_{22} &= -l_2 \sin\lambda + m_2 \cos\lambda \cos\varepsilon + n_2 \cos\lambda \sin\varepsilon \quad , \\
A_{23} &= -T(\theta)\sin\theta_S - (m_2 \sin\varepsilon - n_2 \cos\varepsilon)\cos\theta_S \quad , \\
A_{31} &= -W\cos\theta_S + (m_3 \sin\varepsilon - n_3 \cos\varepsilon)\sin\theta_S \quad , \\
A_{32} &= -l_3 \sin\lambda + m_3 \cos\lambda \cos\varepsilon + n_3 \cos\lambda \sin\varepsilon \quad , \\
A_{33} &= -W\sin\theta_S - (m_3 \sin\varepsilon - n_3 \cos\varepsilon)\cos\theta_S \quad .
\end{aligned}
$$

It is noted that $S(\theta)$, $T(\theta)$ and W are the functions defined by equations (2.7)-(2.9), and that the component of force in the $\underline{Y}_S$ direction is zero for both incident and reflected radiation acting on the satellite.

It may be possible to retain the standard form of Gauss' equations, (2.1)-(2.6), and substitute expressions dependent on $S(\theta)$, $T(\theta)$ and W, to obtain equations that can be analytically integrated, without recourse to numerical methods, which was suspected by Aksnes.

Lucas showed that the force due to reflected radiation is zero for a spherical satellite, as should be expected, and confirms the expression for F used by Aksnes. This expression given by Aksnes employs the factor σ, which in practice is taken as slightly greater than unity, in order to estimate the effect of diffuse radiation from the satellite's surface. Lucas neglects to develop the components of this force, but suggests that this would be possible by treating diffuse reflection in the manner developed for specular reflection.

First, the expressions found for radiation incident on and reflected from a prolate spheroid are given, Lucas (1974) equations (51), (52), (53) and (61), from which

$$\underline{F}_I = - P_o \pi a_s^2 \sqrt{(1-e_s^2)} \sqrt{(1-e_s^2 \sin^2\theta_s)} \times (\cos \theta_s \hat{\underline{X}}_S + \sin \theta_s \hat{\underline{Z}}_S) \qquad (4.1)$$

and

$$\underline{F}_R = - P_o \pi a_s^2 R_s (P_x \cos \theta_s \hat{\underline{X}}_s + P_z \sin \theta_s \hat{\underline{Z}}_s) \qquad (4.2)$$

where e_s is the eccentricity, a_s the semi-major axis of the spheroidal satellite, R_s is the fraction of incident radiation reflected specularly and θ_s is defined in Figure 9. Now substituting

$$C_1 = \{\sqrt{(1-e_s^2)}\ \sqrt{(1 - e_s^2 \sin^2\theta_s)} + R_s p_x\} \quad (-P_o \pi a_s^2)\cos\theta_s$$

and

$$C_2 = \{\sqrt{(1-e_s^2)}\ \sqrt{(1 - e_s^2 \sin^2\theta_s)} + R_s p_z\} \quad (-p_o \pi a_s^2)\sin\theta_s$$

it follows that

$$\underline{F}_I + \underline{F}_R = (C_1 \hat{\underline{X}}_s + C_2 \hat{\underline{Z}}_s)$$

$$= \{C_1 (A_{11} \hat{\underline{S}} + A_{21} \hat{\underline{T}} + A_{31} \hat{\underline{W}})$$

$$+ C_2 (A_{13} \hat{\underline{S}} + A_{23} \hat{\underline{T}} + A_{33} \hat{\underline{W}})\}$$

Grouping components, substituting for the elements of the rotation matrix developed earlier, and rewriting the result in an ordered manner leads to

$$F_S = S^* \cos\theta + T^* \sin\theta \ , \qquad (4.3)$$

$$F_T = T^* \cos\theta - S^* \sin\theta \ , \qquad (4.4)$$

$$F_W = W^* \ , \qquad (4.5)$$

where

$$S^* = -S(C_1 \cos \theta_s + C_2 \sin \theta_s) + S'(C_1 \sin \theta_s - C_2 \cos \theta_s) \quad , \quad (4.6)$$

$$T^* = -T(C_1 \cos \theta_s + C_2 \sin \theta_s) + T'(C_1 \sin \theta_s - C_2 \cos \theta_s) \quad , \quad (4.7)$$

$$W^* = -W(C_1 \cos \theta_s + C_2 \sin \theta_s) + W'(C_1 \sin \theta_s - C_2 \cos \theta_s) \quad , \quad (4.8)$$

with

$$S' = (\sin \omega \cos \Omega \cos i + \cos \omega \sin \Omega) \sin \varepsilon - \sin \omega \sin i \cos \varepsilon \quad ,$$

$$T' = (\cos \omega \cos \Omega \cos i - \sin \omega \sin \Omega) \sin \varepsilon - \cos \omega \sin i \cos \varepsilon \quad ,$$

$$W' = -(\sin i \sin \varepsilon \cos \Omega + \cos i \cos \varepsilon) \quad .$$

S, T and W have been defined on page 9, and for uniformity and overall economisation of computer space, S' and T' are written in the form

$$\begin{Bmatrix} S' \\ T' \end{Bmatrix} = \sin \varepsilon \left[ci \begin{Bmatrix} \sin \\ \cos \end{Bmatrix} (\Omega+\omega) \pm si \begin{Bmatrix} \sin \\ \cos \end{Bmatrix} (\Omega-\omega) \right] - \sin i \cos \varepsilon \begin{Bmatrix} \sin \\ \cos \end{Bmatrix} \omega \quad .$$

For a spherical surface $e_s=0$, $C_1 = -P_0 A \cos \theta_s$ and $C_2 = -P_0 A \sin \theta_s$, therefore

$$S^* = P_0 AS \quad , \quad T^* = P_0 AT \quad \text{and} \quad W^* = P_0 AW \quad ,$$

which are the components expected and those used by Aksnes. It is noted that the factor $(a_\odot/r_\odot)^2$ has been excluded in this treatment; this is for brevity only and is to be included in practice.

When comparing these results with the components of force given by Aksnes, it is seen that the direction cosines are the same but as was noted earlier, PA, the magnitude of the force vector, differs from Aksnes' value by the factor σ, which "equals a constant, whose value lies between 0 and 2, depending on the reflection characteristics of the satellite's surface." This can be misleading, particularly when σ is written in the form $(2-\varepsilon)$ as previous authors have done. Here ε is the fraction of incident radiation absorbed by the satellite. When defined so, it is fair to assume for a balloon surface of high specular reflectivity that ε has a low value. Thus this would lead to a magnitude of force almost twice that of the incident radiation pressure. If an incorrect assumption was made for the satellite's sphericity then the actual magnitude of force F_I+F_R would be represented by $2F_I$ which is true only for a perfectly reflecting plate, and not for a sphere where the resultant force due to specularly reflected radiation is zero. Therefore the value σ should be taken as unity when neglecting the fraction of reflected radiation that is diffuse. This, as has been shown, was done by Lucas. Authors have assumed a spherical satellite and attempted to allow for a diffuse component by trial and error methods. It is then difficult to ascertain to what extent the choice of σ is an unwitting attempt to account for a contribution

to the magnitude of force from reflected radiation, as a result of deformation of the assumed sphere, together with the estimate for diffuse radiation. Aksnes took σ=1.105 for 1963-30D and Slowey (1974) took values of σ between 1.068 and 1.12 for this satellite.

Therefore, it seems expedient not to include such an approximation when considering a prolate spheroid as it is conceivable that some fraction of the effect of F_R will be incorrectly included twice. Before it is possible to discriminate between the differing effects of these forces it is necessary to have knowledge of the parameters defining the satellite's shape and reflective characteristics.

Diffuse Radiation From The Surface of a Sphere

The effect of diffuse radiation for the case of a sphere is considered first. A set of Cartesian coordinates is defined with Z directed towards the Sun and X,Y forming the right-hand set shown in Figure 10.

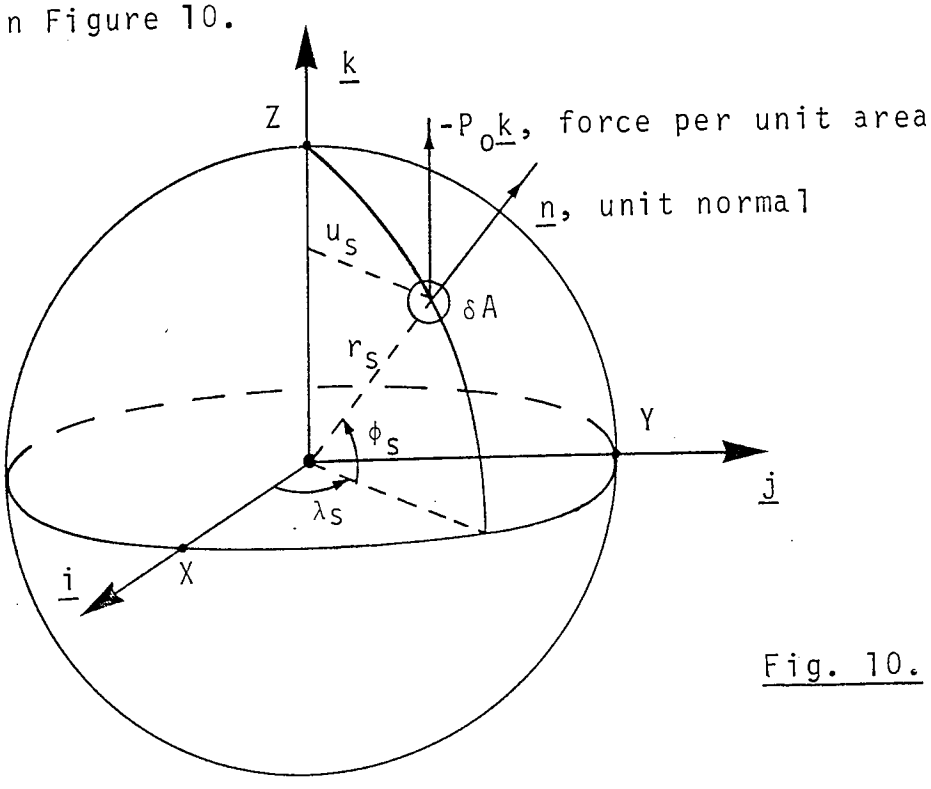

Fig. 10.

The fraction of incident radiation that is diffusely reflected is taken to be R_D and this radiation is assumed to follow Lambert's law. That is, it is assumed the amount of light from a point source, falling normally on unit area of a surface, per second, is inversely proportional to the square of the distance between the surface and the source. If the normal to the surface makes an angle θ with the direction of the rectilinear path along which light is taken to travel, then the illumination is proportional to cos θ.

The force on elemental area δA due to diffuse radiation is

$$\delta \underline{F}_D = -R_D P_o \sin \phi_s \, \delta A \, \underline{n} \quad ,$$

where

$$\underline{n} = (\cos \phi_s \cos \lambda_s, \cos \phi_s \sin \lambda_s, \sin \phi_s) \quad .$$

Integrating over the sunlit half of the sphere for each component results in,

$$\underline{F}_{DX} = -R_D P_o r_s^2 \, \underline{i} \int_0^{\pi/2} \int_0^{2\pi} \sin \phi_s \cos^2 \phi_s \cos \lambda_s \, d\lambda_s \, d\phi_s = \underline{0}$$

$$\underline{F}_{DY} = -R_D P_o r_s^2 \, \underline{j} \int_0^{\pi/2} \int_0^{2\pi} \sin \phi_s \cos^2 \phi_s \sin \lambda_s \, d\lambda_s \, d\phi_s = \underline{0}$$

$$\underline{F}_{DZ} = -R_D P_o r_s^2 \, \underline{k} \int_0^{\pi/2} \int_0^{2\pi} \sin^2 \phi_s \cos \phi_s \, d\lambda_s \, d\phi_s$$

and therefore

$$\underline{F}_D = -\frac{2}{3} R_D P_o \pi r_s^2 \underline{k} \quad .$$

It is noted that

$$\underline{F}_D = \frac{2}{3} R_D \times (\text{Force due to incident radiation on a sphere}) \quad .$$

Diffuse Radiation from the Surface of a Prolate Spheroid

For a prolate spheroid, the set of axes chosen are such that the OZ-axis is in the direction of the satellite's major axis ($2a_s$) with the satellite-Sun vector in the OXZ plane, making an angle θ_s with the OX axis. $\underline{r}_\odot$ is a unit vector in the direction of the Sun, and $\underline{n}$ the general unit vector normal to the surface.

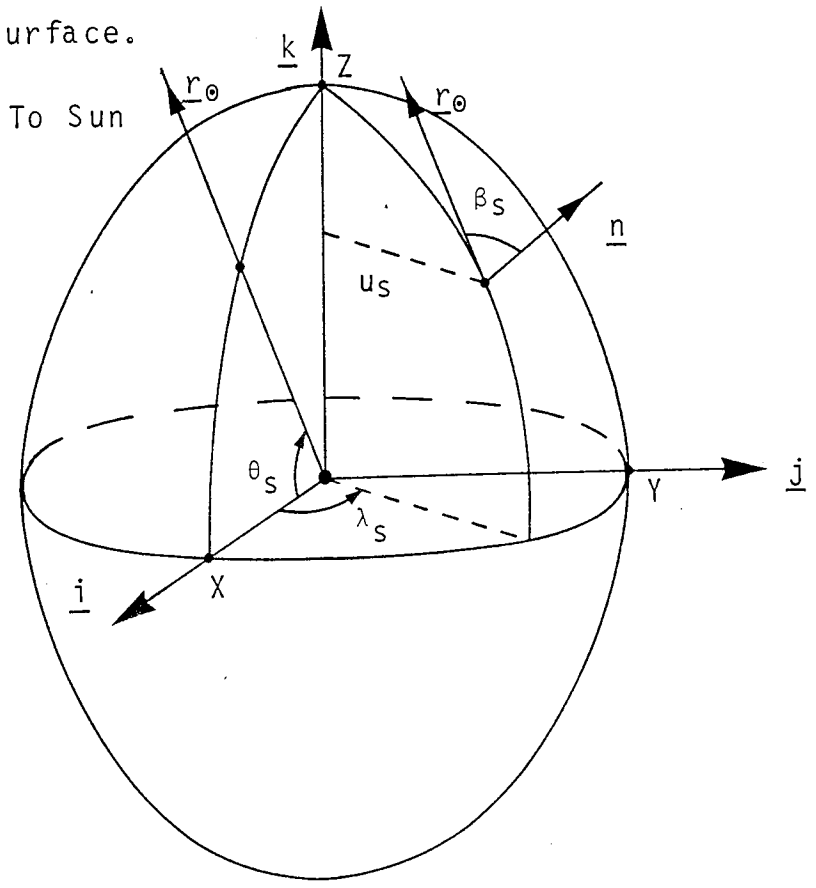

Fig. 11.

From Figure 11,

$$(X,Y,Z) = \{u_s \cos\lambda_s,\ u_s \sin\lambda_s,\ a_s\sqrt{(1 - u_s^2/b_s^2)}\} \qquad (4.9)$$

and

$$\underline{r}_{\odot} = \cos \theta_s \, \underline{i} + \sin \theta_s \, \underline{k} \quad . \qquad (4.10)$$

b_s being the semi-minor axis.

In general terms the surface area of revolution of the complete spheroid is given by (Courant, 1937).

$$A = \int_0^{2\pi} \int_0^{u_{max}} u_s \sqrt{\{1 + (\frac{dz}{du_s})^2\}} \, du_s \, d\lambda_s \quad ,$$

where

$$u_s \, du_s = -(b_s^2 / a_s^2) \, z \, dz$$

and

$$1 + (\frac{dz}{du_s})^2 = \frac{a_s^2 \, (a_s^2 - e_s^2 z^2)}{b_s^2 z^2} \quad ,$$

so that

$$A = -\sqrt{(1-e_s^2)} \iint \sqrt{(a_s^2 - e_s^2 z^2)} \, dz \, d\lambda_s \quad .$$

The limits of integration for the general sunlit area of the spheroid are given in two parts. The boundary of the sunlit area on the spheroid is defined by $\underline{r}_{\odot} \cdot \underline{n} = 0$.

Referring to Figure 12, it is seen that

$$A_1 = \sqrt{(1-e_s^2)} \int_{\eta}^{a_s} \int_{-\pi}^{\pi} \sqrt{(a_s^2 - e_s^2 z^2)} \, d\lambda_s \, dz \quad . \qquad (4.11)$$

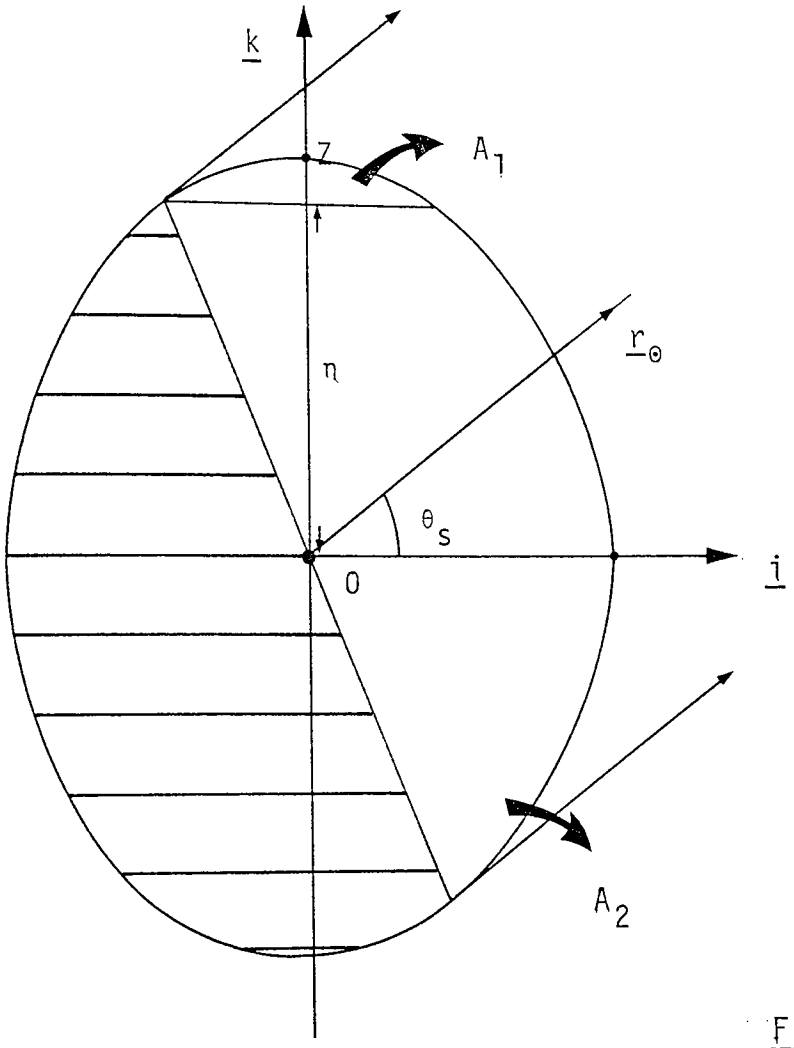

Fig. 12.

Projecting the vectors, from Figure 11, associated with the diffuse radiation forces onto a unit sphere, Figure 13, it is seen that,

$$\underline{n} = (\cos \alpha_s \cos \lambda_s, \cos \alpha_s \sin \lambda_s, \sin \alpha_s) \quad (4.12)$$

so that

$$\underline{r}_\Theta \cdot \underline{n} = \cos \alpha_s \cos \lambda_s \cos \theta_s + \sin \alpha_s \sin \theta_s \quad (4.13)$$

$$= \cos \beta_s \ .$$

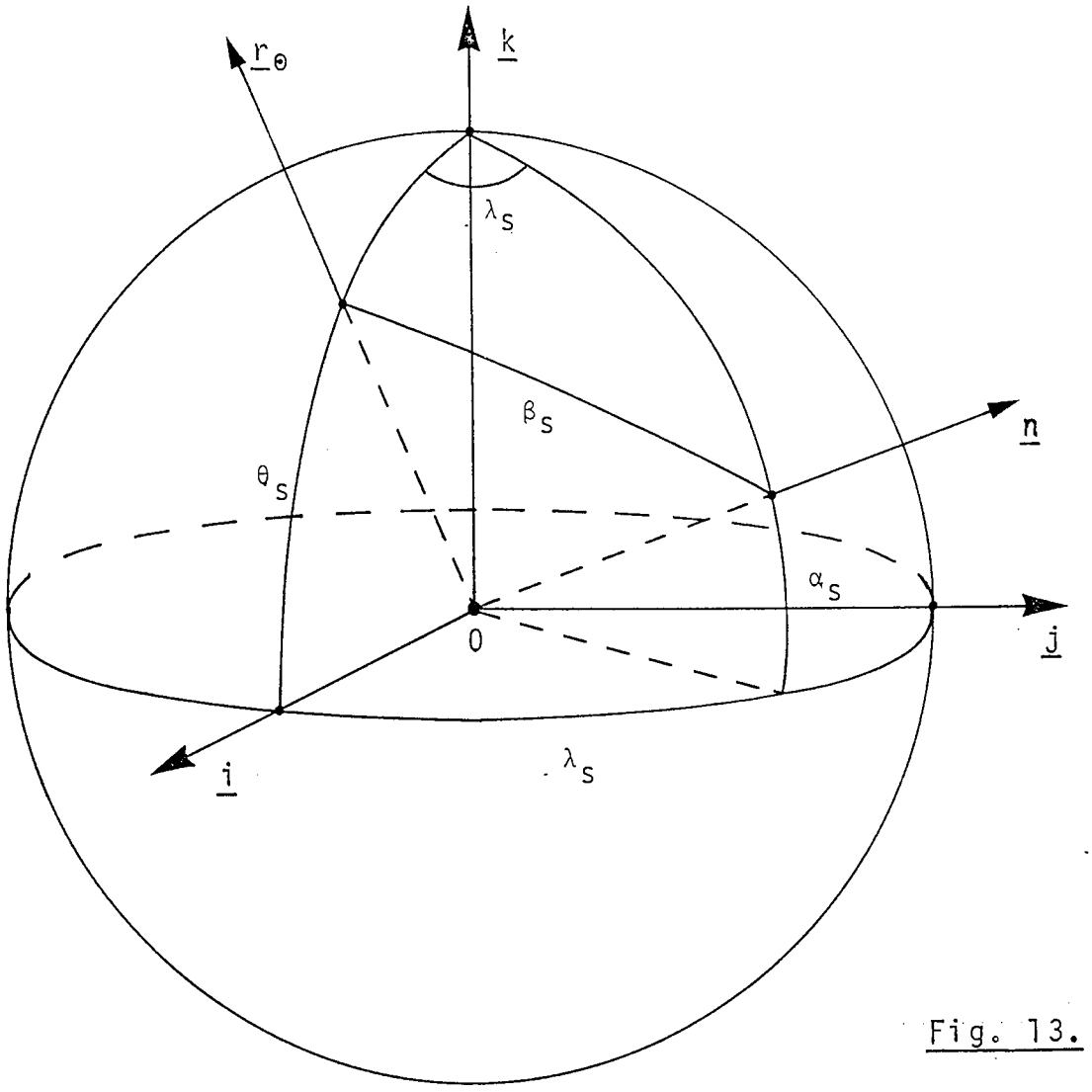

Fig. 13.

From equation (4.9),

$$\frac{dz}{du_s} = - \frac{a_s u_s}{b_s \sqrt{(b_s^2 - u_s^2)}} \quad ,$$

and therefore,

$$\tan \alpha_s = - \frac{du_s}{dz} = \frac{b_s z}{a_s \sqrt{(a_s^2 - z^2)}} \quad . \qquad (4.14)$$

On substituting for terms in α_s, into equation (4.13) and equating the result to zero,

$$\sqrt{(a_s^2 - z^2)} \cos \lambda_s \cos \theta_s + z\sqrt{(1-e_s^2)} \sin \theta_s = 0 \quad , \qquad (4.15)$$

so that with limits of integration for the area A_2 of Figure 12 given by $z=(-\eta,\eta)$ and $\lambda_s=(-\gamma_s,\gamma_s)$, where γ_s is a function of z given by equation (4.15) for $\lambda_s=\gamma_s$,

$$\cos \gamma_s = - \frac{z \sqrt{(1-e_s^2)} \tan \theta_s}{\sqrt{(a_s^2 - z^2)}} \quad . \tag{4.16}$$

In addition noting that $z=\eta$ when $\gamma_s=\pi$, equation (4.16) then gives

$$\eta = \frac{a_s \cos \theta_s}{\sqrt{(1 - e_s^2 \sin^2\theta_s)}}$$

so that

$$A_2 = \sqrt{(1-e_s^2)} \int_{-\eta}^{\eta} \int_{-\gamma_s}^{\gamma_s} \sqrt{(a_s^2 - e_s^2 z^2)} \, d\lambda_s \, dz \quad . \tag{4.17}$$

Combining equations (4.11) and (4.17), and using the same simplifying notation as Lucas,

$$A = A_1 + A_2$$

$$= \sqrt{(1-e_s^2)} \, S_1 \left[\sqrt{(a_s^2 - e_s^2 z^2)} \right] \quad .$$

Now

$$\delta \underline{F}_D = -R_D \, P_o \, (\underline{r}_\odot . \underline{n}) \delta A \underline{n} \quad ,$$

and from equation (4.14)

$$\underline{F}_D = -R_D \, P_o \, (1-e_s^2) \, S_1 \left[z\underline{n} \cos \beta_s \operatorname{cosec} \alpha_s \right] \quad ,$$

so that separating the components gives,

$$\underline{F}_{DX} = -R_D P_o (1-e_s^2) \underline{i} S_1\left[z \cot \alpha_s \cos \lambda_s \cos \beta_s \right] ,$$

$$\underline{F}_{DY} = -R_D P_o (1-e_s^2) \underline{j} S_1\left[z \sin \lambda_s \cot \alpha_s \cos \beta_s \right] ,$$

$$\underline{F}_{DZ} = -R_D P_o (1-e_s^2) \underline{k} S_1\left[z \cos \beta_s \right] .$$

The double integrals represented by S_1 may be evaluated using results derived by Lucas. They are now

$$\underline{F}_{DX} = -R_D P_o (1-e_s^2) \underline{i} \left[\left[\frac{\cos \theta_s}{2} S_1\left[z \operatorname{cosec} \alpha_s \cos^2 \alpha_s \right] + \sin \theta_s S_2\left[z \cos \alpha_s \sin \gamma_s \right] \right]\right] ,$$

$$\underline{F}_{DY} = \underline{0} ,$$

$$\underline{F}_{DZ} = -R_D P_o (1-e_s^2) \underline{k} \left[\left[2 \cos \theta_s S_2\left[z \cos \alpha_s \sin \gamma_s \right] + \sin \theta_s S_1\left[z \sin \alpha_s \right] \right]\right] ,$$

where

$$S_2\left[z \cos \alpha_s \sin \gamma_s \right] = \int_{-\eta}^{\eta} z \cos \alpha_s \sin \gamma_s \, dz .$$

It is now necessary to evaluate the three integrals that were not found by Lucas. The 's' suffix will be dropped during this evaluation.

In the notation of Lucas, the integrals are:

$$\text{I:}\quad S_2\left[z\cos\alpha_s\sin\gamma_s\right],$$

$$\text{II:}\quad S_1\left[z\cot\alpha_s\cos\alpha_s\right],$$

$$\text{III:}\quad S_1\left[z\sin\alpha_s\right].$$

I.

$$S_2\left[z\cos\alpha_s\sin\gamma_s\right] = \frac{\sqrt{(1-e^2\sin^2\theta)}}{\cos\theta}\int_{-\eta}^{\eta}\frac{z\sqrt{(\eta^2-z^2)}}{\sqrt{(a^2-e^2z^2)}}\,dz.$$

Since the integrand is an odd function of z, the integral is zero, and therefore

$$S_2\left[z\cos\alpha_s\sin\gamma_s\right] = 0.$$

II.

$$S_1\left[z\cot\alpha_s\cos\alpha_s\right] = \int_{\eta}^{a}\int_{-\pi}^{\pi} f(z)\,d\lambda\,dz + \int_{-\eta}^{\eta}\int_{-\gamma}^{\gamma} f(z)\,d\lambda\,dz\,.$$

Here, $f(z) = z \cot \alpha \cos \alpha$, and generally

$$S_1\Big[f(z) \Big] = 2\pi \int_{\eta}^{a} f(z)\, dz + 2 \int_{-\gamma}^{\gamma} \gamma\, f(z)\, dz \quad .$$

Let

$$F(z) = \int f(z)\, dz \quad ,$$

so that

$$S_1\Big[f(z) \Big] = 2\pi\Big[F(a) - F(\eta) \Big] + 2\Big[\gamma\, F(z)\Big]_{-\eta}^{\eta} - 2\int F(z)\, d\gamma \quad .$$

The integration limits are defined so that when $z = \eta$, $\gamma = \pi$ and for $z = -\eta$, $\gamma = 0$, therefore

$$S_1\Big[f(z) \Big] = 2\pi\, F(a) - 2 \int_{0}^{\pi} F(z)\, d\gamma \quad .$$

For this case,

$$F(z) = \int z \cot \alpha \cos \alpha\, dz = \frac{a}{b} \int \frac{(a^2 - z^2)}{\sqrt{(a^2 - e^2 z^2)}}\, dz$$

$$= \frac{a}{b}\left[\frac{a^2}{e}\left(1 - \frac{1}{2e^2}\right) \sin^{-1}\left(\frac{ez}{a}\right) + \frac{z}{2e^2} \sqrt{(a^2 - e^2 z^2)} \right]$$

and

$$F(a) = \frac{a}{b}\left[\frac{a^2}{e}\left(1 - \frac{1}{2e^2}\right) \sin^{-1}(e) + \frac{a^2}{2e^2} \sqrt{(1 - e^2)} \right]$$

It is now required to evaluate

$$\int_0^{\pi} F(z)\, d\gamma = \frac{a^3}{be}\left(1 - \frac{1}{2e^2}\right) \int_0^{\pi} \sin^{-1}\left(\frac{ez}{a}\right) d\gamma$$

$$+\frac{a}{2be^2} \int_0^{\pi} z\sqrt{(a^2 - e^2z^2)}\, d\gamma \quad .$$

Suppose that $f(z)$ is any odd function of z and that $z = g(\gamma)$ where $g(\pi-\gamma) = -g(\gamma)$.

If $f\{g(\gamma)\} = G(\gamma)$ say, then

$$\begin{aligned} G(\pi-\gamma) &= f\{g(\pi-\gamma)\} \\ &= f\{-g(\gamma)\} \\ &= -f\{g(\gamma)\} \\ &= -G(\gamma), \end{aligned}$$

and hence

$$\int_0^{\pi} f(z)\, d\gamma = \int_0^{\pi} G(\gamma)\, d\gamma = 0.$$

Now $\sin^{-1}\left(\frac{ez}{a}\right)$ and $z\sqrt{(a^2 - e^2z^2)}$ are both odd functions of z, and

$$z = g(\gamma) = \frac{a \cos \gamma}{\sqrt{\{(1-e^2)\tan^2\theta + \cos^2\gamma\}}} \quad ,$$

from equation (4.16).

Thus $g(\gamma)$ has the property stated and it follows that

$$\int_0^{\pi} \sin^{-1}\left(\frac{ez}{a}\right)\, d\gamma = 0$$

and

$$\int_0^{\pi} z\sqrt{(a^2 - e^2z^2)}\, d\gamma = 0.$$

Hence

$$S_1\left[z \cot \alpha_s \cos \alpha_s\right] = \frac{2\pi a}{b}\left[\frac{a^2}{e}\left(1 - \frac{1}{2e^2}\right)\sin^{-1}(e) + \frac{a^2}{2e^2}\sqrt{(1-e^2)}\right]$$

III.

$$S_1\left[z \sin \alpha_s\right] = \int_{\eta}^{a}\int_{-\pi}^{\pi} z \sin \alpha \, d\lambda \, dz + \int_{-\eta}^{\eta}\int_{-\gamma}^{\gamma} z \sin \alpha \, d\lambda \, dz$$

$$= 2\pi F(a) - 2\int_0^{\pi} F(z)\, d\gamma$$

where

$$F(z) = \int \frac{z^2\sqrt{(1-e^2)}}{\sqrt{(a^2-e^2z^2)}}\, dz$$

$$= \frac{\sqrt{(1-e^2)}}{e^2}\left[\frac{a^2}{2e}\sin^{-1}\left(\frac{ez}{a}\right) - \frac{z}{2}\sqrt{(a^2-e^2z^2)}\right]$$

and

$$F(a) = \frac{\sqrt{(1-e^2)}}{e^2}\left[\frac{a^2}{2e}\sin^{-1}(e) - \frac{a}{2}\sqrt{(1-e^2)}\right] \quad .$$

The integral of F(z) is

$$\int_0^{\pi} F(z)\, d\gamma = \frac{a^2\sqrt{(1-e^2)}}{2e^3}\int_0^{\pi}\sin^{-1}\left(\frac{ez}{a}\right) d\gamma$$

$$-\frac{\sqrt{(1-e^2)}}{2e^2}\int_0^{\pi} z\sqrt{(a^2 - e^2z^2)}\, d\gamma$$

which is zero, as before, and therefore

$$S_1\left[z \sin \alpha_s\right] = \frac{2\pi\sqrt{(1-e^2)}}{e^2}\left[\frac{a^2}{2e}\sin^{-1}(e) - \frac{a^2}{2}\sqrt{(1-e^2)}\right]$$

The two components for diffuse radiation are now given, viz.,

$$\underline{F}_{DX} = -\frac{R_D P_0 a_s^2}{2}\frac{\sqrt{(1-e_s^2)}}{e_s^3}\cos\theta_s\left[\pi(2e_s^2 - 1)\sin^{-1}(e_s) + \pi e_s\sqrt{(1-e_s^2)}\right]\underline{i} \qquad (4.18)$$

$$\underline{F}_{DZ} = -\frac{R_D P_0 a_s^2\sqrt{(1-e_s^2)}}{e_s^3}\sin\theta_s\left[\pi\sin^{-1}(e_s) - \pi e_s\sqrt{(1-e_s^2)}\right]\underline{k} \qquad (4.19)$$

The components are now expressed in terms of the vectors $\hat{\underline{S}}$, $\hat{\underline{T}}$ and $\hat{\underline{W}}$ for substitution into the planetary equations (2.1)-(2.6),

$$\underline{F}_D = \underline{F}_{DX} + \underline{F}_{DZ} = F_{DX}\,\underline{i} + F_{DZ}\,\underline{k}$$

$$= F_{DX}(A_{11}\hat{\underline{S}} + A_{21}\hat{\underline{T}} + A_{31}\hat{\underline{W}}) + F_{DZ}(A_{13}\hat{\underline{S}} + A_{23}\hat{\underline{T}} + A_{33}\hat{\underline{W}})$$

$$= (A_{11}F_{DX} + A_{13}F_{DZ})\hat{\underline{S}} + (A_{21}F_{DX} + A_{23}F_{DZ})\hat{\underline{T}}$$

$$+(A_{31}F_{DX} + A_{33}F_{DZ})\hat{\underline{W}} \quad .$$

These three components can be expressed in terms of S^* , T^* and W^* by replacing C_1 and C_2 by F_{DX} and F_{DZ} , from equations (4.18) and (4.19), into equations (4.6)-(4.8). Here,

$$F_{DX} = -\frac{R_D P_o\, \pi a_s^2 \cos\theta_s}{2} \frac{\sqrt{(1-e_s^2)}}{e_s^3}\Big[(2e_s^2 - 1)\sin^{-1}(e_s) + e_s\sqrt{(1-e_s^2)}\Big] \quad , \qquad (4.20)$$

and

$$F_{DZ} = -R_D P_o\, \pi a_s^2 \sin\theta_s \frac{(1-e_s^2)^{\frac{3}{2}}}{e_s^3}\Big[\sin^{-1}(e_s) - e_s\sqrt{(1-e_s^2)}\Big] \quad . \qquad (4.21)$$

The presence of e_s^{-3} in equations (4.20) and (4.21) suggests that the components could tend to infinity as the eccentricity approaches zero. F_{DX} and F_{DZ} can be developed as a power series in terms of e_s, noting that

$$\sqrt{(1-e_s^2)} = 1 - \frac{e_s^2}{2} - \frac{e_s^4}{8} - \frac{e_s^6}{16} - \frac{5e_s^8}{128} - \cdots ,$$

$$(1-e_s^2)^{\frac{3}{2}} = 1 - \frac{3e_s^2}{2} + \frac{3e_s^4}{8} + \frac{e_s^6}{16} + \frac{3e_s^8}{128} + \cdots ,$$

and

$$\sin^{-1}(e_s) = e_s + \frac{e_s^3}{6} + \frac{3e_s^5}{40} + \frac{5e_s^7}{112} + \frac{35e_s^9}{1152} + \cdots .$$

Substituting these series into equations (4.20) and (4.21), and performing the multiplications that occur, leads to

$$\underline{F}_D = - R_D P_o \pi a_s^2 (q_X \cos\theta_s, 0, q_Z \sin\theta_s) ,$$

where

$$q_X = \frac{2}{3} - \frac{4e_s^2}{15} - \frac{2e_s^4}{21} - \frac{16e_s^6}{315} - \cdots , \qquad (4.22)$$

and

$$q_Z = \frac{2}{3} - \frac{4e_s^2}{5} + \frac{2e_s^4}{35} + \frac{8e_s^6}{315} + \cdots . \qquad (4.23)$$

Therefore when $e_s = 0$, from equations (4.20)-(4.23)

$$\underline{F}_D = - \frac{2}{3} R_D P_o \pi a_s^2 (\cos\theta_s, 0, \sin\theta_s)$$

which is the result expected for a diffusely radiating sphere.

The effects of incident, specularly reflected and diffusely reflected radiation on the motion of a balloon satellite, can now be evaluated separately or together. This can be achieved without making any alterations to the integrated form of the planetary equations derived by Aksnes.

In summary the result for the combined effects of the different radiation forces acting on the satellite are now given. Let this total effect be expressed by,

$$\underline{F} = C_{T1}\,\hat{\underline{X}}_s + C_{T2}\,\hat{\underline{Z}}_s$$

where

$$C_{T1} = -P_o\,\pi a_s^2 \cos\theta_s \left[\sqrt{(1-e_s^2)}\,\sqrt{(1-e_s^2\sin^2\theta_s)} + R_S p_X + R_D q_X\right]$$

and

$$C_{T2} = -P_o\,\pi a_s^2 \sin\theta_s \left[\sqrt{(1-e_s^2)}\,\sqrt{(1-e_s^2\sin^2\theta_s)} + R_S p_Z + R_D q_Z\right] .$$

C_{T1} and C_{T2} are expressed in series form as,

$$C_{T1} = -P_o\,\pi a_s^2 \cos\theta_s \left[\left(1 + \frac{2R_D}{3}\right) - e_s^2\left\{\left(\frac{1}{2} - \frac{R_S}{6} + \frac{4R_D}{15}\right) + \frac{1}{6}(3-R_S)\sin^2\theta_s\right\}\right.$$

$$\left. - e_s^4\left\{\left(\frac{1}{8} + \frac{R_S}{48} + \frac{2R_D}{21}\right) - \frac{1}{24}(6-5R_S)\sin^2\theta_s + \frac{1}{16}(2-R_S)\sin^4\theta_s\right\}\right]$$

$$- e_s^6 \left\{\left(\frac{1}{16} + \frac{R_S}{48} + \frac{16R_D}{315}\right) - \frac{1}{48}(3-R_S)\sin^2\theta_s \right.$$

$$\left. - \frac{1}{16}(1-R_S)\sin^4\theta_s + \frac{1}{80}(5-3R_S)\sin^6\theta_s\right\} \Bigg] \quad ,$$

and

$$C_{T2} = - P_o \pi a_s^2 \sin\theta_s \left[\left(1 + \frac{2R_D}{3}\right) - e_s^2\left\{\left(\frac{1}{2} + \frac{R_S}{2} + \frac{4R_D}{5}\right) \right.\right.$$

$$\left. + \frac{1}{6}(3-R_S)\sin^2\theta_s\right\}$$

$$- e_s^4\left\{\left(\frac{1}{8} - \frac{R_S}{16} - \frac{2R_D}{35}\right) - \frac{1}{24}(6+R_S)\sin^2\theta_s \right.$$

$$\left. + \frac{1}{16}(2-R_S)\sin^4\theta_s\right\}$$

$$- e_s^6\left\{\left(\frac{1}{16} - \frac{R_S}{16} - \frac{8R_D}{315}\right) - \frac{1}{48}(3-R_S)\sin^2\theta_s \right.$$

$$\left.\left. - \frac{1}{80}(5-R_S)\sin^4\theta_s + \frac{1}{80}(5-3R_S)\sin^6\theta_s\right\} \right] \quad .$$

C_{T1} and C_{T2} may now be substituted into equations (4.6)-(4.8) .

EARTH REFLECTED SOLAR RADIATION PRESSURE

The amount of solar radiation reflected from the Earth that affects an Earth satellite is investigated.

The albedo, a_b, of a surface is defined as,

$$a_b = \frac{\text{radiant energy reflected}}{\text{radiant energy received}} .$$

The radiance of the Sun is defined as the flux radiated by unit surface area of the source in all directions. If luminance is the same in all directions then it can be said that the source radiates according to Lambert's Law. The luminance of a source, in the direction considered, is its intensity per unit area of apparent surface.

The solar energy flux, I_o, at one A.U. is taken as a constant value. Such disturbances as sunspots, solar flares, whilst causing large variations in flux in such regions of the spectrum as the cosmic, gamma, X-ray and radio waves, have negligible effect on the total flux.

Solar flux varies inversely with the square of the distance from the Sun, and therefore the flux incident on a planet will change as its orbital position changes. The solar constant has been measured as $I_o = 1396 \pm 3.4\%$ Joules per sec. per sq. m., the area here refers to the projected area. The albedo flux is generally taken as varying with the cosine of the angle between the direction of the normal to the surface

and the line joining the centres of the Sun and the planet.

If c is the velocity of light then I_0/c is the force of solar radiation on unit area at a distance $a_\odot$ from the Sun, $a_\odot$ is the mean distance of the Earth from the Sun, so that

$$I = \frac{I_0}{c} (a_\odot/r_\odot)^2$$

is the force per unit area at a distance $r_\odot$ from the Sun. Albedo flux is also assumed to be diffuse, that is each ray of solar radiation is reflected and backscattered in all directions. From observations for differing atmospheric conditions and latitudes it is found that the mean albedo is approximately 0.35, but this can vary by upto 50% for extreme conditions of clear and overcast skies, (Slowey, 1974). Prior (1970) determined the approximate effects of albedo by considering only the radial component of force when the cap of the Earth's surface that is visible to the satellite, is completely sunlit. Slowey (1974) allowed the albedo to vary for four seasonal models.

The radiation force acting on the surface of the Earth is,

$$F_a = I \times (\text{apparent surface area}) \quad .$$

A set of Cartesian axes, dependent on the instantaneous position of the Sun and satellite, is shown in Figure 15, where

$\hat{\underline{r}}$ = unit position vector of satellite from the Earth's centre,

$\hat{\underline{r}}_\odot$ = unit position vector of the Sun from the Earth's centre.

(R_E, ϕ, ψ) are the polar coordinates of a general elemental area of terrestrial surface, restricted to lie within the bounds of the Earth's surface that is visible from the satellite. This region will be referred to as the visible cap. The vector, $\underline{d}$, defines the position of the satellite with respect to the elemental area, and $\underline{n}$ is the unit normal to this element.

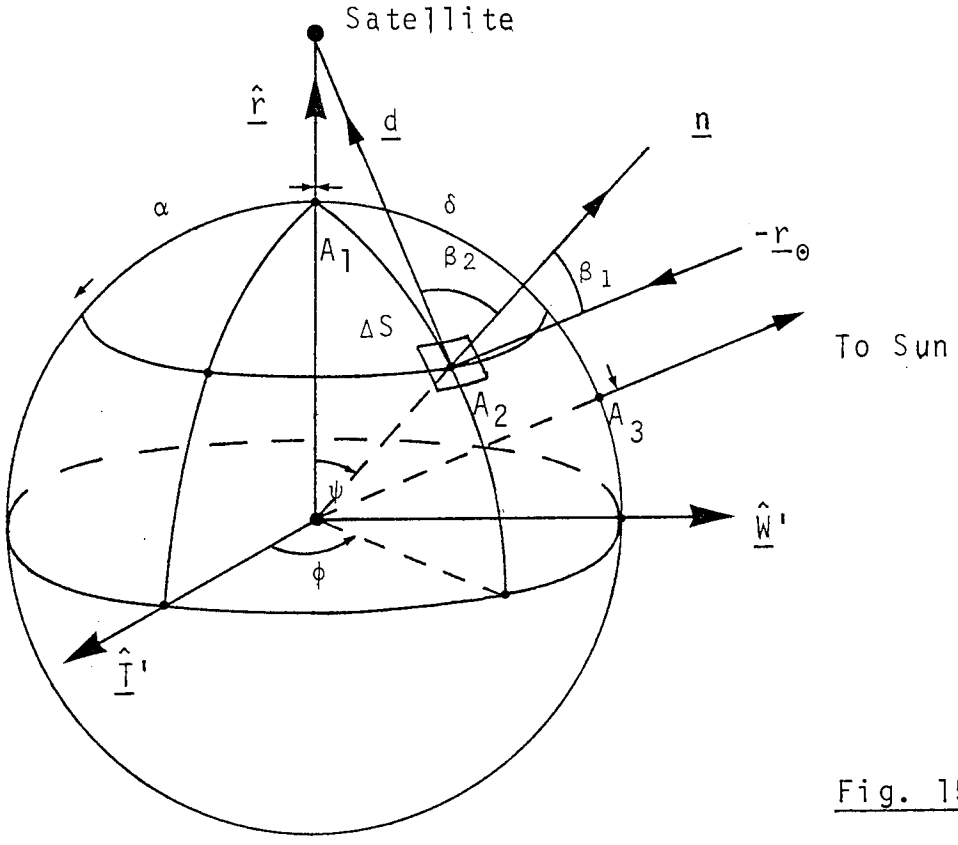

Fig. 15.

The model assumes: (i) that the Earth can be replaced by a sphere of radius equal to the Earth's mean radius, R_E = 6378.140 km; (ii) that the mean solar constant is equal to 1.395×10^6 erg cm^{-2} sec; (iii) that the mean albedo of the Earth is equal to 0.35; and (iv) that the satellite retains

a spherical shape.

The visible cap defines a solid angle that is dependent on the angle α, shown in Figure 16, such that

$$\alpha = \cos^{-1}(R_E/r) \quad . \tag{5.1}$$

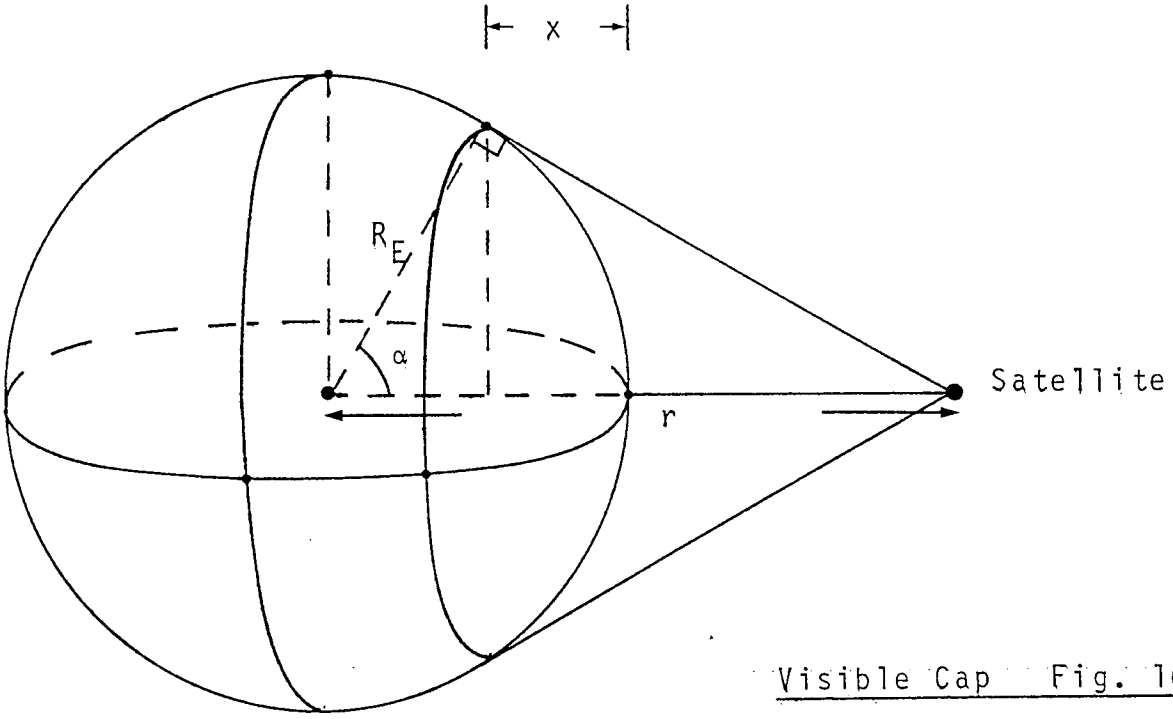

Visible Cap Fig. 16.

The area of the visible cap is $2\pi R_E x = 2\pi R_E^2 (1-\cos \alpha)$. It should be noted that the amount of the visible cap that will be sunlit is dependent on the value of $\hat{\underline{r}}.\hat{\underline{r}}_\odot$, and is discussed later.

Now applying the sine and cosine laws to Figure 15 results in

$$d^2 = r^2 + R_E^2 - 2rR_E \cos \psi \quad ,$$

$$\underline{d} = \underline{r} - \underline{n}R_E$$

$$= -R_E \sin\psi \cos\phi\, \hat{\underline{T}}' - R_E \sin\psi \sin\phi\, \hat{\underline{W}}' + (r - R_E \cos\psi)\hat{\underline{r}} \quad ,$$

and

$$\sin\beta_2 = \frac{r \sin\psi}{d} \quad .$$

Therefore

$$\cos\beta_2 = (r\cos\psi - R_E)/d \quad ,$$

and from the spherical triangle $A_1A_2A_3$

$$\cos\beta_1 = \cos\psi\cos\delta + \sin\psi\sin\delta\cos(\pi/2 - \phi) \quad .$$

In terms of polar coordinates the elemental area may be written as,

$$\Delta S = R_E^2 \sin\psi \quad \delta\phi\, \delta\psi \quad .$$

If κ is defined as a factor dependent on the reflective characteristics of the satellite and the satellite's surface area, then the force acting on the satellite due to reflected radiation is,

$$\underline{F}_a = a_b \kappa I \iint_{\substack{\text{sunlit area} \\ \text{of visible cap}}} \frac{\cos\beta_1 \cos\beta_2\, \hat{\underline{d}}}{\pi d^2}\, \Delta S$$

$$= \frac{a_b \kappa I R_E^2}{\pi} \int_{\psi_1}^{\psi_2} \int_{\phi_1}^{\phi_2} \frac{(r \cos\psi - R_E)(\cos\psi \cos\delta + \sin\psi \sin\delta \sin\phi)}{(r^2 + R_E^2 - 2rR_E \cos\psi)^{3/2}}$$

$$\times \hat{\underline{d}} \sin\psi \; d\phi \; d\psi \qquad (5.2)$$

where ψ_1, ψ_2, ϕ_1 and ϕ_2 are dependent on the orientation of the visible cap with respect to the Sun. These limits of integration are now developed for four separate situations reliant on the relative magnitudes of δ and α. It is assumed here that the threshold of light and dark can be defined by a distinct great circle drawn on the Earth's surface.

(a) $(\delta - \alpha) \geq \pi/2$: The complete visible cap is in darkness, therefore $\underline{F}_a = \underline{0}$.

(b) $(\delta + \alpha) \leq \pi/2$ and $\delta \geq 0$; The visible cap is totally sunlit so that the limits of integration for equation (5.2) are

$\psi = (0, \alpha)$ and $\phi = (0, 2\pi)$.

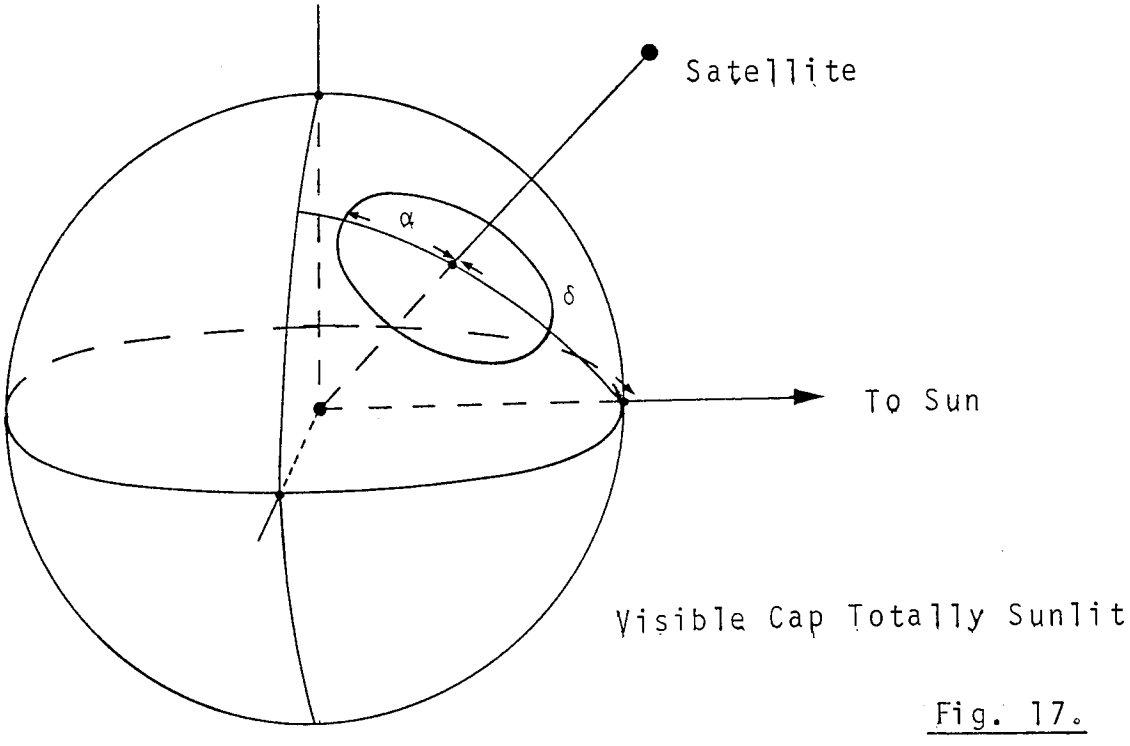

Visible Cap Totally Sunlit

Fig. 17.

(c) $(\delta-\alpha) \leq \pi/2$ and $\delta > \pi/2$: Here the visible cap is partially sunlit and the centre of the circular boundary is within the Earth's dark hemisphere. To evaluate the limits here it is necessary to consider the three spherical triangles $B_1B_2B_3$, $B_1B_3B_5$ and $B_3B_4B_5$ shown in Figure 18.

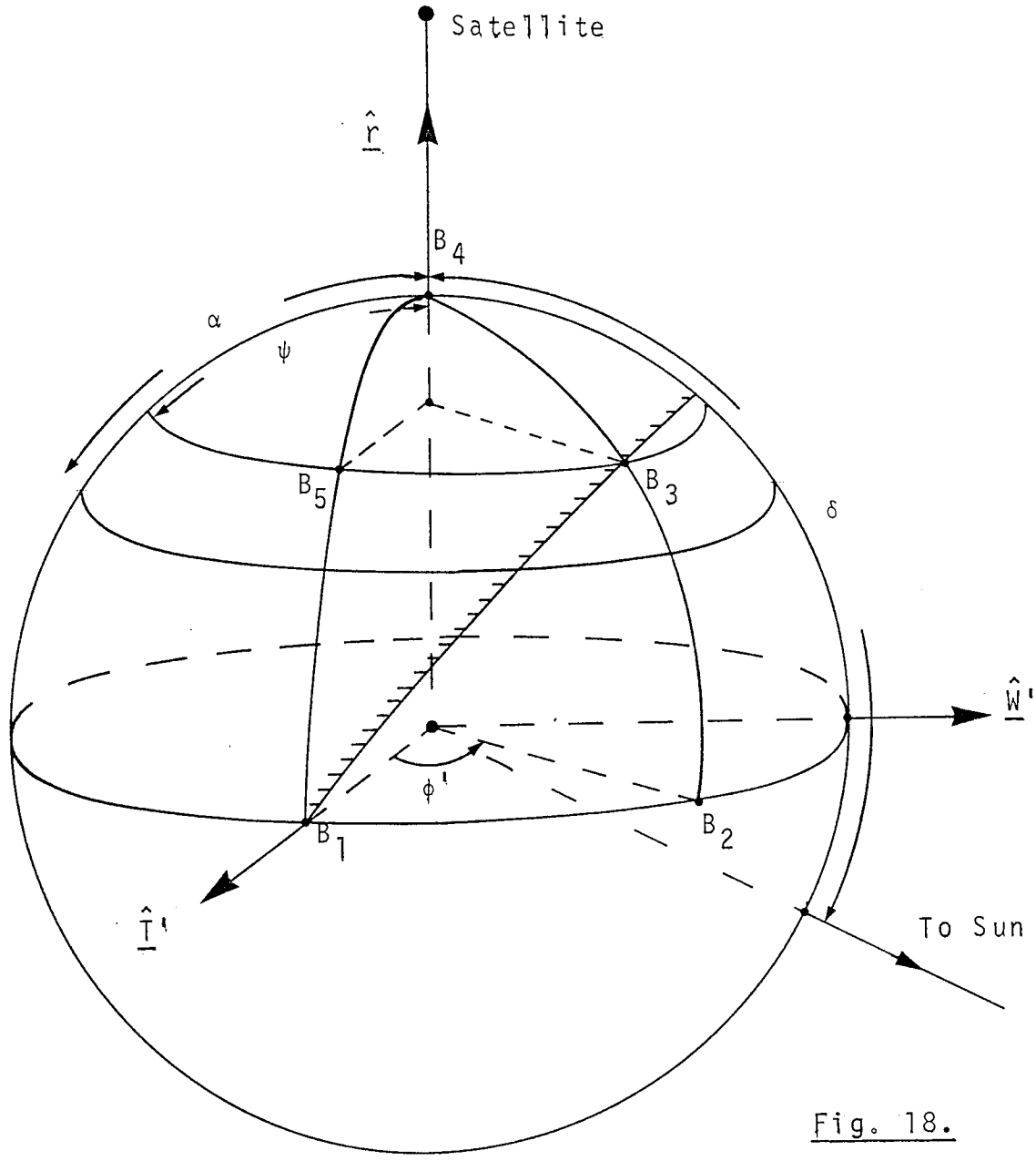

Fig. 18.

From Figure 18 the limits are

$$\psi = (\delta-\pi/2, \alpha) \quad \text{and} \quad \phi = (\phi', \pi-\phi')$$

where $\phi' = f(\psi)$. Considering the spherical triangle $B_1B_2B_3$,

$$\sin(\overline{B_1B_3}) = \frac{\cos\ \psi}{\sin\ \delta} \quad , \tag{5.3}$$

the spherical triangle $B_1B_3B_5$,

$$\sin(\overline{B_1B_3}) = \frac{\sin(\phi'\ \sin\ \psi)}{\sin(\delta-\pi/2)} \tag{5.4}$$

and using $B_3B_4B_5$,

$$\frac{\sin(\phi'\ \sin\ \psi)}{\sin\ \phi'} = \frac{\sin\ \psi}{1} \quad . \tag{5.5}$$

Now from equations (5.3) and (5.4)

$$\sin(\phi'\ \sin\ \psi) = -\frac{\cos\ \psi\ \cos\ \delta}{\sin\ \delta} \quad ,$$

therefore, from equation (5.5) .

$$\sin\ \phi' = -\ \cot\ \psi\ \cot\ \delta$$

so that the limits for equation (5.2) are,

$$\psi = (\delta-\pi/2, \alpha)$$

and

$$\phi = \left[\sin^{-1}(-\cot\ \psi\ \cot\ \delta),\ \pi-\ \sin^{-1}(-\cot\ \psi\ \cot\ \delta)\right]$$

$$= \left[-\ \sin^{-1}(\cot\ \psi\ \cot\ \delta),\ \pi+\sin^{-1}(\cot\ \psi\ \cot\ \delta)\ \right] \quad .$$

(d) $(\delta+\alpha) > \pi/2$ and $\delta \leq \pi/2$; The visible cap is partially sunlit and the centre of the boundary is in the sunlit hemisphere of the Earth.

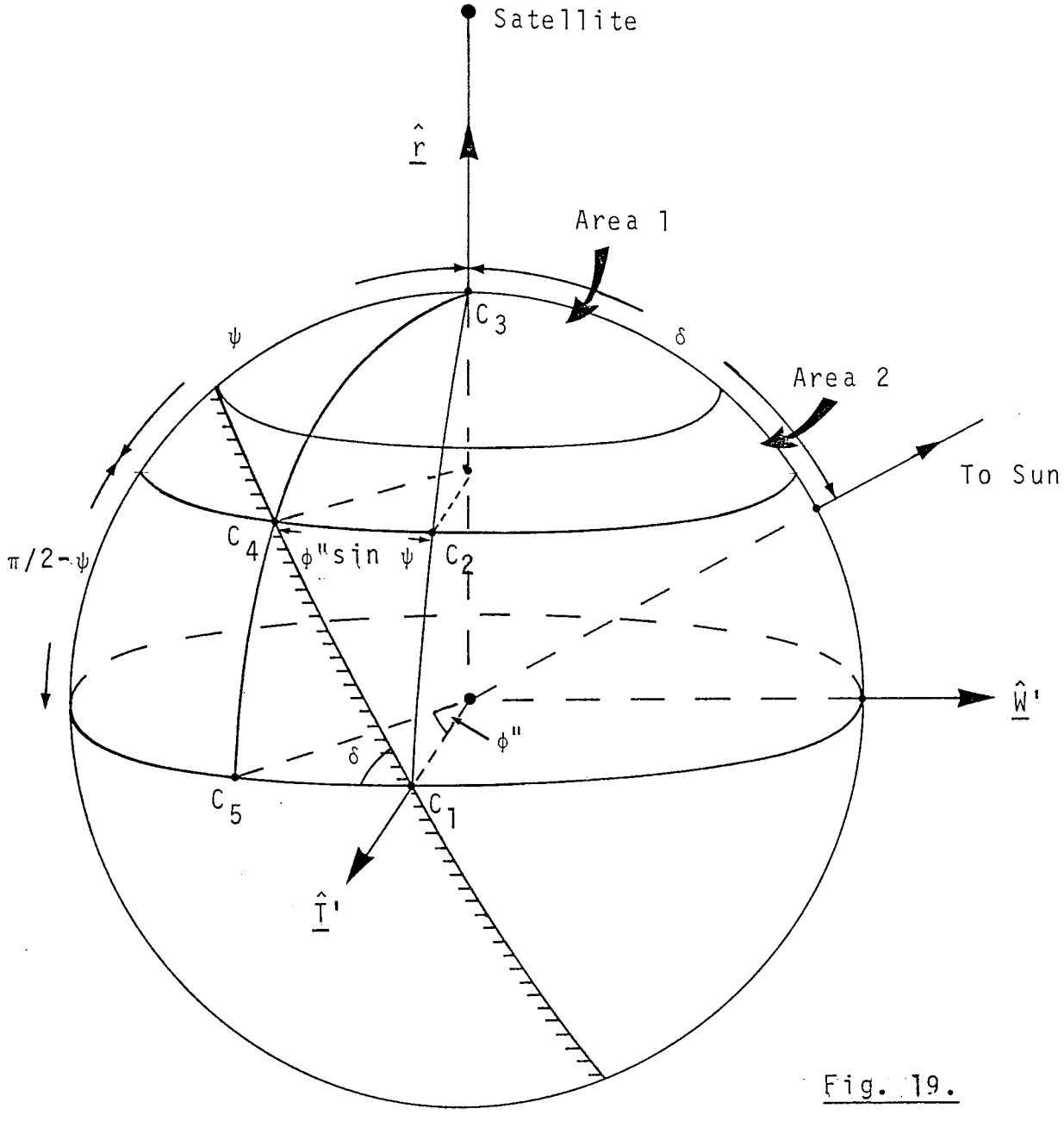

Fig. 19.

The sunlit area, as shown in Figure 19, is divided into two areas. The limits corresponding to Area 1 are

$$\psi = (0, \pi/2-\delta) \quad \text{and} \quad \phi = (0, 2\pi) \quad ,$$

and for Area 2,

$$\psi = (\pi/2 - \delta, \alpha) \quad \text{and} \quad \phi = (-\phi'', \pi + \phi'') \quad .$$

From the spherical triangle $C_1C_4C_5$ in Figure 19,

$$\sin \overline{C_1C_4} = \frac{\cos \psi}{\sin \delta}$$

and the spherical triangle $C_1C_2C_4$ gives,

$$\sin \overline{C_1C_4} = \frac{\sin(\phi'' \sin \psi)}{\sin(\pi/2-\delta)} \quad .$$

Now using the triangle $C_2C_3C_4$ gives,

$$\sin(\phi'' \sin \psi) = \sin \phi'' \sin \psi$$

so that the limits corresponding to Area 1 are,

$$\psi = (0, \pi/2-\delta) \quad \text{and} \quad \phi = (0,2\pi) \quad ,$$

and for Area 2,

$$\psi = (\pi/2-\delta, \alpha)$$

and

$$\phi = \left[-\sin^{-1}(\cot \psi \cot \delta), \pi+\sin^{-1}(\cot \psi \cot \delta)\right] \quad .$$

Each set of limits is applied to the equation (5.2) after $\underline{F}_a$ has been separated into the three components defined by $\hat{\underline{T}}'$, $\hat{\underline{W}}'$ and $\hat{\underline{r}}$ from Figure 15. These components are now given:

$$F_1 = - \frac{a_b \kappa I R_E^3}{\pi} \int_\psi \int_\phi \frac{(\cos\psi \cos\delta + \sin\psi \sin\delta \sin\phi)\sin^2\psi \cos\phi}{(r^2 + R_E^2 - 2rR_E \cos\psi)^2}$$

$$\times (r \cos\psi - R_E)\, d\phi\, d\psi$$

$$F_2 = - \frac{a_b \kappa I R_E^3}{\pi} \int_\psi \int_\phi \frac{(\cos\psi \cos\delta + \sin\psi \sin\delta \sin\phi)\sin^2\psi \sin\phi}{(r^2 + R_E^2 - 2rR_E \cos\psi)^2}$$

$$\times (r \cos\psi - R_E)\, d\phi\, d\psi$$

$$F_3 = \frac{a_b \kappa I R_E^2}{\pi} \int_\psi \int_\phi \frac{(\cos\psi \cos\delta + \sin\psi \sin\delta \sin\phi)\sin\psi}{(r^2 + R_E^2 - 2rR_E \cos\psi)^2}$$

$$\times (r \cos\psi - R_E)(r - R_E \cos\psi)\, d\phi\, d\psi \quad .$$

The terms $\cos\delta$ and r can be expressed in terms of the orbital elements of the satellite and the standard elements defining the Sun's position. The above integrals can be evaluated, noting that δ and r vary as the satellite orbits, and the results of the double integrals will give the components of force, F_a, for instantaneous values of δ and r. For the case (b), for a totally sunlit visible cap, the components are,

$$F_1^T = 0 \quad , \tag{5.6}$$

$$F_2^T = - a_b \kappa I R_E^3 \int_0^\alpha \frac{(r \cos\psi - R_E)\sin^3\psi \sin\delta}{(r^2 + R_E^2 - 2rR_E \cos\psi)^2}\, d\psi \quad , \tag{5.7}$$

and

$$F_3^T = a_b \kappa I R_E^2 \int_0^{\alpha} \frac{(r \cos\psi - R_E)\sin 2\psi \cos\delta}{(r^2 + R_E^2 - 2rR_E \cos\psi)^2}$$

$$\times (r - R_E \cos\psi)\, d\psi \quad . \qquad (5.8)$$

For the limits defined by (c), the components are,

$$F_1^{Pc} = 0 \quad ,$$

$$F_2^{Pc} = -\frac{a_b \kappa I R_E^3}{\pi} \int_{\delta - \frac{\pi}{2}}^{\alpha} \frac{(r \cos\psi - R_E)}{(r^2 + R_E^2 - 2rR_E \cos\psi)^2}$$

$$\times \Big[2 \cos\psi \sin^2\psi \cos\delta \sqrt{(1 - \cot^2\psi \cot^2\delta)}$$

$$+ \sin^3\psi \sin\delta \{\cos^{-1}(-\cot\psi \cot\delta)$$

$$- (\cot\psi \cot\delta) \sqrt{(1 - \cot^2\psi \cot^2\delta)}\}\Big]\, d\psi \quad , \qquad (5.10)$$

$$F_3^{Pc} = \frac{a_b \kappa I R_E^2}{\pi} \int_{\delta - \frac{\pi}{2}}^{\alpha} \frac{(r \cos\psi - R_E)(r - R_E \cos\psi)}{(r^2 + R_E^2 - 2rR_E \cos\psi)^2}$$

$$\times \Big[\sin 2\psi \cos\delta \cos^{-1}(-\cot\psi \cot\delta)$$

$$+ 2 \sin^2\psi \sin\delta \sqrt{(1 - \cot^2\psi \cot^2\delta)}\Big]\, d\psi \quad . \qquad (5.11)$$

Finally for the limits defined in (d) the components are,

$$F_1^{Pd} = 0 \quad , \tag{5.12}$$

$$F_2^{Pd} = - a_b \kappa I R_E^3 \int_0^{\frac{\pi}{2} - \delta} \frac{(r \cos \psi - R_E)}{(r^2 + R_E^2 - 2rR_E \cos \psi)^2} \sin^3 \psi \sin \delta \, d\psi$$

$$- \frac{a_b \kappa I R_E^3}{\pi} \int_{\frac{\pi}{2} - \delta}^{\alpha} \frac{(r \cos \psi - R_E)}{(r^2 + R_E^2 - 2rR_E \cos \psi)^2}$$

$$\times \Big[2 \cos \psi \sin^2 \psi \cos \delta \sqrt{(1 - \cot^2 \psi \cot^2 \delta)}$$

$$+ \sin^3 \psi \sin \delta \{ \cos^{-1} (-\cot \psi \cot \delta)$$

$$- (\cot \psi \cot \delta) \sqrt{(1 - \cot^2 \psi \cot^2 \delta)} \} \Big] \, d\psi \quad , \tag{5.13}$$

$$F_3^{Pd} = a_b \kappa I R_E^2 \int_0^{\frac{\pi}{2} - \delta} \frac{(r \cos \psi - R_E)(r - R_E \cos \psi) \sin 2\psi \cos \delta}{(r^2 + R_E^2 - 2rR_E \cos \psi)^2} \, d\psi$$

$$+ \frac{a_b \kappa I R_E^2}{\pi} \int_{\frac{\pi}{2} - \delta}^{\alpha} \frac{(r \cos \psi - R_E)(r - R_E \cos \psi)}{(r^2 + R_E^2 - 2rR_E \cos \psi)^2}$$

$$\times \Big[\sin 2\psi \cos \delta \cos^{-1} (-\cot \psi \cot \delta)$$

$$+ 2 \sin^2 \psi \sin \delta \sqrt{(1 - \cot^2 \psi \cot^2 \delta)} \Big] \, d\psi \quad . \tag{5.14}$$

Each revolution has been separated into four regions (a), (b), (c) and (d) that have been represented by equations (5.6)-(5.14). These components are now expressed in terms of S^*, T^* and W^* so that they may be substituted into the relevant

equations for the rates of change of the orbital elements. Generally, for any of the four regions, let

$$\underline{F}_a = F_1\hat{\underline{T}}' + F_2\hat{\underline{W}}' + F_3\hat{\underline{r}} \quad .$$

Then from

$$S^* = \hat{\underline{S}}.\underline{F}_a, \quad T^* = \hat{\underline{T}}.\underline{F}_a \quad \text{and} \quad W^* = \hat{\underline{W}}.\underline{F}_a \quad ;$$

$$S^* = F_3 \quad ,$$

$$T^* = F_2 \operatorname{cosec} \delta \; T(\theta) \quad ,$$

and

$$W^* = F_2 \operatorname{cosec} \delta \; W \quad .$$

The term $(r^2 + R_E^2 - 2rR_E \cos \psi)^{-2}$ appears in all the non-zero components and may be expanded by Taylor's series, to facilitate the integration of these components with respect to ψ. The convergence of this series depends on the magnitude of the expression,

$$(2rR_E \cos \psi - R_E^2)/r^2$$

and it was found that for usual values of r and for $0 \leq \psi \leq \alpha$, the series converged in such a manner that it was necessary to take at least 30 terms in the summation, in order that an accuracy of one decimal place was maintained. An alternative to this method is to resort to numerical integration.

This method requires a step by step search around the orbit so that the exit and entry points of the four regions might be ascertained. The value of the components of force

are assumed constant within each region for the orbit. After the components have been substituted into the Lagrange equations the double integration that results, requires numerical computation, firstly with respect to ψ and then with respect to the eccentric anomaly, over the limits defined by the bounds of the relevant region. This was applied to the equations for the eccentricity and semi-major axis, viz.,

$$\frac{da}{dE} = \frac{2}{n^2}\left[e \sin E\, S^* + \sqrt{(1-e^2)}\, T^*\right]$$

$$\frac{de}{dE} = \frac{\sqrt{(1-e^2)}}{n^2 a}\left[\sqrt{(1-e^2)} \sin E\, S^* - \left(\frac{3e}{2} - 2\cos E + \frac{e}{2}\cos 2E\right)T^*\right]$$

so that it is possible to investigate the effect of Earth reflected radiation pressure on the perigee height and on the orbital acceleration, $\dot{n}$, from

$$\frac{dn}{dt} = -\frac{3}{2}\frac{n}{a}\frac{da}{dt} .$$

When the satellite is within region (a) the rates of change of the orbital elements are zero, so that it will be necessary to evaluate only,

$$\delta M = -\frac{3}{2}\int \frac{\delta a}{a}\, dM$$

when the perturbation of the mean anomaly is considered.

Figure 20 shows the calling structure for the program units required to evaluate the perturbations due to the forces

resulting from Earth reflected radiation. Descent of a vertical line in this figure indicates the call of a subroutine.

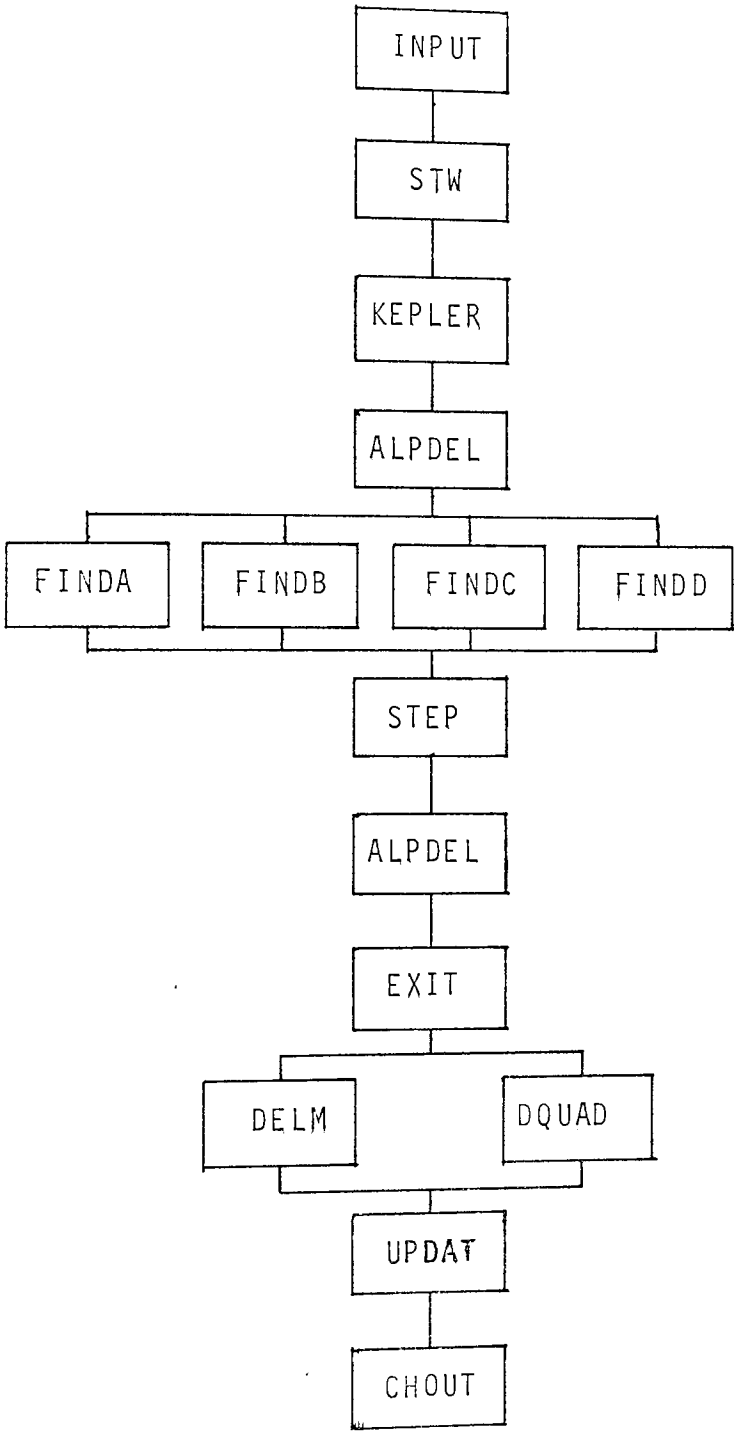

Fig. 20.

INPUT: Reads initial elements and prints this set together with the values input for n, $\dot{\omega}$ and $\dot{\Omega}$.

STW: Calculates the direction cosines from the latest values of ω, Ω and i together with derived values for λ and ε.

KEPLER: Evaluates E_o from $M_o = E_o + e_o \sin E_o$ using the second order iterative technique of Newton-Raphson.

ALPDEL: Calculates the values of α and δ in the range $(0,\pi)$ from

$$\alpha = \cos^{-1}\left[\frac{R_E}{a(1 - e\cos E)}\right]$$

and

$$\delta = \cos^{-1}\left[\frac{S(\cos E - e) + T\sqrt{(1-e^2)}\sin E}{(1 - e\cos E)}\right] .$$

FINDA,(B,C,D): Using a step by step loop, this subroutine evaluates, to an accuracy of one degree, the entry point of the region relevant to the present value of E.

STEP: $E_1 = E_o + \frac{2\pi}{100}$ and evaluates new values of α and δ. Finds the exit point from the present region and assigns this value to E_1.

DELM: $$\delta M = -\frac{3}{2}\int \frac{\delta a}{a}\, dM .$$

DQUAD: This routine is provided for the evaluation of the repeated integrals of the form

$$\int_a^b \int_{\phi_1(y)}^{\phi_2(y)} f(x,y)\, dy\, dx .$$

The method is based on the repeated use of Gauss quadrature.

UPDAT: This calculates the updated elements, allowing for perturbations due to reflected radiation pressure and allows for the effect of J_2 in $\dot{\omega}$, $\dot{\Omega}$ and $\dot{M}_o$. The new mean motion is evaluated together with the new epoch MJD + $\frac{2\pi}{n}$.

CHOUT: The subroutine checks when the final epoch required has been reached and outputs the variational results at the intervals requested. These intervals are to be not less than one revolution. The program operation is returned to INPUT together with the updated elements.

6.

ANALYSIS OF THE ORBIT OF EXPLORER 19

i) Orbital Data:

The balloon satellite Explorer 19, 1963-53A, was designed and built at the NASA Langley Research Centre in order to obtain measurements of the atmospheric density. Explorer 19 was launched on 19th. December 1963 into an orbit of inclination 78.6 degrees, with a perigee height of 592 km. and an apogee height of 2392 km. The spherical balloon with a diameter of 3.66 m., had a mass of 8.069 kg. (Keating, Mullins and Prior, 1970)

The orbit was determined at 60 separate epochs using the RAE orbit determination program PROP, in the PROP 6 version. (Gooding and Tayler, 1968 and Gooding, 1974) There were 2765 observations used, assembled from five sources. The most accurate observations were those made by the Hewitt Camera at Malvern, having an accuracy of about 2 arc sec. in position and 1 m. sec. in time. Unfortunately these observations were only available for seven of the 60 epochs, and comprised only 2% of all the observations. The two largest groups consisted of 1169 visual observations supplied by the Appleton Laboratory at Slough and 1162 U.S. Navy observations supplied by courtesy of the U.S. Naval Laboratory, the former generally having an accuracy of within 1-3 arc min. and the latter having an average accuracy of about 2 arc min. in position and 1 km. in range. Of the epochs, 24 used important data from the Southern hemisphere with 161 observations made by the kinetheodolite at the Cape Observatory, accurate to 1 arc min.

The fifth source was supplied by the Finnish Meteorological Instituteand was generally accurate to within 3 arc min.

For the first time observations from the Appleton Laboratory included Russian data. The accuracy of these visual observations was of the same order as that generally found for this type of data.

The 60 sets of orbital parameters obtained are presented in Table 1, together with the standard deviations below each value. The epochs chosen correspond to 0 hr. on the day of determination and were selected so as to be equally spaced every four days from 14th. February to the 7th. October, 1976 inclusively. There are no observations overlapping from one epoch to the next so as to avoid the repetition of errors obtained by poor distribution. For 48 of the epochs the mean anomaly was represented by

$$M = M_0 + M_1 t + M_2 t^2 \quad ,$$

and in the remaining 12 orbits an extra term, $M_3 t^3$, was required. The orbits fit the observations reasonably well, with ε, the parameter measuring the degree of fit, ranging from 0.42 to 0.94 .

The values for the semi-major axis have standard deviations in the range 0.4 m. to 8.2 m. and the standard deviation in eccentricity lies between 0.000009 and 0.000042. The average standard deviations for the semi-major axis and eccentricity are 1.9 m. and 0.000018 respectively. These

figures correspond to an error of between 69 m. and 320 m. in perigee height. The mean motion, M_1, generally accurate to 1.2×10^{-4} %, while the accuracy of the higher coefficients, M_2 and M_3, depends essentially on the number of observations used and their geographical distribution.

The epoch, measured in Modified Julian Days (MJD = JD - 2400000.5), appears in the first column of Table 1. The nine columns following contain the semi-major axis, a km., the eccentricity, e, the orbital inclination, i deg., the right ascension of the ascending node, Ω deg., the argument of the perigee, ω deg., the mean anomaly at epoch, M_0 deg., the mean motion, M_1=n deg./day, and the later coefficients of the polynomial for M. The final columns of Table 1 give the measure of fit of the orbit by the observations, ε, the number of observations used, N, and the time in days covered by the observations, D. The orbits utilising Hewitt Camera observations are signified with * on the left hand side of Table 1.

Figure 21 shows the observed values of eccentricity for the orbit of Explorer 19, given by Table 1. It would appear that the value of eccentricity obtained at epoch 49, MJD 43010.0, is in error. This is possibly the result of a bias in the observations. This orbit was included in the analysis for the sake of continuity.

The effects of the Earth's gravity and those of Lunar and Solar gravity may be removed from the initial orbital data with the aid of the computer program PROD developed at

Table 1. Orbital Parameters of Explorer 19 at the 60 Epochs, with Standard Deviations

	MJD	a	e	i	Ω	ω	M_0	M_1	M_2	M_3	ε	N	D
1	42822	7639.226 1	0.06501 2	78.808 2	334.350 1	308.40 2	31.85 2	4682.112 1	-0.0045 9		.60	70	3.7
2	42826	7639.231 2	0.06465 2	78.807 2	330.201 2	299.87 2	40.13 2	4682.107 2	-0.0088 18		.63	65	4.8
3	42830	7639.288 1	0.06440 1	78.803 2	326.054 2	291.19 1	48.46 1	4682.055 1	-0.0112 9		.60	68	3.8
* 4	42834	7639.388 1	0.06405 1	78.805 1	321.914 1	282.50 1	56.50 1	4681.963 1	-0.0059 16	-0.0062 11	.89	62	3.2
* 5	42838	7639.460 1	0.06371 1	78.813 1	317.758 2	273.70 2	64.30 2	4681.897 1	-0.0050 4		.74	91	3.8
* 6	42842	7639.514 0	0.06344 1	78.816 1	313.607 1	265.05 1	71.73 1	4681.847 0	-0.0115 6	-0.0033 4	.74	88	3.7
* 7	42846	7639.621 3	0.06316 1	78.812 2	309.468 2	256.09 2	79.21 2	4681.749 2	-0.0091 7	0.0029 9	.62	78	3.7
8	42850	7639.669 1	0.06295 2	78.814 2	305.323 2	247.14 2	86.38 2	4681.704 1	-0.0063 12		.62	46	3.7
9	42854	7639.655 1	0.06280 1	78.815 1	301.183 1	238.15 1	93.50 1	4681.717 1	0.0015 11		.50	52	3.1

Table 1, continued.

	MJD	a	e	i	Ω	ω	M_0	M_1	M_2	M_3	ε	N	D
10	42858	7639.635 1	0.06283 1	78.816 2	297.037 1	229.23 1	100.65 1	4681.735 1	0.0037 8		.82	60	3.8
11	42862	7639.590 1	0.06287 2	78.825 3	292.904 2	220.27 2	107.91 1	4681.777 1	0.0115 8		.84	30	3.8
12	42866	7639.454 3	0.06291 2	78.819 1	288.758 1	211.39 1	115.45 1	4681.902 3	0.0150 13	0.0003 10	.51	33	3.7
13	42870	7639.330 1	0.06314 1	78.824 1	284.618 1	202.56 1	123.42 1	4682.016 1	0.0113 9		.61	40	3.0
14	42874	7639.250 2	0.06341 2	78.823 2	280.473 1	193.81 1	131.72 1	4682.090 1	0.0093 19		.86	19	3.9
15	42878	7639.159 2	0.06373 1	78.823 2	276.336 1	185.05 1	140.32 1	4682.174 2	0.0060 10	0.0078 8	.65	34	3.9
16	42882	7638.996 1	0.06403 2	78.823 3	272.192 1	176.51 2	149.19 2	4682.324 1	0.0133 7		.44	18	3.9
17	42886	7638.904 4	0.06426 1	78.826 2	268.052 1	168.03 1	158.48 1	4682.409 4	0.0096 21	0.0064 25	.63	38	3.1
18	42890	7638.803 2	0.06449 2	78.821 3	263.913 2	159.59 2	168.04 2	4782.502 2	0.0117 11		.56	35	3.9

Table 1, continued.

	MJD	a	e	i	Ω	ω	M_0	M_1	M_2	M_3	ε	N	D
19	42894	7638.666 1	0.06463 2	78.821 2	259.770 2	151.05 1	178.14 1	4682.627 1	0.0143 8		.47	53	3.9
20	42898	7638.569 1	0.06477 2	78.825 3	255.629 2	142.76 2	188.50 2	4682.717 1	-0.0001 13		.74	34	3.9
21	42902	7638.518 4	0.06477 3	78.827 4	251.488 3	134.50 3	199.00 3	4682.764 4	0.0001 27		.63	30	3.0
22	42906	7638.509 2	0.06476 2	78.828 2	247.350 2	126.00 2	209.89 2	4682.772 2	0.0010 13		.70	39	3.9
23	42910	7638.499 2	0.06463 2	78.827 2	243.216 2	117.77 3	220.56 2	4682.781 1	-0.0055 15		.62	45	3.0
24	42914	7638.565 2	0.06452 2	78.822 3	239.070 3	109.27 3	231.40 3	4682.721 1	-0.0126 13		.66	43	3.7
25	42918	7638.649 2	0.06423 2	78.821 3	234.931 2	100.96 2	241.78 2	4682.643 2	-0.0092 19		.60	22	3.1
26	42922	7638.706 2	0.06410 2	78.826 3	230.793 4	92.58 5	251.94 4	4682.591 1	-0.0046 12		.94	58	3.7
27	42926	7638.785 1	0.06373 1	78.832 2	226.652 2	83.97 2	262.13 2	4682.518 1	-0.0136 7		.71	50	3.9

Table 1, continued.

	MJD	a	e	i	Ω	ω	M_o	M_1	M_2	M_3	ε	N	D
28	42930	7638.886 3	0.06332 3	78.826 3	222.514 3	75.57 4	271.74 4	4682.425 3	-0.0229 25		.59	23	3.1
29	42934	7638.992 1	0.06309 2	78.829 2	218.379 2	67.00 2	281.08 2	4682.327 1	-0.0076 9		.66	45	3.8
*30	42938	7639.045 2	0.06274 2	78.834 1	214.245 2	58.34 2	290.26 2	4682.279 1	-0.0114 12		.70	48	3.2
31	42942	7639.124 2	0.06239 2	78.834 1	210.113 2	49.88 2	299.02 2	4682.206 1	0.0090 13		.76	34	3.7
32	42946	7639.171 2	0.06207 2	78.836 3	205.976 2	41.15 2	307.78 2	4682.163 2	0.0006 19		.61	23	3.1
33	42950	7639.111 1	0.06186 2	78.837 2	201.845 2	32.43 1	316.56 1	4682.218 1	0.0068 5		.57	23	3.7
34	42954	7639.066 1	0.06153 1	78.837 2	197.714 1	23.75 1	325.50 1	4682.259 1	0.0033 8		.67	36	3.4
35	42958	7639.042 1	0.06128 1	78.838 2	193.583 1	15.09 1	334.54 1	4682.282 1	0.0029 11		.57	22	3.6
36	42962	7638.992 4	0.06104 1	78.838 1	189.449 1	6.45 1	343.70 1	4682.327 3	0.0057 19		.56	26	2.1

Table 1, continued.

	MJD	a	e	i	Ω	ω	M_0	M_1	M_2	M_3	ε	N	D
37	42966	7638.920 6	0.06076 2	78.838 3	185.322 2	357.88 1	353.08 1	4682.394 6	0.0086 29		.46	18	2.0
38	42970	7638.876 2	0.06059 1	78.843 2	181.192 2	349.21 1	2.74 1	4682.434 2	0.0011 11		.53	36	3.9
39	42974	7638.827 8	0.06024 1	78.847 2	177.061 1	340.66 1	12.45 1	4682.479 8	0.0088 39		.50	24	2.0
40	42978	7638.742 1	0.05995 2	78.846 2	172.930 2	332.00 2	22.50 2	4682.557 1	0.0075 10		.51	40	4.0
41	42982	7638.726 1	0.05962 2	78.844 2	168.802 2	323.44 2	32.69 2	4682.572 1	-0.0050 9		.65	70	3.9
42	42986	7638.771 2	0.05926 4	78.844 3	164.668 3	314.86 3	42.77 4	4682.530 2	0.0015 20		.43	36	3.9
43	42990	7638.796 2	0.05891 2	78.844 2	160.538 2	306.10 2	52.93 2	4682.507 1	-0.0037 14		.57	70	3.9
44	42994	7638.807 4	0.05849 2	78.839 2	156.408 2	297.36 2	62.95 3	4682.497 4	-0.0055 20	-0.0070 14	.56	65	3.9
45	42998	7638.925 5	0.05822 2	78.840 2	152.277 2	288.49 3	72.90 3	4682.388 4	-0.0108 13	0.0039 15	.52	52	3.7

Table 1, continued.

	MJD	a	e	i	Ω	ω	M_o	M_1	M_2	M_3	ε	N	D
46	43002	7638.967 3	0.05778 2	78.843 2	148.150 2	279.76 2	82.41 2	4682.350 3	-0.0088 33	-0.0031 20	.57	57	3.2
47	43006	7639.030 3	0.05757 2	78.839 2	144.021 2	270.86 3	91.90 3	4682.291 3	-0.0083 8	-0.0004 9	.56	75	3.9
* 48	43010	7639.095 2	0.05721 1	78.840 1	139.894 1	261.96 1	101.17 2	4682.232 2	-0.0105 7	-0.0028 9	.69	77	3.8
* 49	43014	7639.183 1	0.05738 3	78.844 3	135.765 3	252.70 2	110.53 2	4682.151 1	-0.0091 9		.64	78	3.0
50	43018	7639.206 2	0.05669 1	78.843 2	131.637 2	243.95 2	119.06 2	4682.129 2	-0.0040 7	-0.0022 7	.52	53	3.8
51	43022	7639.228 2	0.05659 2	78.844 2	127.510 2	234.92 2	127.86 2	4682.110 2	-0.0102 14		.59	51	3.1
52	43026	7639.281 1	0.05664 2	78.844 2	123.386 2	225.96 2	136.47 2	4682.061 1	-0.0037 8		.49	72	3.8
53	43030	7639.284 2	0.05656 2	78.848 3	119.261 2	216.87 2	145.09 2	4682.058 2	0.0033 18		.60	37	2.9
54	43034	7639.231 2	0.05656 2	78.849 3	115.137 2	207.94 2	153.67 2	4682.107 1	0.0031 1		.42	22	3.7

Table 1, continued.

	MJD	a	e	i	Ω	ω	M_0	M_1	M_2	M_3	ε	N	D
55	43038	7639.194 1	0.05680 2	78.847 2	111.016 2	198.92 1	162.52 1	4682.141 1	0.0016 10		.68	53	3.7
56	43042	7639.148 2	0.05702 2	78.853 3	106.892 2	189.99 3	171.39 3	4682.184 1	0.0085 20		.76	25	3.1
57	43046	7639.059 1	0.05717 1	78.852 2	102.769 1	181.19 1	180.38 1	4682.266 1	0.0134 11		.63	49	3.7
58	43050	7638.978 1	0.05745 2	78.858 2	98.650 1	172.46 1	189.65 1	4682.340 1	0.0067 8		.71	37	3.6
59	43054	7638.937 1	0.05763 1	78.860 2	94.525 1	163.81 1	199.06 1	4682.378 1	0.0056 7		.49	37	3.7
60	43058	7638.858 1	0.05777 1	78.859 1	90.402 1	155.24 1	208.58 1	4682.450 1	0.0111 5		.68	50	3.9

RAE Farnborough (Cook, 1972). The zonal harmonics in the Earth's potential that were included were upto and including J_{20}. Solar and Lunar gravity perturbations both included the second harmonic together with periodic terms. That is, the six monthly oscillations in the case of Solar gravity and the fourteen day oscillations in the case of Lunar gravity.

ii) Radiation Pressure Effects:

In order to evaluate the effects of direct SRP it is necessary to integrate the planetary equations (2.1)-(2.6) over each revolution of Explorer 19, over the period MJD 42822.0 to MJD 43058.0, that is over 3070 revolutions. The limits of the integration are defined by the relevant shadow position of each revolution as described in Section 3. The equations defining the changes in a,e and i due to SRP are derived from equations (2.1),(2.2) and (2.3) respectively, by a change of variable from the true anomaly, θ, to the eccentric anomaly, E, and integrating with respect to E while holding constant the terms not explicitly dependent on E. The remaining three elements defining the satellite's position ω, Ω and M are integrated similarly and the small changes in these elements due to the interaction of SRP and the first order oblateness of the Earth's gravitational field are added. These changes are derived from equations (2.22)-(2.24) by substituting the first order secular term of the gravitational potential R, where

$$R = \frac{J_2 \mu R_E^2}{2a^3(1-e^2)^{3/2}} \left(1 - \frac{3}{2}\sin^2 i\right) .$$

Fig. 21. OBSERVED VALUES OF ECCENTRICITY, e.

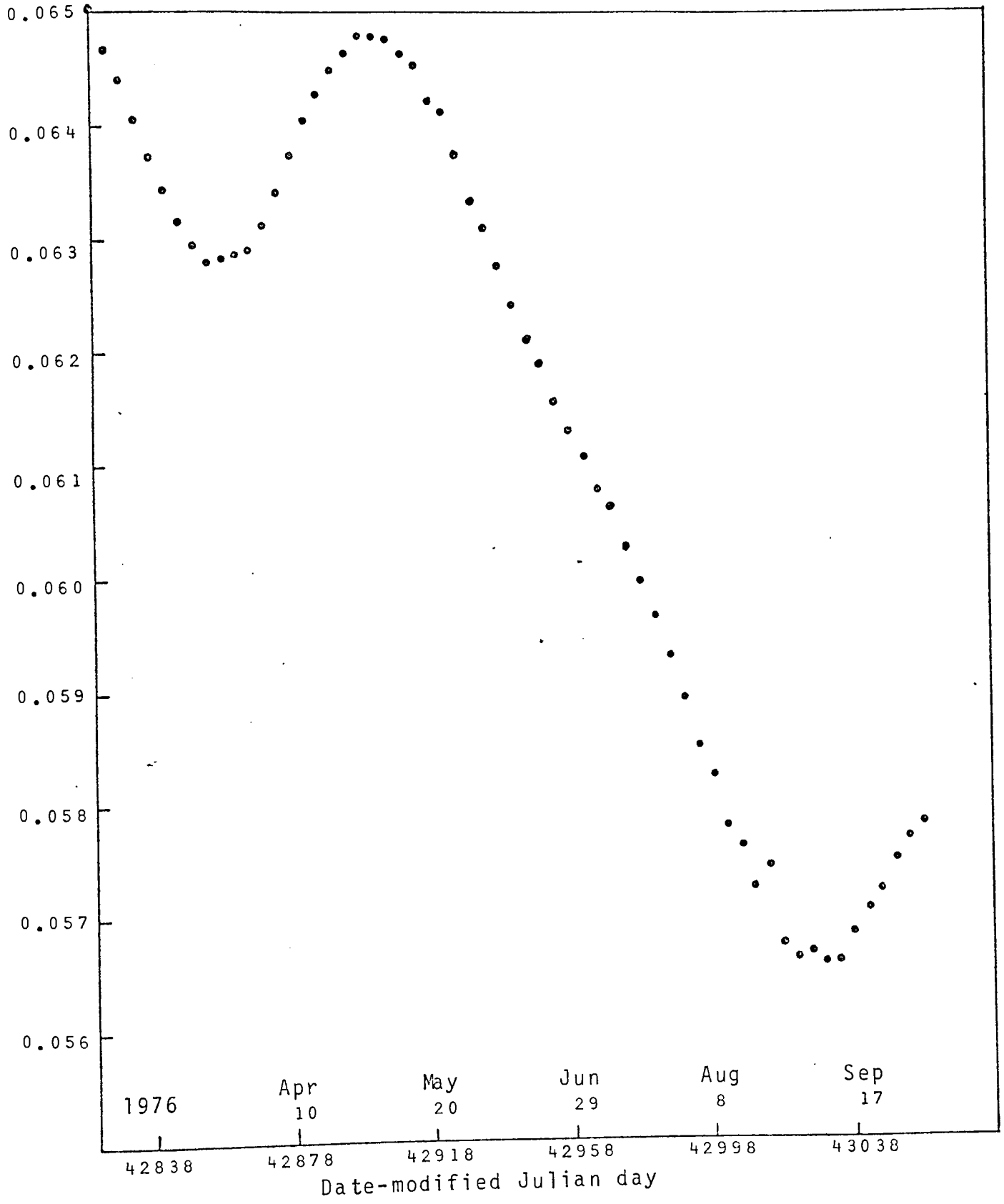

It is also important when considering short-period changes of M, to include the variations of M due to the changes in n caused by the perturbations of a by SRP. This will then result in the equations (6) given by Aksnes, 1976.

The long-period perturbations due to SRP are computed over the 236 days defined by the data of Table 1, by summing the changes over complete revolutions and adding the fractions of the revolutions that occur at the start and end of the period of time defined by MJD 42822.0 to 43058.0 . The step by step method described in Section 3 is used to evaluate the integration limits defining the shadow phase of each revolution. The initial data employed was line 1 of Table 1 together with values for n, $\dot{\omega}$ and $\dot{\Omega}$, taken as the mean values over the period considered, the rates $\dot{\omega}$ and $\dot{\Omega}$ being given by the equations 1.1 and 1.2 of King-Hele (1964). The variable data describing the Sun's position is given by the Explanatory Supplement to the Astronomical Ephemeris, 1961.

It only remains to assign a value to $s\frac{A}{m}$, defined in the introduction. $\frac{A}{m}$ is taken as 1.304 m^2 kg^{-1} while the trial and error method of fitting the results to the observed values of the perturbations, is at first applied, to find a suitable value for s. The satellite was assumed to be spherical. The points plotted in Figure 22 give the residual change in eccentricity after the perturbations due to the Luni-Solar gravitational fields and those due to the Earth's gravitational field have been removed, by using the computer program PROD. The computed results for SRP are also shown in this figure, for s=1.0, 1.1 and 1.14 . Taking s=1.1 gives quite a good fit

Fig. 22. RESIDUAL ECCENTRICITY AFTER PROD, PLOTTED AS POINTS AND RESULTS COMPUTED FOR SRP.

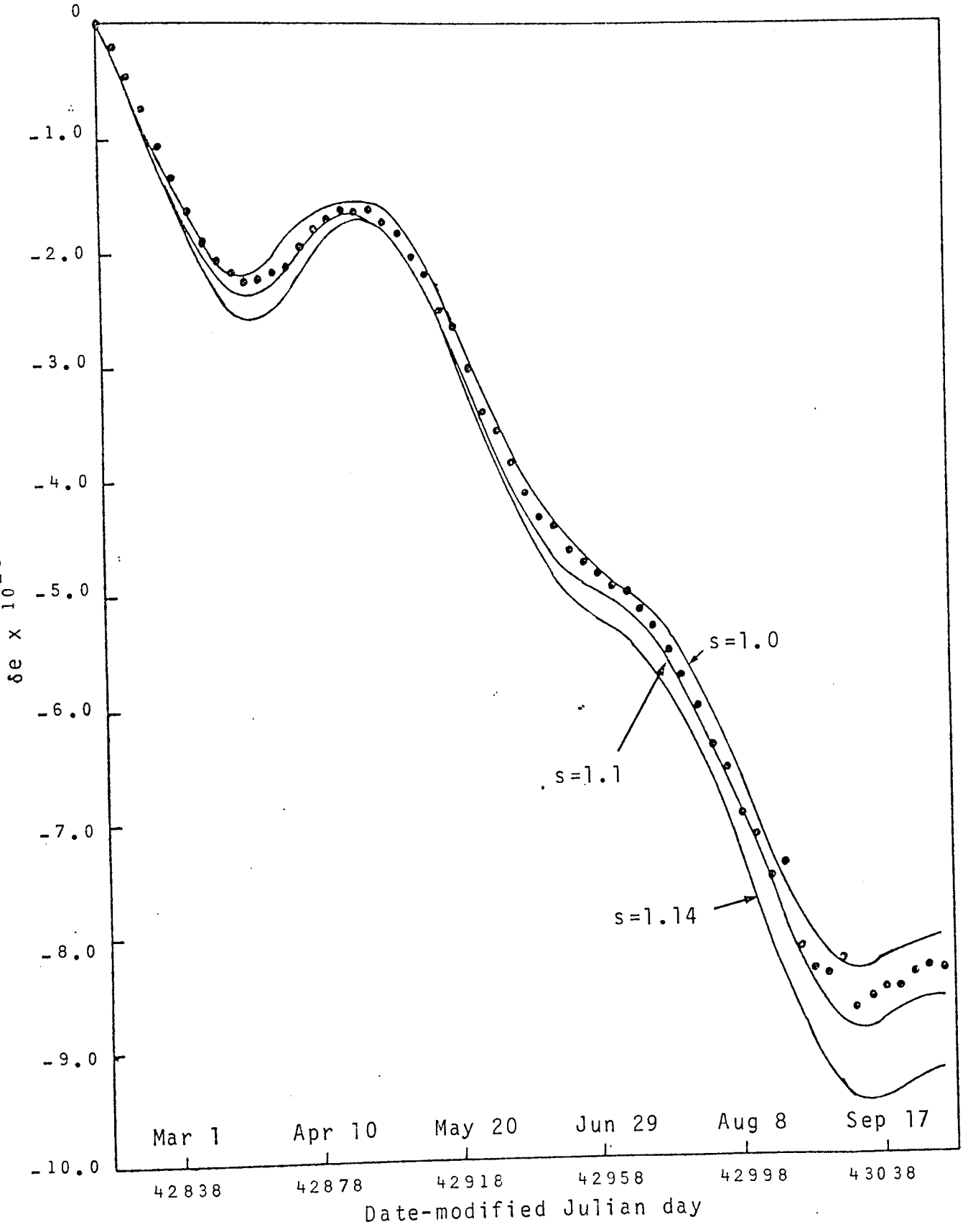

of the observed data by the predicted effects of SRP. The choice of s=1.1 results in a maximum difference of 0.0003 between the observed residues and the computed values for SRP. It should be remembered that it is not possible to remove precisely the effects on the observations due to atmospheric drag, which for the height of Explorer 19 is by no means negligible. The approximate perigee height of this satellite is 800 km. so that the perturbing effect on the mean motion by atmospheric drag is of the same order as that of SRP. In the absence of precise data describing the change in the elements due to air drag or data defining the reflective characteristics of Explorer 19, it is not possible to compare accurately the magnitude of the effects of SRP and the aerodynamic forces acting on the satellite. However, it can be seen that the variation of the computed results for SRP follows the variation of the residual eccentricity of Figure 22 very closely.

The revolutions within the ranges of MJD 42858-42888, 42946-42978 and 43038-43058 were completely sunlit. The perturbations of the orbital elements for 1 revolution (111 min) of the satellite, are plotted against time, in Figures 23 and 24 the revolution commencing on 42822.0 and including a period of time when the satellite was in shadow. Figures 25 and 26 show the perturbation of the elements during 1 revolution starting on 42966.0 when the satellite did not enter the Earth's shadow. The smooth curves here show the results evaluated by using the step by step method to find the shadow boundaries. For the revolution starting at 42822.0 the satellite entered the Earth's shadow after 41 min. and

Fig. 23.

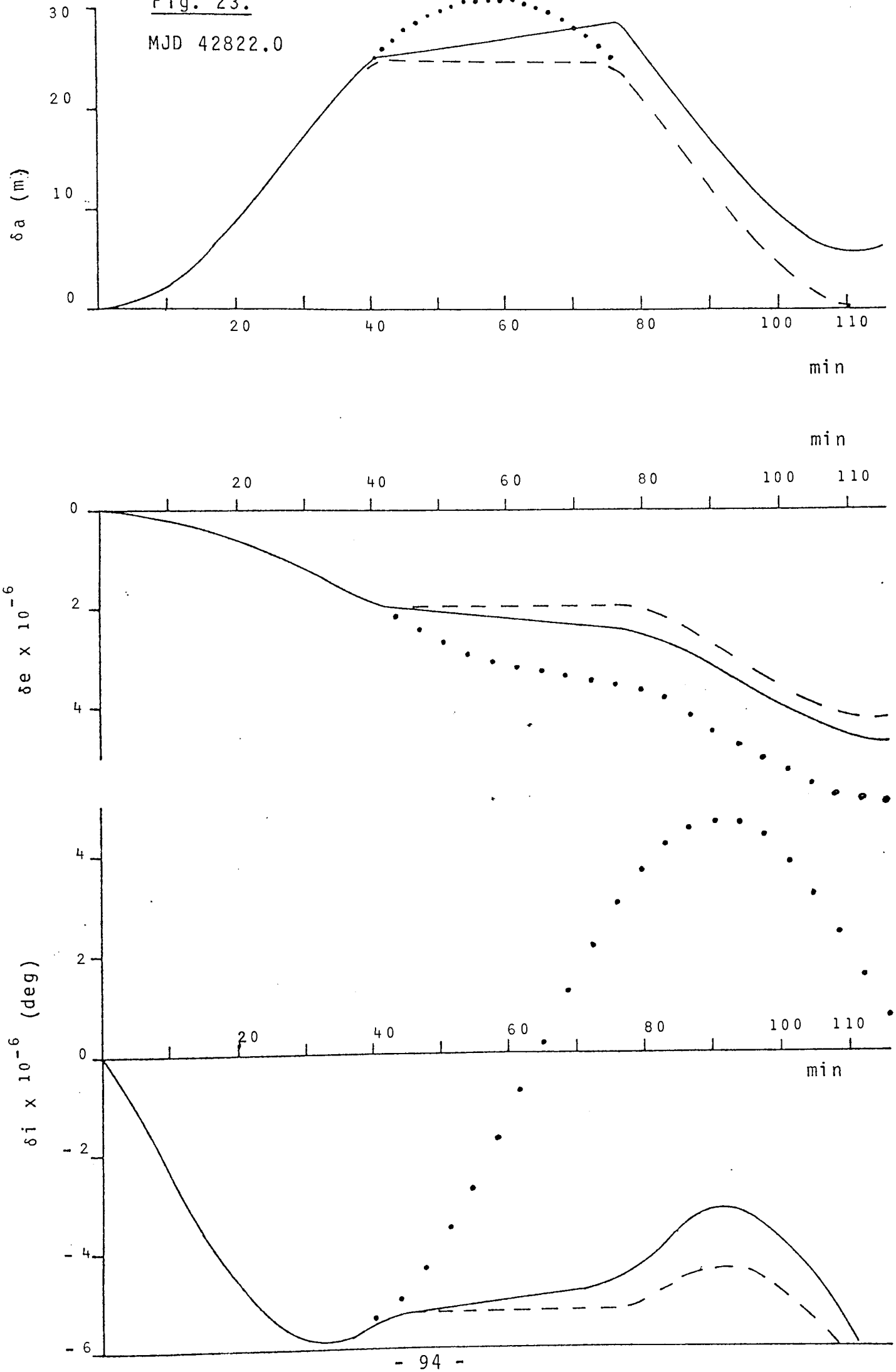
MJD 42822.0
δa (m)
30
20
10
0
20
40
60
80
100
110
min
δe x 10^-6
0
2
4
δi x 10^-6 (deg)
4
2
0
- 2
- 4
- 6

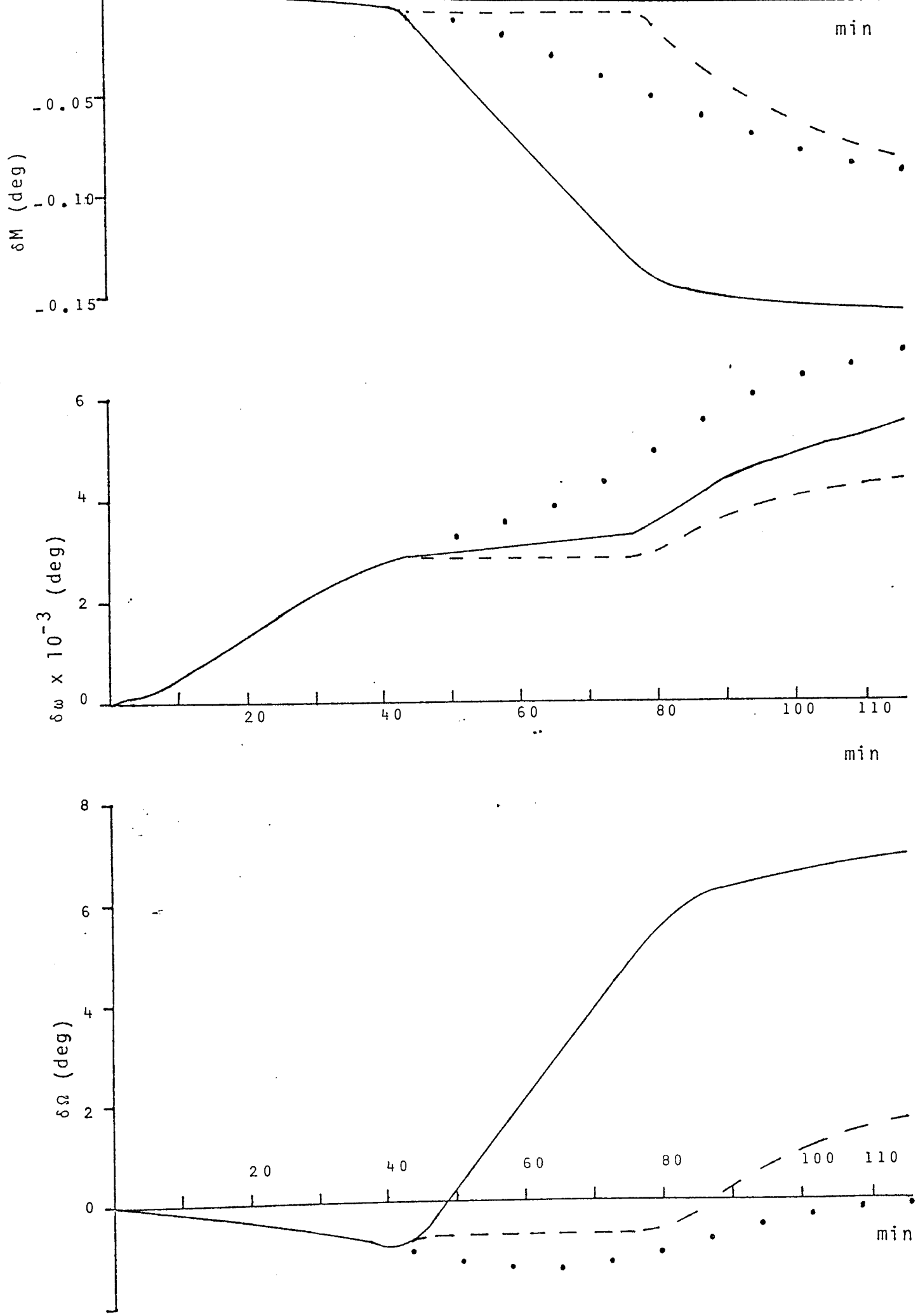

Fig. 24. MJD 42822.0

Fig. 25.

MJD 42966.0

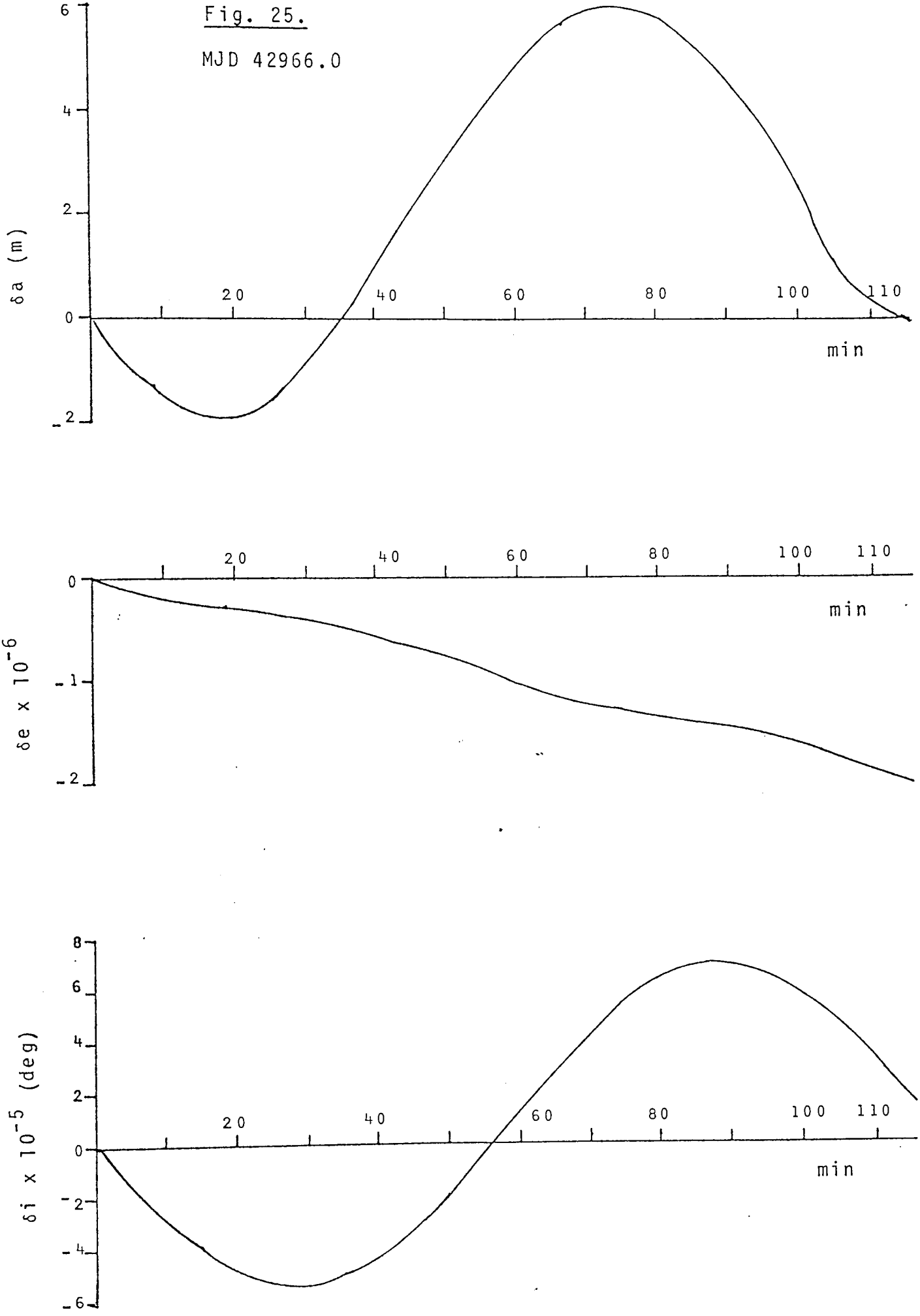

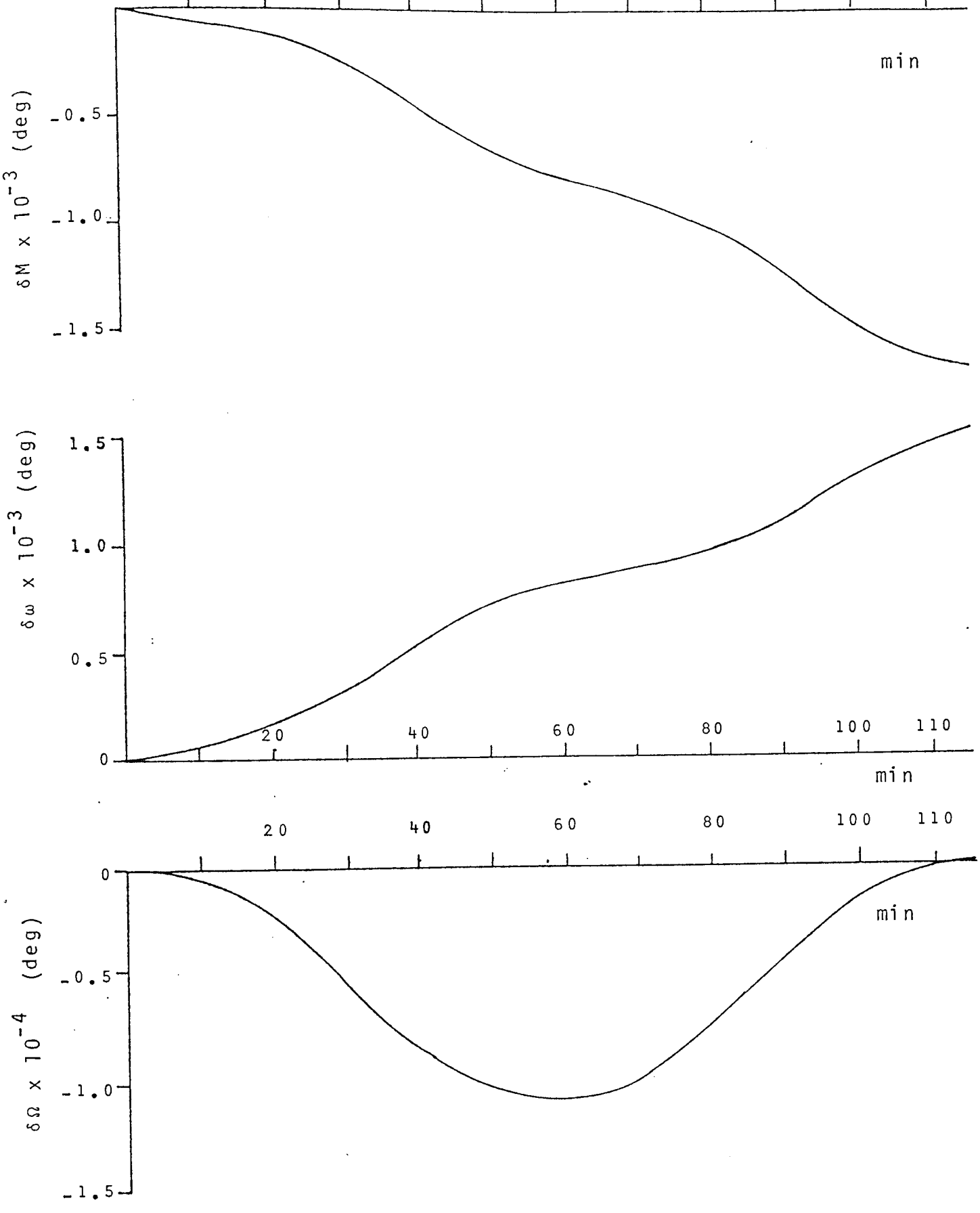

Fig. 26.

MJD 42966.0

remained eclipsed for 35 min. before entering sunlight again. The data in these figures, plotted as dashed lines are the result of applying the continuous shadow function given by Lala and Sehnal (1969) and described in Section 3. This process was applied with the relevant number of terms required in the expansions, chosen so that the results coincide with the portion of the curve representing that period before the satellite entered the Earth's shadow. The portion of the revolution eclipsed by the shadow, is shown by the horizontal part of the curves. The difference between the smooth curves and the individual points is the result of approximating linearly, the changes of the direction cosines S,T and W, when summing the perturbations over a revolution. The inclusion of this approximation was not possible when applying the continuous shadow function. The individual points plotted in Figures 23 and 24 show the effect of neglecting the shadow phase, that is $\Gamma(x)=0$ from equation (3.5).

Figures 25 and 26 show the perturbations of the elements over a revolution that is completely sunlit. The small net change in a, of about 0.4 m., over this revolution is again the result of including a linear approximation to δS, δT and δW, the small changes in S, T and W over the time interval, δt. When integrating the perturbations represented in Figures 23-26, δt was taken as 0.001 day. These effects of linear variation in the orbital elements when the satellite is in shadow and the net change in a during a sunlit revolution, cannot be detected in the results given by Aksnes. They were checked by taking S, T and W as constant during a complete revolution

so that δS, δT and δW were zero. As expected from equation (2.10), $\delta a = 0$ when $E_1 = 0$, $E_2 = 2\pi$ and all the terms not explicitly dependent on E were held constant.

As suggested in Section 5, radiation coming from the Earth as reflected sunlight can also effect the orbital behaviour of satellites. The effect on the elements is of course quite small compared to the effect of direct SRP, and in the example of Explorer 19, small compared to atmospheric drag. When the effect of terrestrial radiation pressure was considered it was necessary to integrate around the orbit numerically and at each point in that integration, to integrate numerically again in order to obtain the force on the satellite. The semi-analytical method described in Section 5 was employed to calculate this form of radiation pressure perturbation. The assumptions made in that section were made at this stage, that is, that the solar radiation reflected from the Earth, is reflected diffusely according to Lambert's Law, the satellite is spherical and that the Earth's albedo, a_b, is taken as constant. The value chosen for a_b was unduly large, 0.5, so as to obtain an idea of the magnitude of the perturbation involved. The albedo suggested by Slowey (1974ii) was less than 0.4.

The results for the perturbations in the semi-major axis and the eccentricity are given in Figures 27 and 28 respectively. The maximum magnitude of δa found was 53 m. and that for δe was -2.4×10^{-5} so that the maximum perturbation in the perigee height is of the order of 183 m. The effect of Earth reflected radiation pressure on a was found to give

values for $\dot{n}$ of 6×10^{-7} revs/day^2. The mean standard deviation of M_2 is 0.0020 deg/day^2 which results in a value for $\dot{n}$ of 1.1×10^{-5} revs/day^2 , so that it is possible to neglect this perturbation when evaluating the rate of change of the mean motion. The maximum value of $\dot{n}$ found due to this force was 8×10^{-6} revs/day^2 corresponding to the epoch 42902.0 (MJD). The perturbations to the perigee height were also neglected as the values of δe lead to changes of height of less than 0.1 km.

Figure 29 shows the perturbation of the semi-major axis, due to SRP, over 236 days starting at MJD 42822.0 . The periods when the satellite's revolutions were completely sunlit are clearly discernable. The total effect of SRP on a is shown to be , δa_{SRP}=+3.77km. After the same period of time the observed value is δa_{OBS}=-0.37 km. If SRP and air drag are the only forces relevant then the total change in a, that can be assumed due to air drag, is of the order of 4 km. This leads to the approximate value of $\dot{n} = 4.5 \times 10^{-5}$, which may be considered as a mean value for the rate of change of the mean motion due to atmospheric drag acting on Explorer 19 for MJD 42822-43058.

Figure 30 provides a comparison of the observed values of the orbital inclination, (points) after removal of gravitational perturbations, with the perturbations calculated for SRP (smooth curve). Again the effect of the aerodynamic forces have not been eliminated and the differences between observed and computed results are due, in part, to the variation in the rate of rotation of the Earth's upper

Fig. 27. THE EFFECTS OF EARTH REFLECTED RADIATION ON THE SEMI-MAJOR AXIS, a.

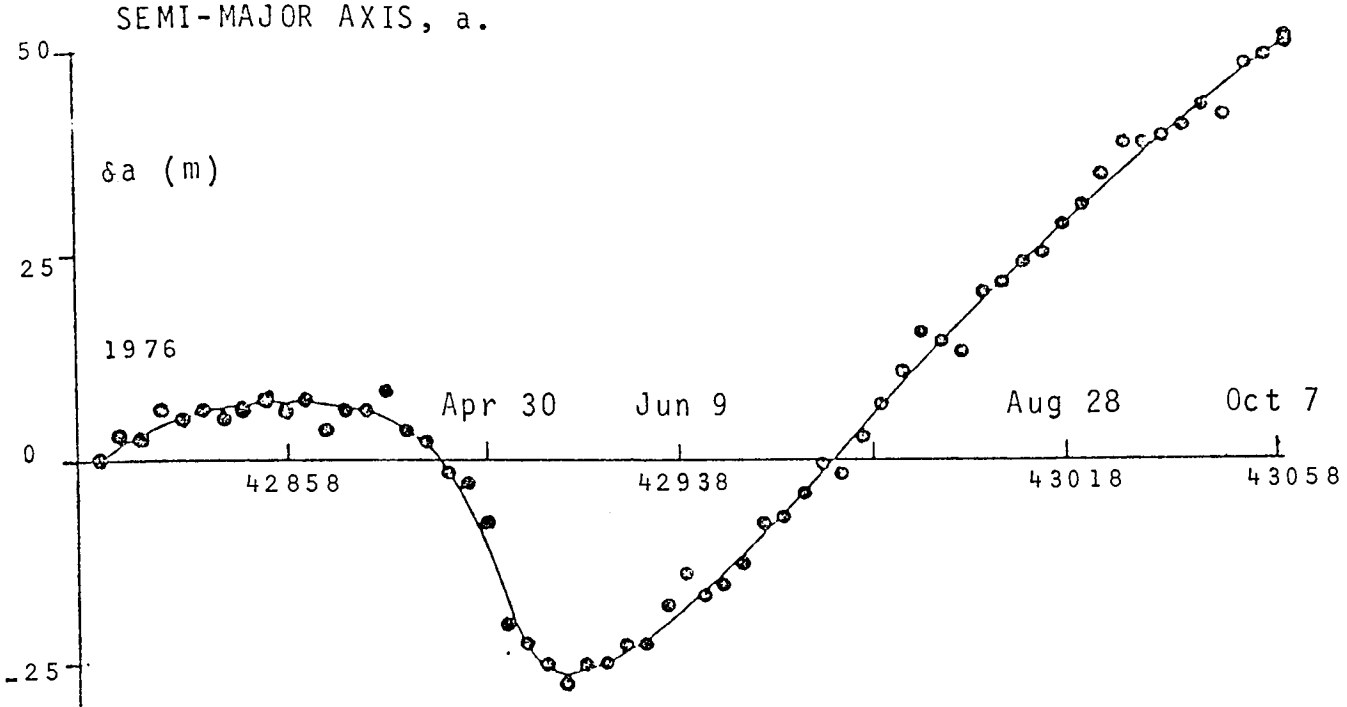

Fig. 28. THE EFFECTS OF EARTH REFLECTED RADIATION ON THE ECCENTRICITY, e.

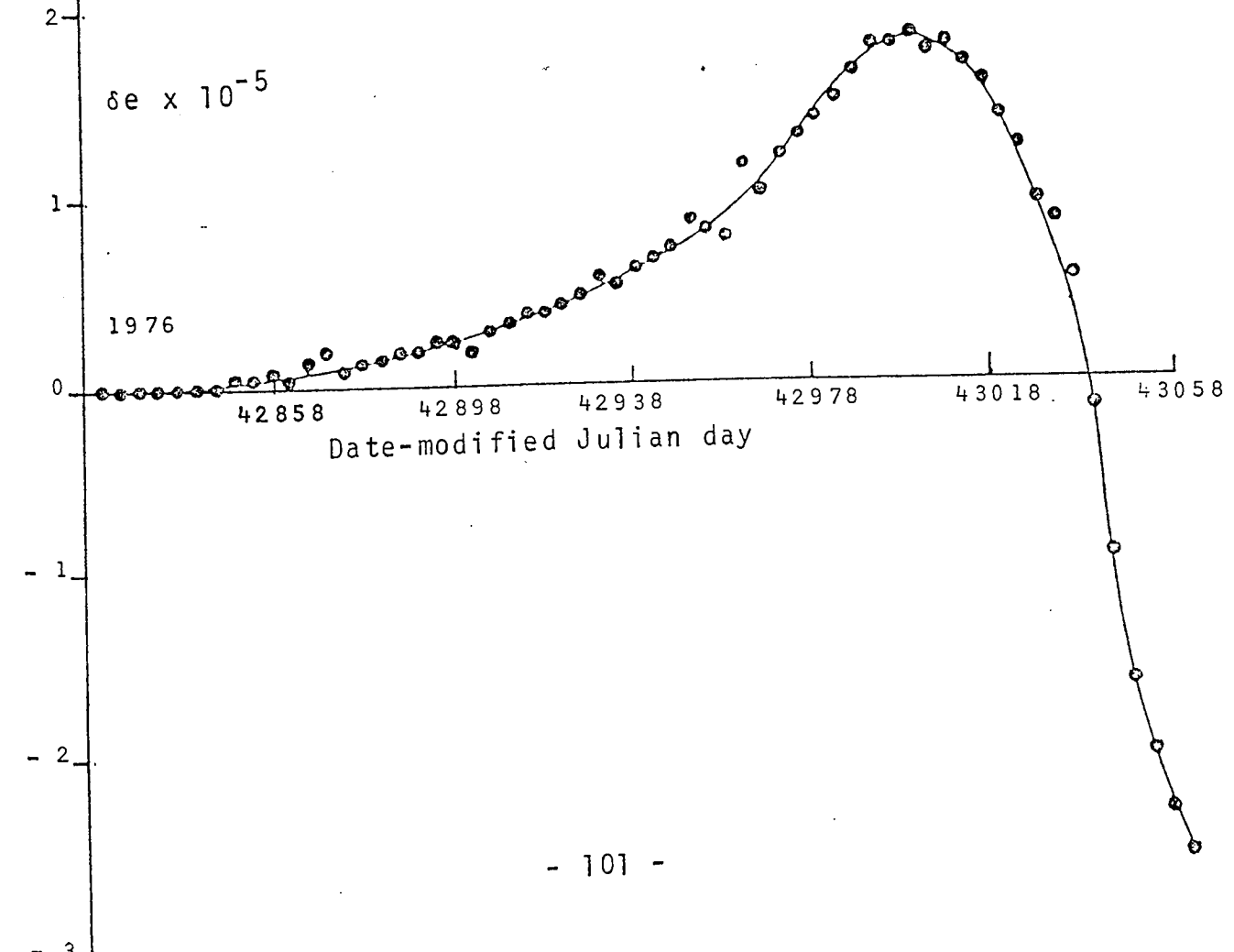

Fig. 29. THE EFFECTS OF SRP ON THE SEMI-MAJOR AXIS.

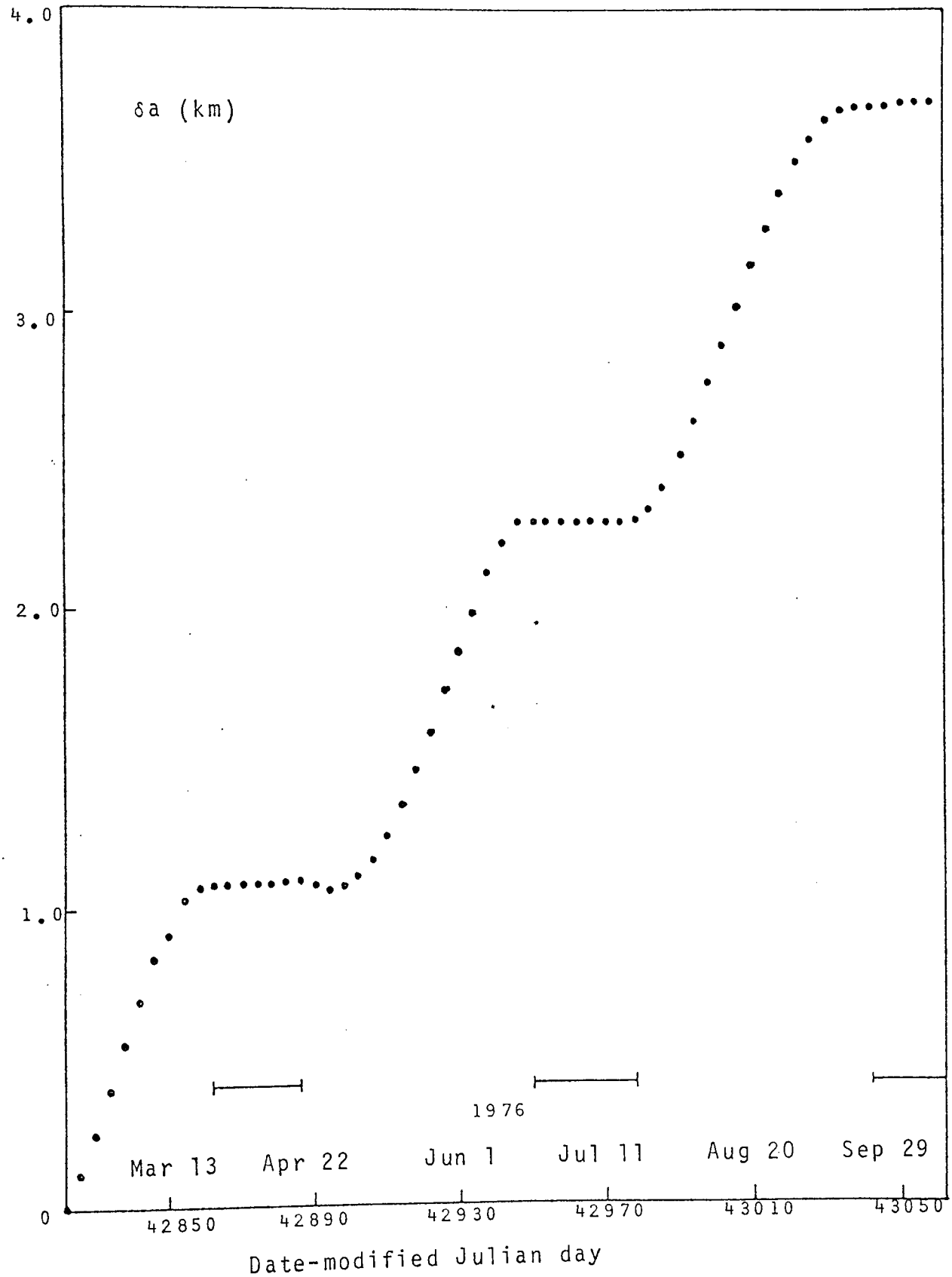

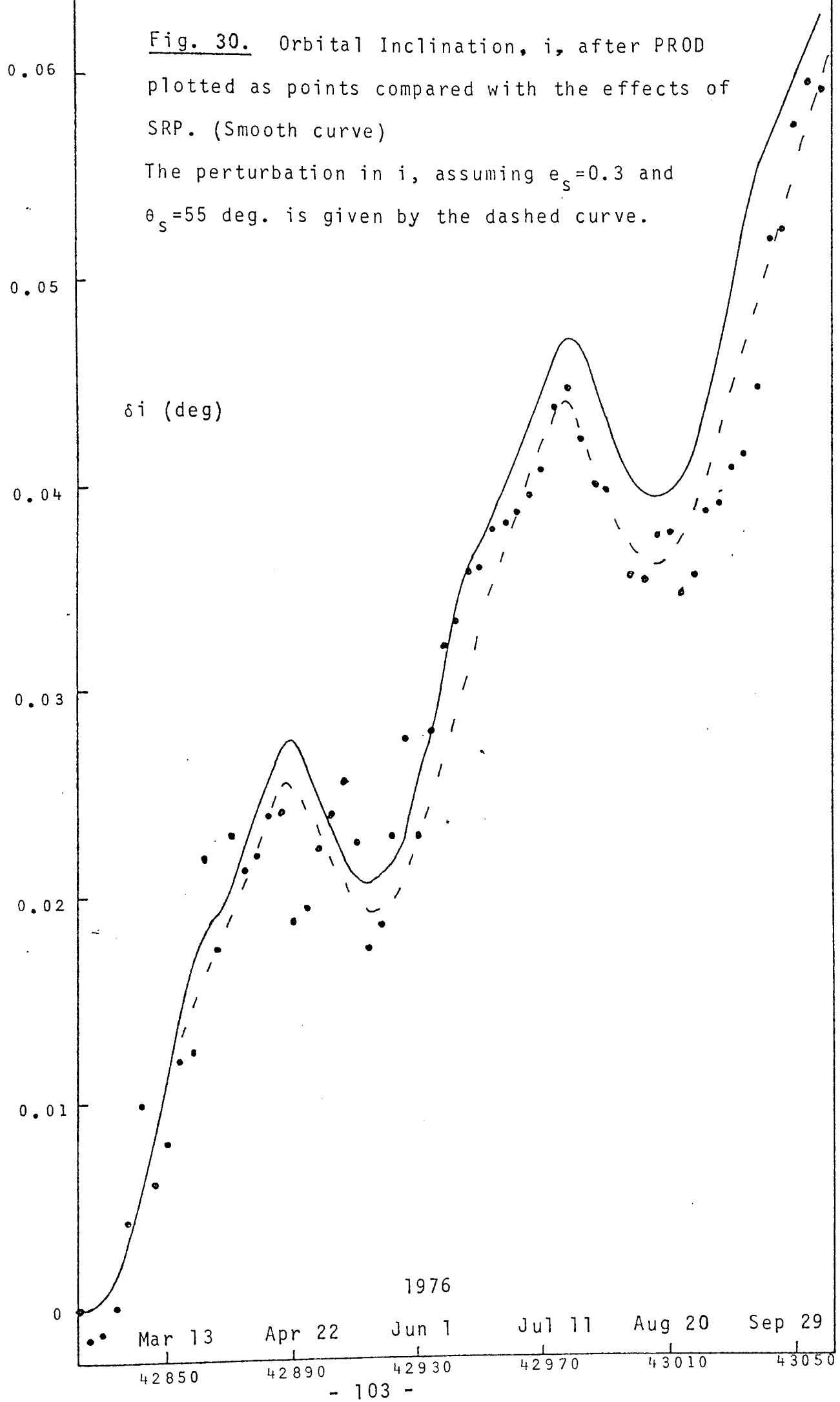

Fig. 30. Orbital Inclination, i, after PROD plotted as points compared with the effects of SRP. (Smooth curve)
The perturbation in i, assuming e_s=0.3 and θ_s=55 deg. is given by the dashed curve.

Fig. 31. THE EFFECTS OF SRP ON ECCENTRICITY ASSUMING A DEFORMED SATELLITE WITH PARAMETERS, e_s=0.3 AND Θ_s=55 (deg).

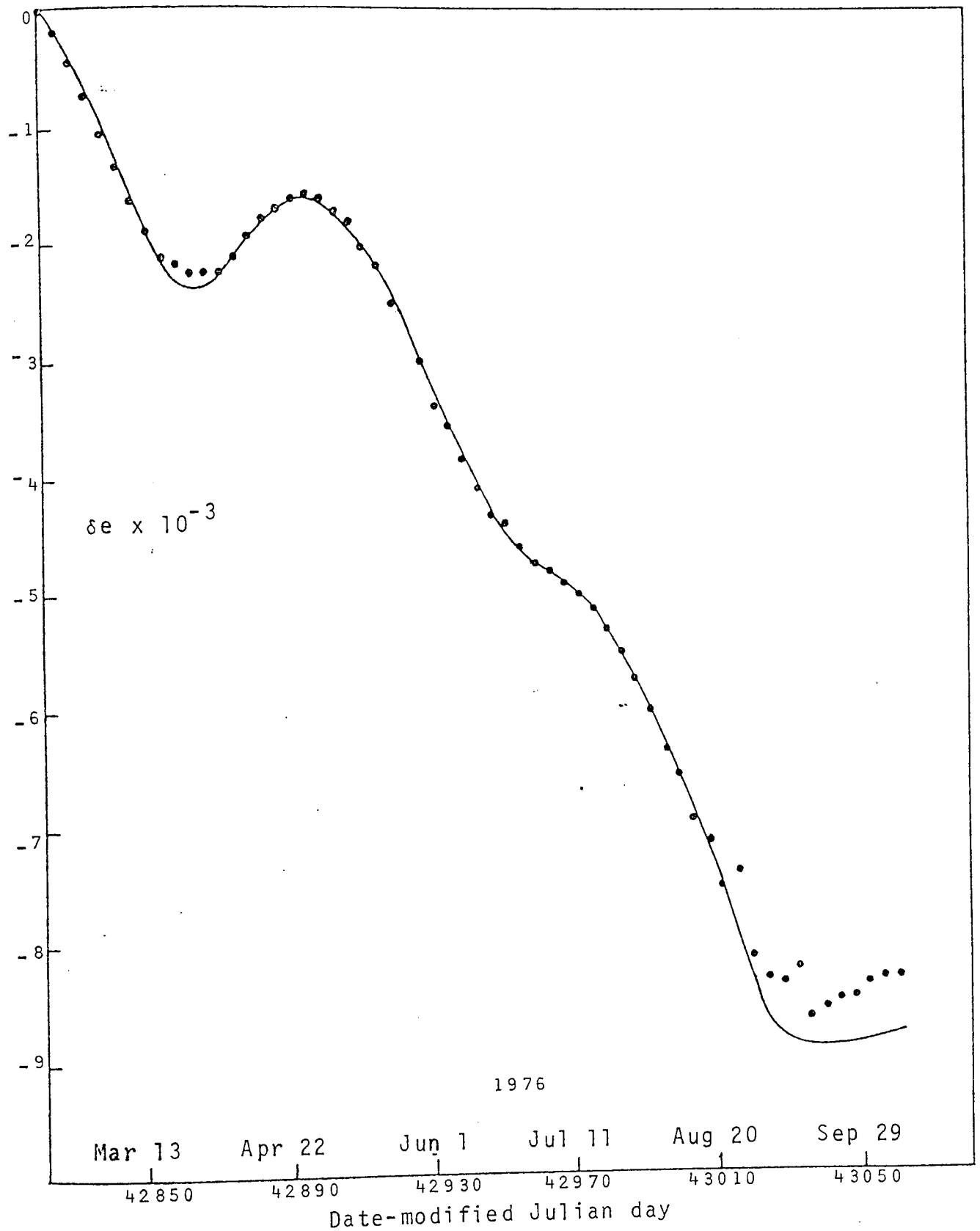

atmosphere. The values for this rotation can usually vary in the range 0.8 to 1.4 times the rate of the Earth's rotation.

An effect not yet mentioned is that described in Section 4. In this analysis Explorer 19 has been assumed to be spherical in shape. The only data available for the period of time considered here, is that of visual observations made during September 1976. These gave the stellar magnitude as +5.4 to +6.2 and the optical appearance as invariant, suggesting that the satellite was not rotating. The theory of Section 4 has been applied by using trial and error methods to select suitable values for θ_s and e_s, defined in that section. The best fit obtained in this way is shown in Figure 31 for eccentricity and Figure 30 for inclination (dashed curve). Here e_s=0.3 and θ_s=55 deg. R_s was taken as 0.8 and R_D as 0.02. It should be noted that if the satellite is in fact spherical then the integrated specular component would be zero. If the value of the reflection coefficient, s, is taken as 1.14 then this process, by virtue of the equations derived in Section 4, would suggest a value of 0.21 for R_D, a value that would seem unduly high.

iii) Air Drag Effects:

The 60 values for the rate of change of the mean motion given by Table 1 are plotted in Figure 32. It can be seen that the periods when $\dot{n}$ are positive coincide with those periods of time when the revolutions were totally sunlit. During these periods the major perturbation responsible for these values of $\dot{n}$ is that of air drag. The effect of SRP on

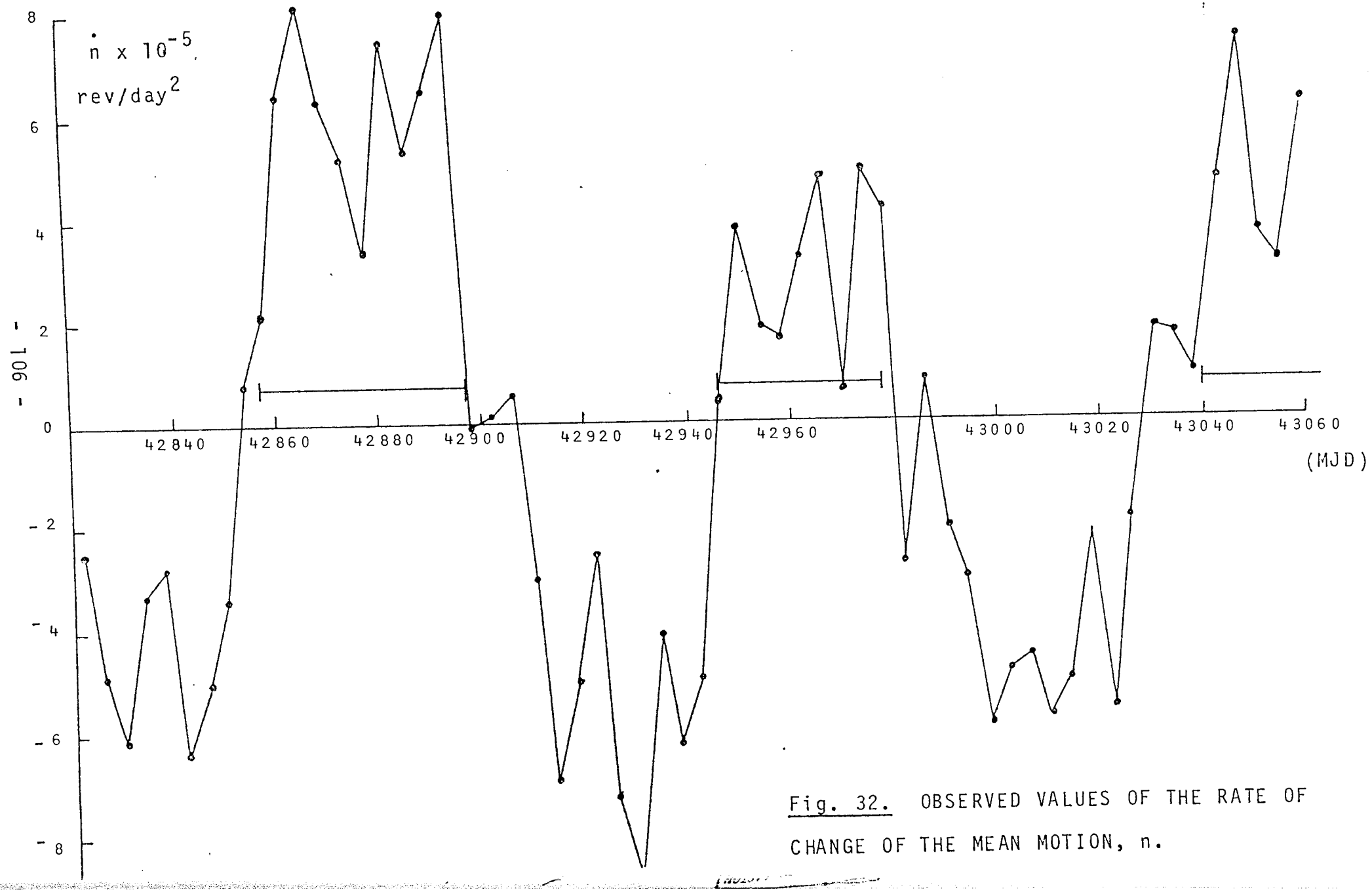

Fig. 32. OBSERVED VALUES OF THE RATE OF CHANGE OF THE MEAN MOTION, n.

Fig. 33. THE EFFECTS OF SRP ON $\dot{n}$, REV/DAY^2.

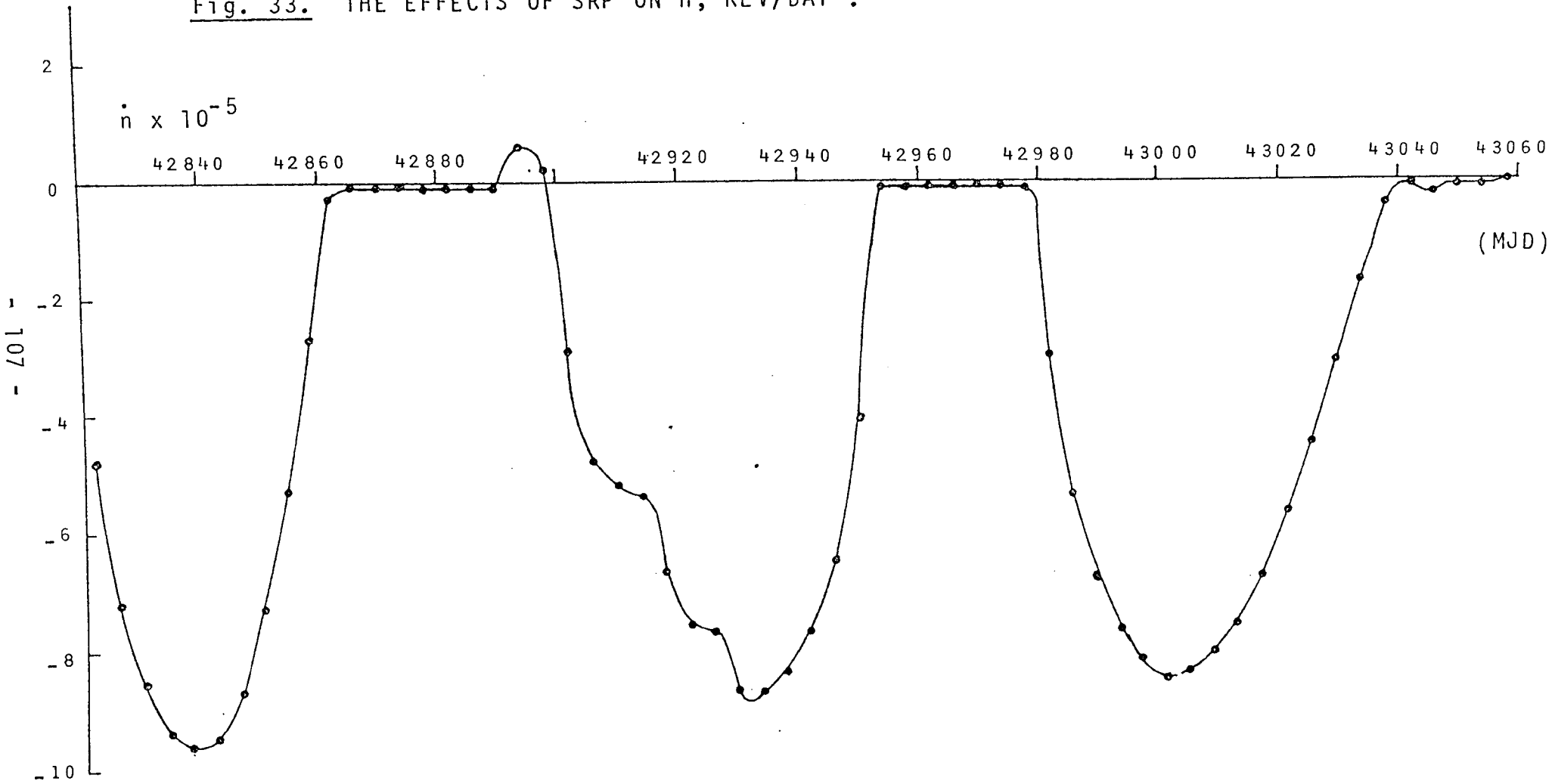

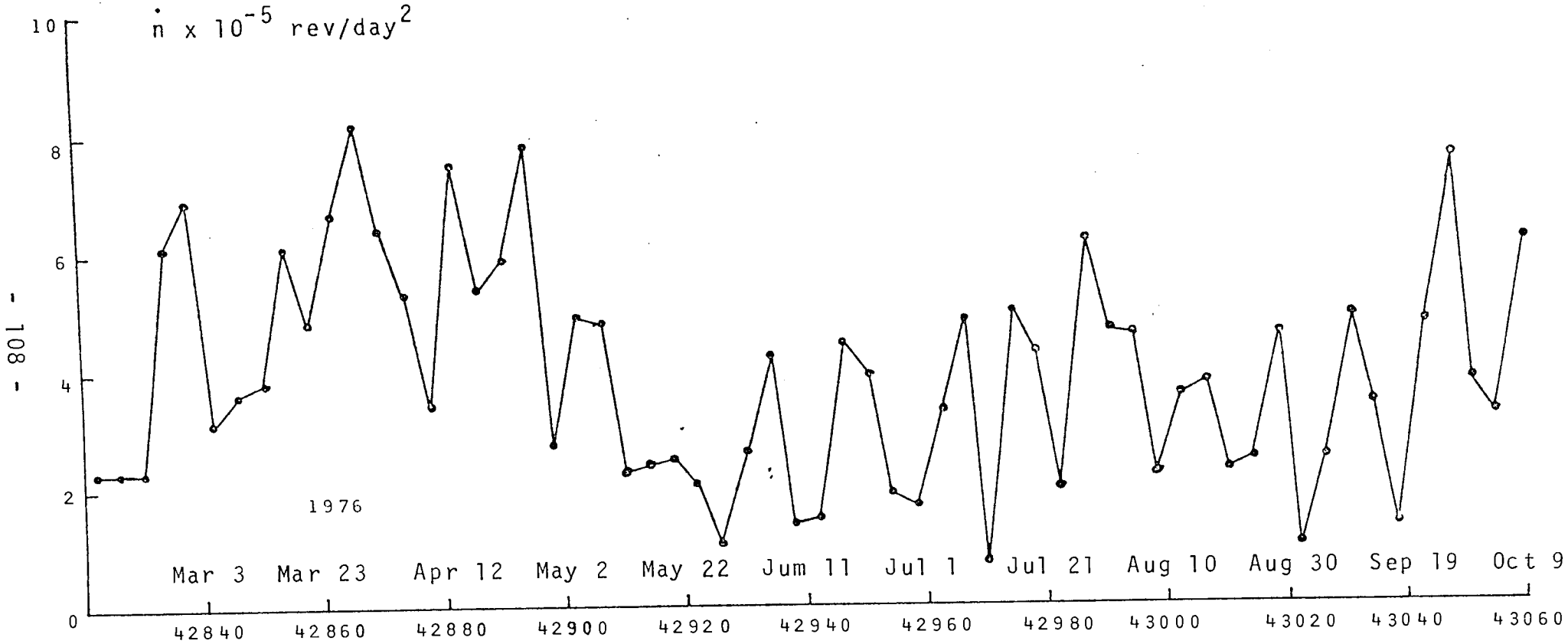

Fig. 34. THE RATE OF CHANGE OF THE MEAN MOTION AFTER THE REMOVAL OF THE EFFECTS OF SRP.

$\dot{n}$ is shown in Figure 33, again those epochs when the revolutions are totally sunlit are apparent from the horizontal portions of the curve. Figure 34 shows residual perturbations in $\dot{n}$ after the removal of the variation due to SRP.

It is now possible to evaluate the air density from these values of $\dot{n}$, so that comparison with Jacchia's atmospheric model (Jacchia, 1971) should ascertain the effectiveness of the removal of the perturbations due to solar radiation. The analysis follows the lines of Brookes and Ryland, 1977 with the exception that the phase , defined by King-Hele (1964), is $z=\frac{ae}{H} < 3$, where H is the density scale height.

Figure 35 shows the values of the perigee height over a spherical Earth, $y = a(1-e) - R_E$, where R_E=6378.14 km. Figure 36 gives the perigee height after the effects of SRP have been removed from y. The regular oscillation here is caused by the odd zonal harmonics in the geopotential. Figure 37 demonstrates the results calculated for the perigee height when the effects of SRP, the zonal harmonics upto J_{20} and the Luni-Solar perturbations have been removed. The graph exhibits the steady decrease due to the influence of air drag.

The actual perigee height y_p above the Earth's surface is derived from y, by subtracting the local Earth radius at latitude ϕ_p, which differs from R_E by

$$21.38 \sin^2\phi_p = 20.57 \sin^2\omega \text{ km.},$$

Fig. 35. OBSERVED VALUES OF PERIGEE HEIGHT, $a(1-e)-R_E$.

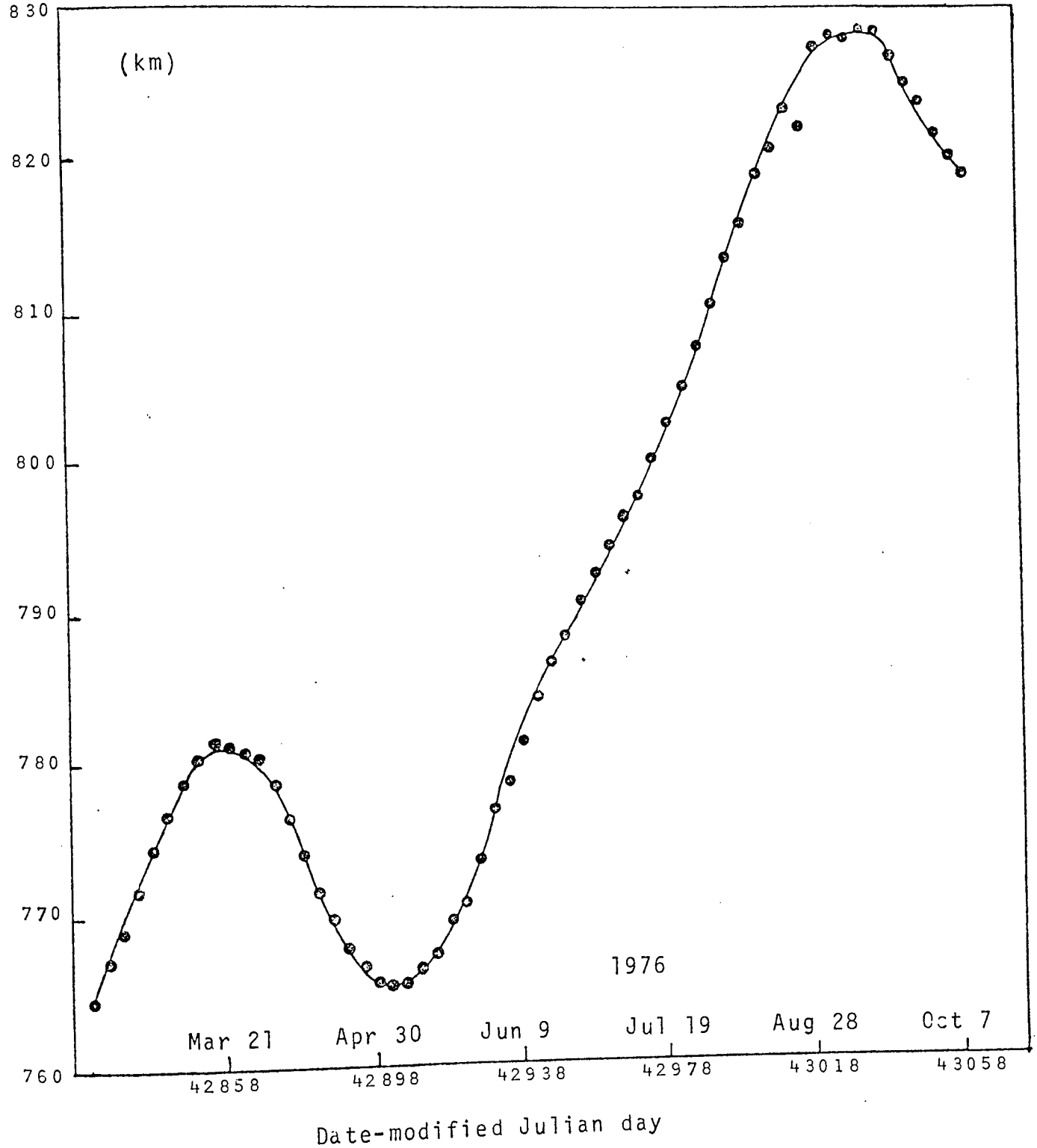

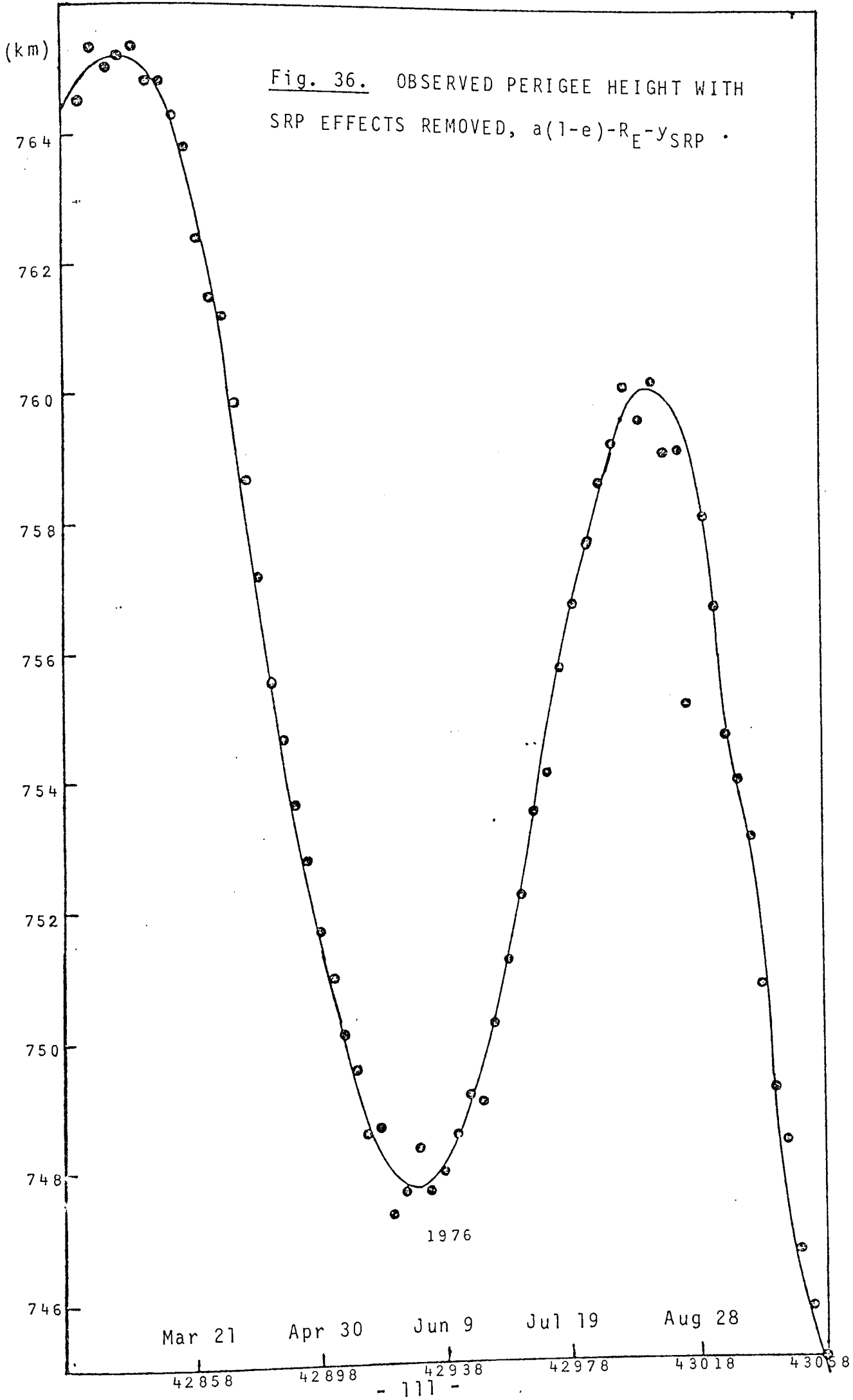

Fig. 36. OBSERVED PERIGEE HEIGHT WITH SRP EFFECTS REMOVED, $a(1-e)-R_E-y_{SRP}$.

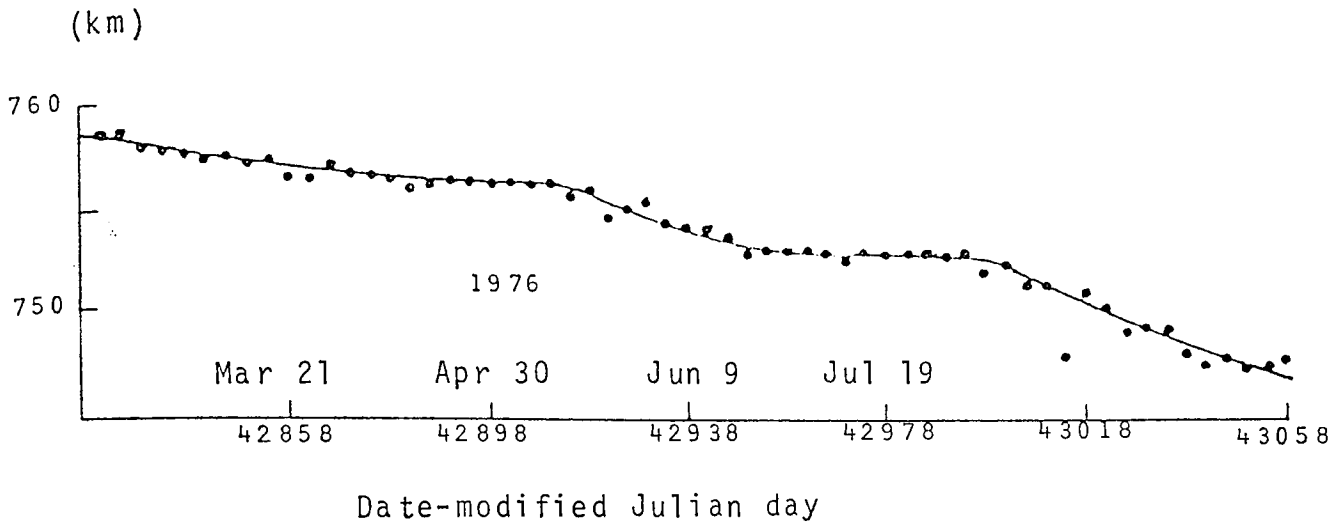

Fig. 37. VALUES OF PERIGEE HEIGHT PARAMETER. THE EFFECTS OF THE ZONAL HARMONICS, LUNI-SOLAR PERTURBATIONS AND SRP HAVE BEEN REMOVED.

and adding the small amount by which the actual perigee distance differs from a(1-e). Following Kozai (1959) the correction is found to be $1.34-0.81\sin^2\omega$. Figure 38 shows the values of y_p for Explorer 19 defined by

$$y_p = a(1-e) - R_E + 1.34 + 17.78 \sin^2\omega \quad .$$

In the phase $z<3$ the air density is obtained from $\dot{n}$, after the effects of air drag have been removed, at a height λH^* above perigee, where H^* is the best estimate of the density scale height. This is evaluated by means of the equation, (King-Hele, 1964)

$$\rho_\lambda = \frac{\dot{n}\Phi}{3000\ \pi a n^2 \delta}\left[\frac{I_0(z^*)\exp(c\cos 2\omega)}{I_0(z^*) + 2eI_1(z^*) + cI_2(z^*)\cos 2\omega}\right]$$

Fig. 38. VARIATION OF PERIGEE HEIGHT, $y_p = a(1-e) - R_E + 1.34 + 17.78\sin^2\omega$.

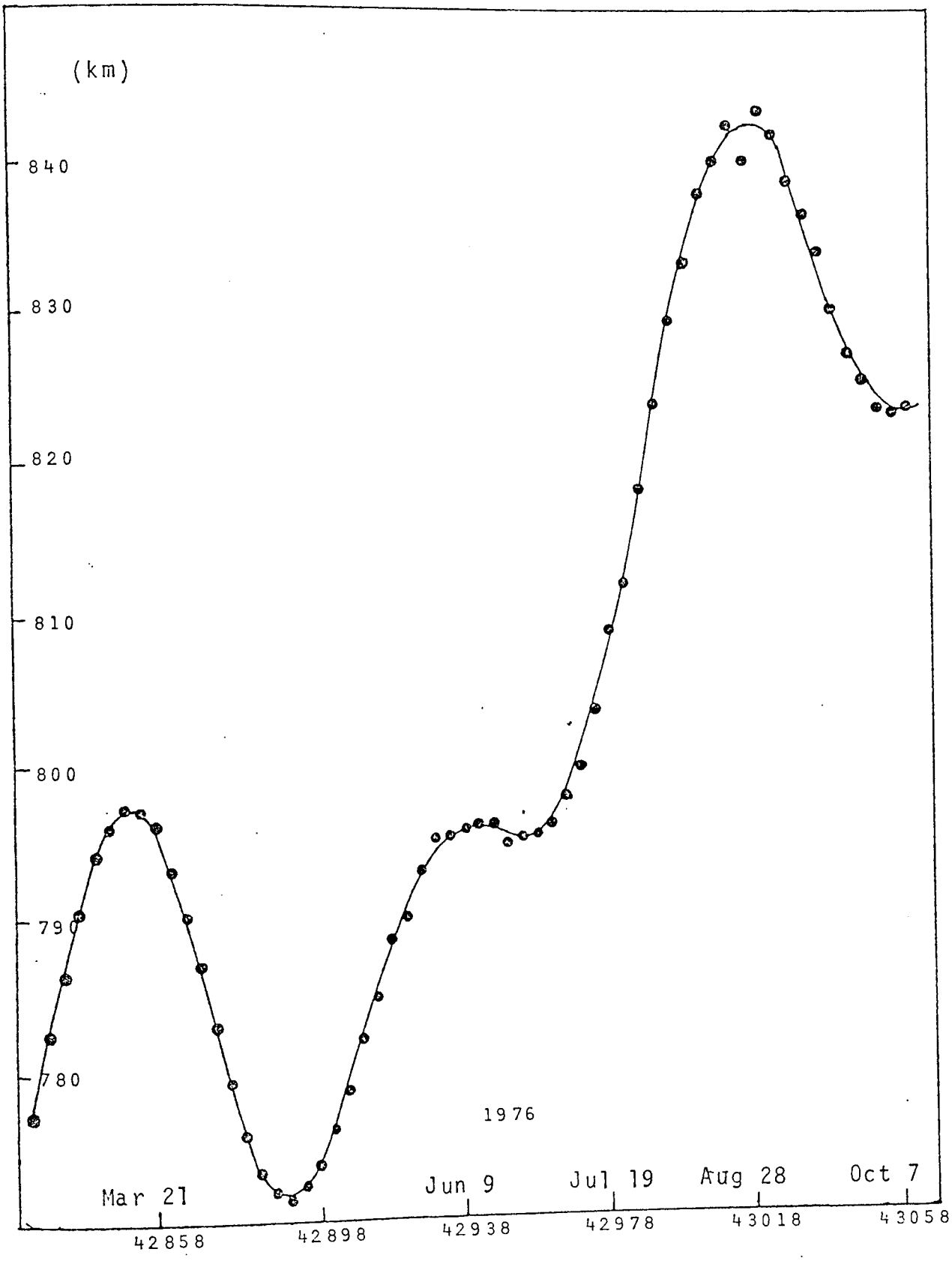

where

$$z^* = \frac{ae}{H^*} \quad ,$$

$\dot{n}$ = mean motion corrected for SRP ,

$$\lambda = z^* - \frac{z^{*2}}{2} \quad \text{when} \quad 0 \leq z^* \leq 1$$

$$= \tfrac{1}{2} \qquad \text{when} \quad z^* \geq 1 \quad ,$$

$$\Phi = \left(1 + \frac{\mu\lambda^2}{2}\right) \frac{\exp(Z-\lambda)}{I_0(Z)} \quad ,$$

$$Z = \frac{z^*}{1 + \mu\xi} \quad ,$$

$$\xi = \frac{(0.88+z^*)^2}{3.52} \left| z^* \exp(-z^*) \right| \left| 3I_0(z^*) - 4I_1(z^*) + I_2(z^*) \right| \quad ,$$

and

$$c = \frac{\varepsilon a}{2H^*} (1-e) \sin^2 i \quad .$$

Here I_n (n=0,1,2) is the Bessel function of the first kind and imaginary argument of order n, μ is the rate of increase of H with height and is given by,

$$\mu = \frac{2(H' - H^*)}{H^*} \quad ,$$

where $H' = 227$ km., is the best estimate of H at height $\bar{y}_p + H^*/2$. $\bar{y}_p$ is the mean perigee height, which for Explorer 19 is 803 km. δ is an area to mass parameter and ε is the ellipticity of the atmosphere, taken as 0.00335.

The value of H^* was taken as 194 km. throughout the computations, this corresponded to an exospheric temperature of 700 ^oK at a height of 800 km.

The value of the drag parameter δ is given by

$$\delta = \frac{FAC_D}{m} \quad ,$$

where A/m is again taken as 1.304 $m^2\ kg^{-1}$, F is a factor related to the atmospheric rotation and C_D the drag coefficient. The value for δ was taken as 3.088 $m^2\ kg^{-1}$ which corresponds to C_D=2.4 and F=0.98 .

The values of density, ρ_A, are evaluated at a height $y_A = y_p + \frac{1}{2}H^*$, as $\lambda=\frac{1}{2}$ for all values of z^* given by the 60 epochs of Table 1. The values of ρ_A are converted to a fixed height y_B, which was taken as $y_B = \overline{y}_p + \frac{1}{2}H^* = 900$ km. This conversion is effected by using,

$$\rho_B = \rho_A \exp\left(\frac{y_A - y_B}{H'}\right) \quad .$$

These values of ρ_B corresponding to a standard height of 900 km. are listed in Table 2 and plotted in Figure 39 against time and compared with the daily geomagnetic index A_p, as given by the Institut für Geophysik, Göttingen, plotted with a 12 hr. time lag. In the Figure 40 ρ_B is compared with solar 10.7-cm. radiation energy as measured by NRC, Ottawa. In Figure 41 the Sun-perigee angle and the local time at perigee are given.

Table 2. Values of y_A, ρ_A and ρ_B from 1963-53A

Time (MJD)	y_A (km)	$10^{15}\rho_A$ (kg/m^3)	$10^{15}\rho_B$ (kg/m^3)	Time (MJD)	y_A (km)	$10^{15}\rho_A$ (kg/m^3)	$10^{15}\rho_B$ (kg/m^3)
42822	873.8	1.16	1.03	42882	870.1	3.76	3.30
42826	878.9	1.16	1.05	42886	869.0	2.72	2.37
42830	883.0	1.15	1.07	42890	868.5	2.97	2.59
42834	887.2	3.05	2.88	42894	869.3	3.93	3.43
42838	890.6	3.43	3.30	42898	870.6	1.41	1.24
42842	892.7	1.54	1.49	42902	873.0	2.47	2.19
42846	894.1	1.78	1.74	42906	875.7	2.41	2.17
42850	894.0	1.88	1.83	42910	879.0	1.15	1.05
42854	892.9	3.02	2.93	42914	881.8	1.20	1.11
42858	890.0	2.38	2.28	42918	885.4	1.25	1.17
42862	886.9	3.32	3.14	42922	887.0	2.64	2.40
42866	883.9	4.07	3.79	42926	889.7	0.55	0.53
42870	879.8	3.19	2.92	42930	892.1	1.29	1.25
42874	876.1	2.65	2.38	42934	892.3	2.08	2.01
42878	872.7	1.70	1.51	42938	892.8	0.69	0.67

Table 2 (cont.). Values of y_A, ρ_A and ρ_B from 1963-53A

Time (MJD)	y_A (km)	$10^{15}\rho_A$ (kg/m^3)	$10^{15}\rho_B$ (kg/m^3)	Time (MJD)	y_A (km)	$10^{15}\rho_A$ (kg/m^3)	$10^{15}\rho_B$ (kg/m^3)
42942	893.1	0.74	0.72	43002	935.0	1.70	1.99
42946	892.9	2.22	2.15	43006	937.2	1.79	2.11
42950	891.8	1.92	1.85	43010	939.7	1.08	1.29
42954	892.1	0.93	0.90	43014	937.2	1.18	1.39
42958	892.3	0.83	0.81	43018	940.7	2.16	2.58
42962	893.2	1.62	1.57	43022	939.0	0.05	0.06
42966	895.0	2.40	2.34	43026	936.0	1.17	1.38
42970	896.9	0.34	0.34	43030	933.8	2.30	2.67
42974	900.8	2.43	2.44	43034	931.2	1.60	1.84
42978	905.0	2.08	2.13	43038	927.3	0.61	0.69
42982	909.9	2.46	2.57	43042	924.3	2.27	2.53
42986	915.3	2.98	3.19	43046	922.5	3.60	3.98
42990	920.6	2.25	2.46	43050	920.6	1.81	1.98
42994	926.3	2.19	2.46	43054	920.3	1.52	1.66
42998	930.3	1.05	1.19	43058	920.9	2.95	3.24

It is difficult to see the correlation of the day to day values of A_p as the density values are given at 4 day intervals. The two largest values of ρ_B occur at MJD 42866.0 and MJD 43046.0, coinciding with values of A_p=138 and A_p=51, respectively.

The corrections for day to night, solar and geomagnetic activity variations were made to the values of ρ_B, in the manner outlined in Section 9.2 of Brookes and Ryland, 1977. The resulting densities were then standardized to the exospheric temperature of 800 ^{o}K. The results of the standardized values of density, ρ_B^*, are shown in Figure 42 together with a comparison with results found for the same period of time at a height of 435 km. and 850 ^{o}K by Brookes and Moore, 1978.

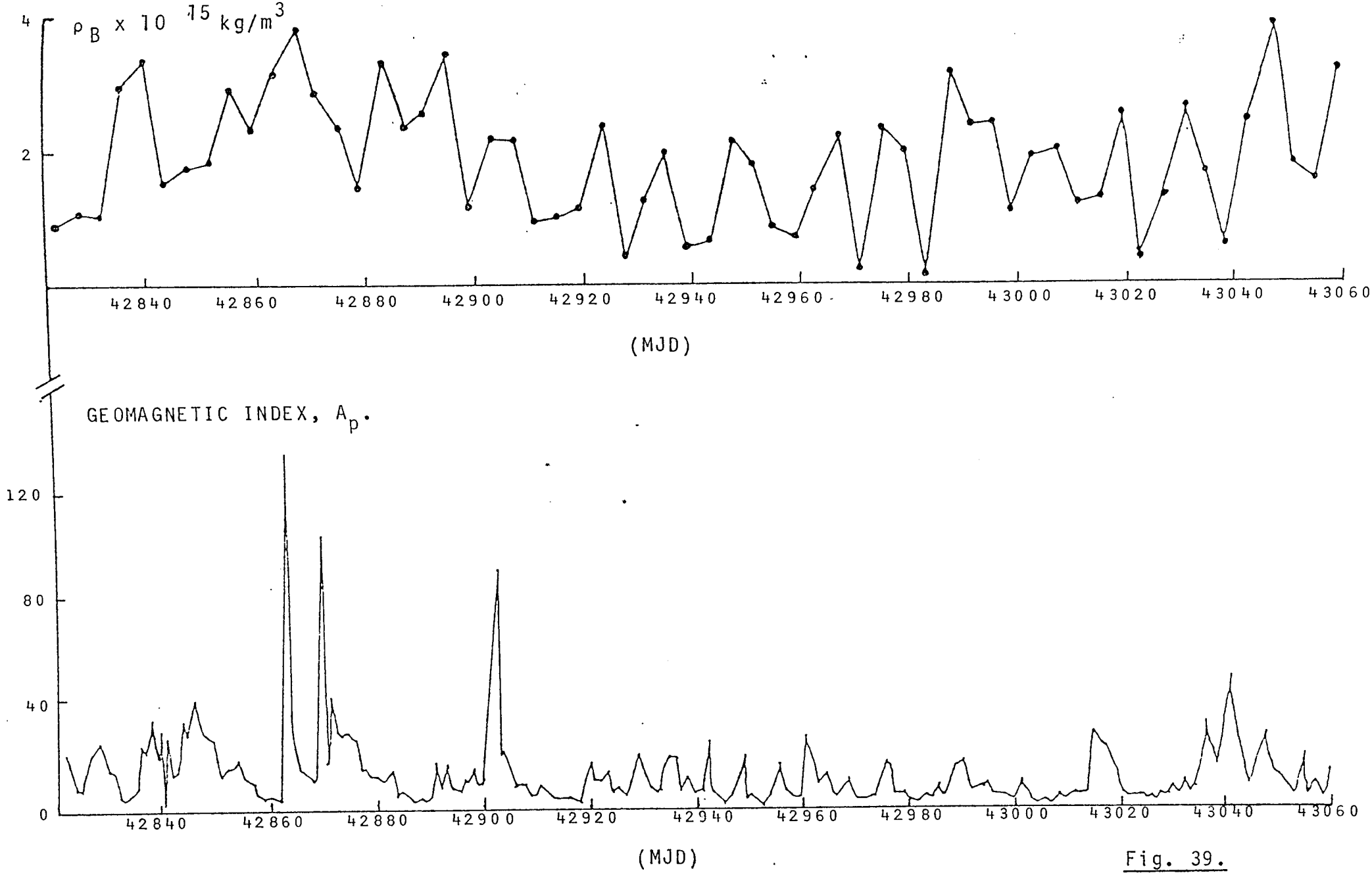
ρ_B x 10 $^{-15}$ kg/m^3
4
2
42840
42860
42880
42900
42920
42940
42960
42980
43000
43020
43040
43060
(MJD)
GEOMAGNETIC INDEX, A_p.
120
80
40
0
42840
42860
42880
42900
42920
42940
42960
42980
43000
43020
43040
43060
(MJD)

Fig. 39.

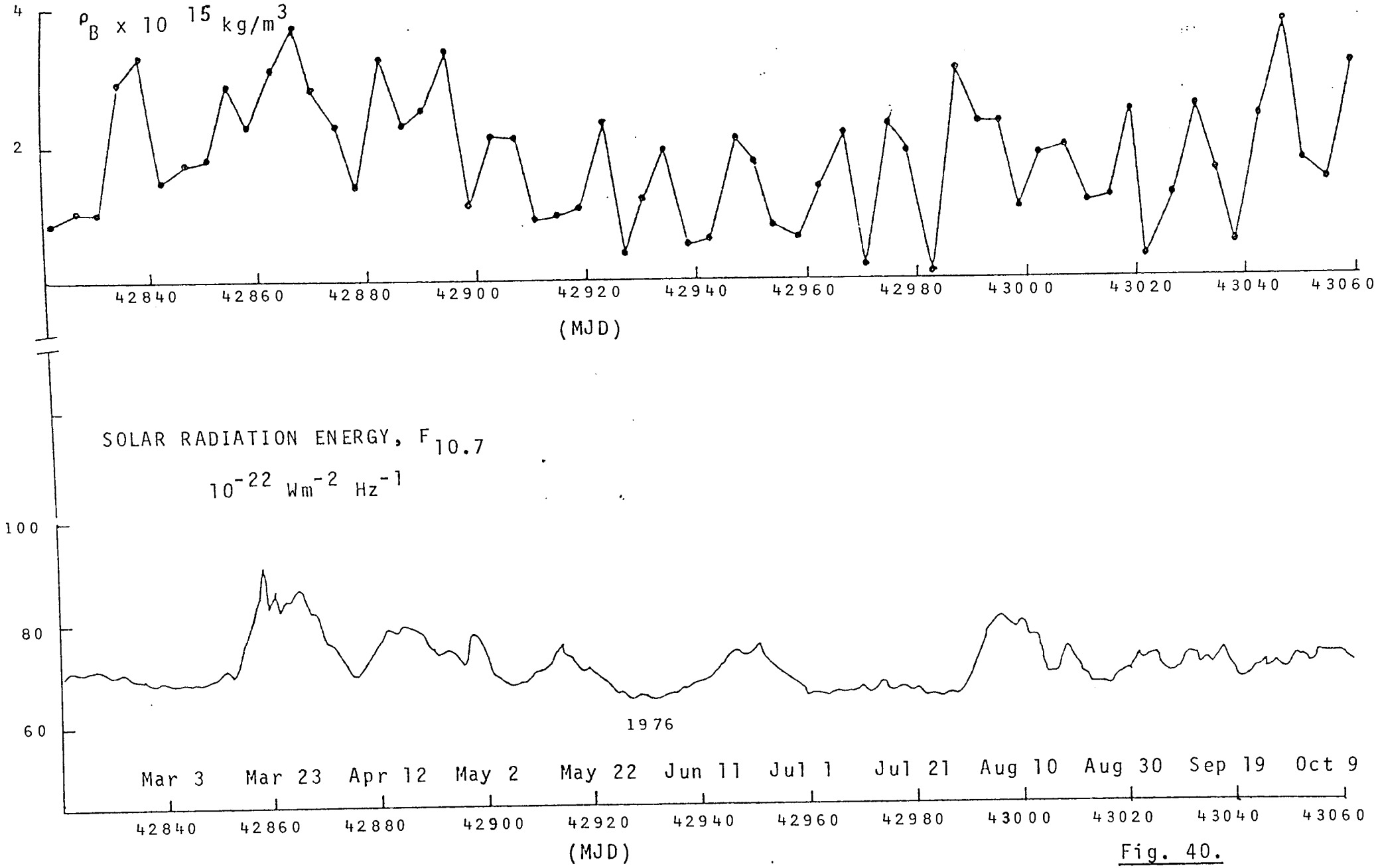
4
ρ_B x 10 ^{15} kg/m^3
2
42840
42860
42880
42900
42920
42940
42960
42980
43000
43020
43040
43060
(MJD)
SOLAR RADIATION ENERGY, $F_{10.7}$
10^{-22} Wm^{-2} Hz^{-1}
100
80
60
1976
Mar 3
Mar 23
Apr 12
May 2
May 22
Jun 11
Jul 1
Jul 21
Aug 10
Aug 30
Sep 19
Oct 9
42840
42860
42880
42900
42920
42940
42960
42980
43000
43020
43040
43060
(MJD)

Fig. 40.

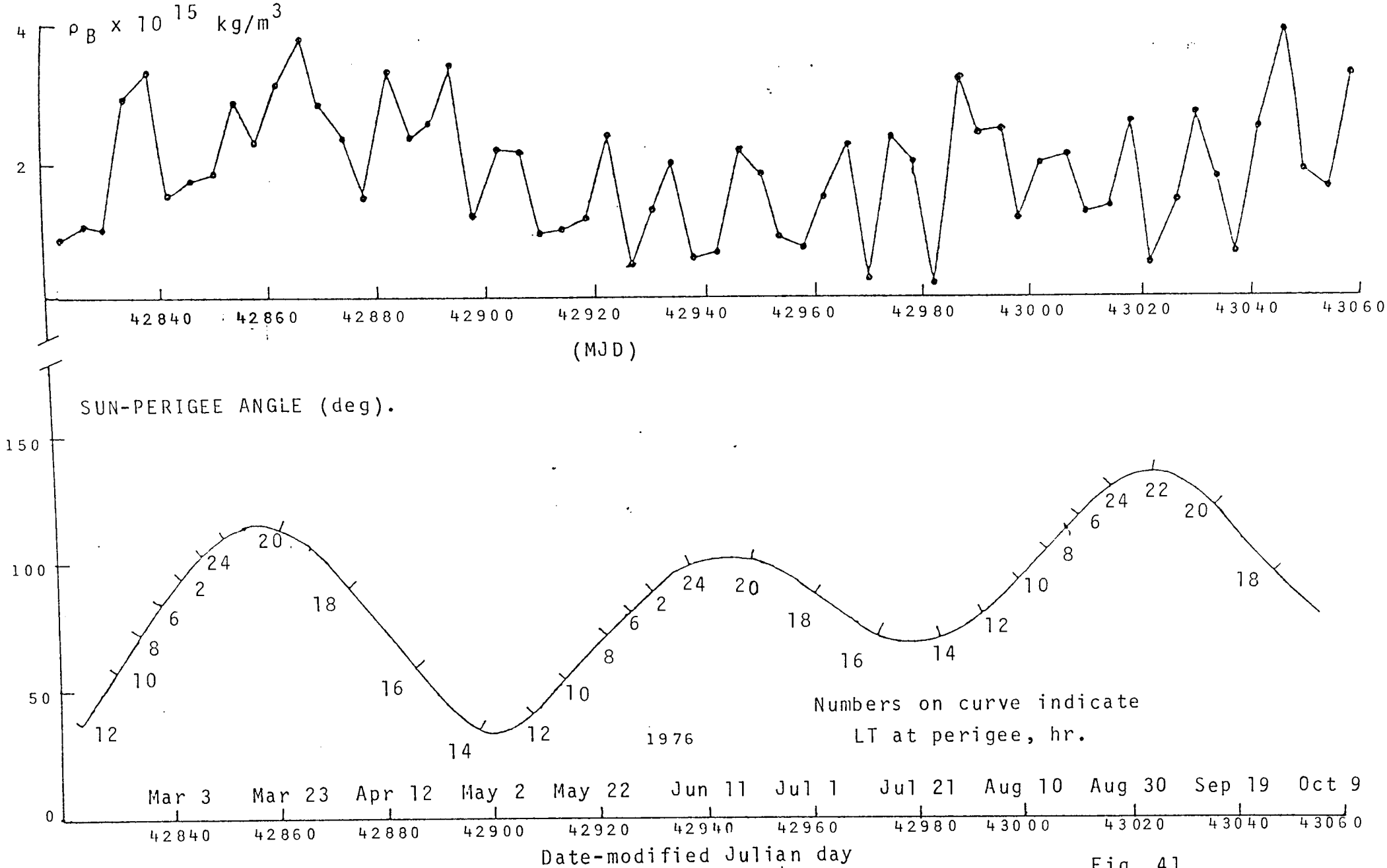
$\rho_B \times 10^{15}$ kg/m^3
4
2
42840
42860
42880
42900
42920
42940
42960
42980
43000
43020
43040
43060
(MJD)
SUN-PERIGEE ANGLE (deg).
150
100
50
0
12
10
8
6
2
24
20
18
16
14
12
10
8
6
2
24
20
18
16
14
12
10
8
6
24
22
20
18
1976
Numbers on curve indicate
LT at perigee, hr.
Mar 3
Mar 23
Apr 12
May 2
May 22
Jun 11
Jul 1
Jul 21
Aug 10
Aug 30
Sep 19
Oct 9
42840
42860
42880
42900
42920
42940
42960
42980
43000
43020
43040
43060
Date-modified Julian day

Fig. 41.

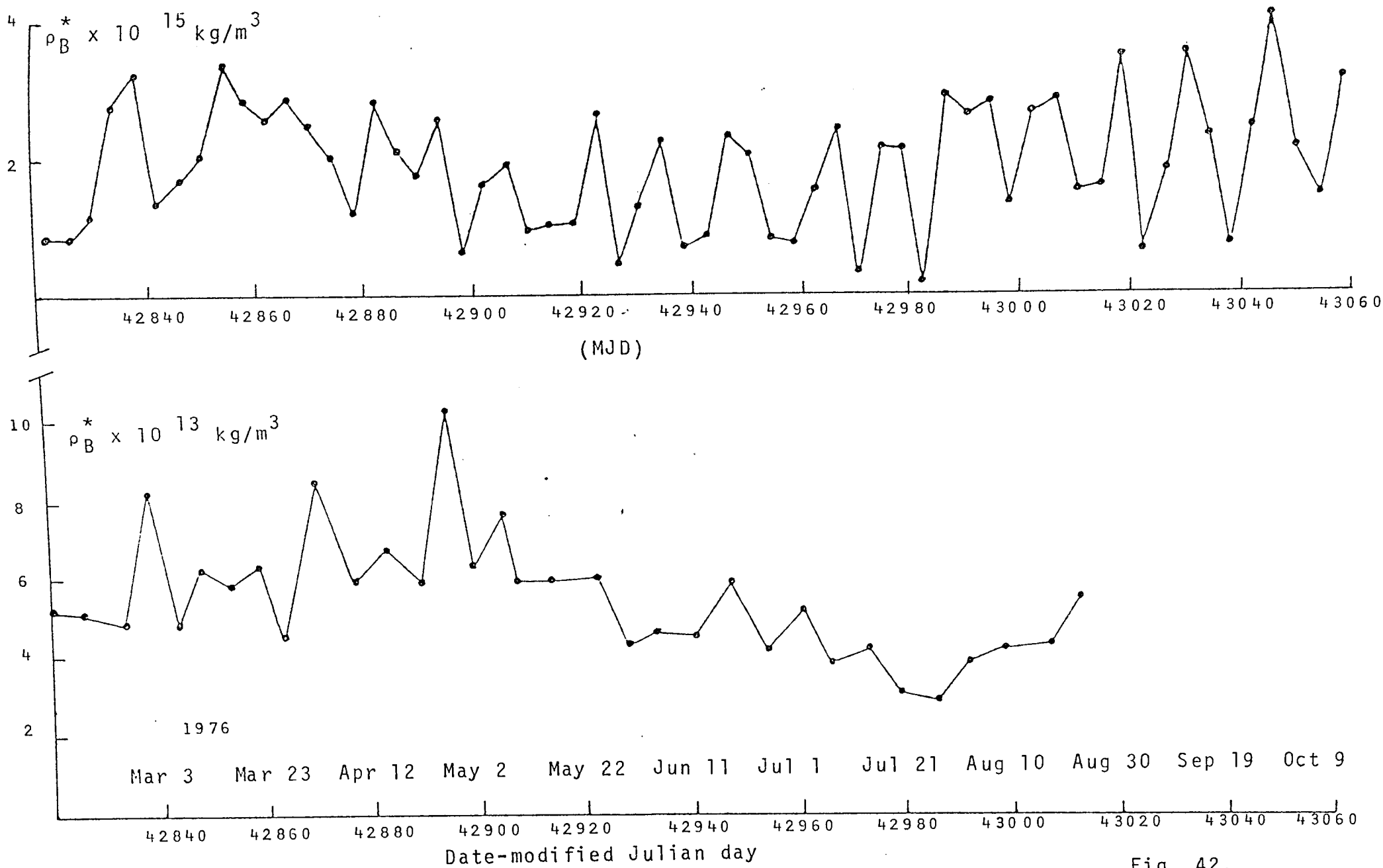
4
ρ_B^* x 10 ^{15} kg/m^3
2
42840
42860
42880
42900
42920
42940
42960
42980
43000
43020
43040
43060
(MJD)
10
ρ_B^* x 10 ^{13} kg/m^3
8
6
4
2
1976
Mar 3
Mar 23
Apr 12
May 2
May 22
Jun 11
Jul 1
Jul 21
Aug 10
Aug 30
Sep 19
Oct 9
42840
42860
42880
42900
42920
42940
42960
42980
43000
43020
43040
43060
Date-modified Julian day

Fig. 42.

7.

CONCLUSION

Studies of the motion of an artificial satellite in the atmospheric zone above about 800 km. are complicated by the extraneous effects that rival those of aerodynamic drag. This competing force of solar radiation is known to be significant whenever the area to mass ratio is large, and can be evaluated and eliminated by means of the theory developed in this study. It has been shown that the effects of SRP are greatest when the satellite orbit includes the Earth's shadow. The disadvantages of employing a continuous method to derive the results that define the orientation of this shadow, with respect to the orbit, have been outlined. In Section 3 this method was shown to be unnecessarily lengthy and in the application in Section 6, the inherent inaccuracies are highlighted by Figures 23 and 24. It is concluded that the method best suited to the evaluation of the shadow angles is that of a discrete, numerical method that allows the introduction of suitable approximations for those terms whose variations over one revolution may not be neglected. This 'step by step' method can be altered to allow for second order, or greater variations in S, T and W , though it is felt that a linear approximation for these variables is adequate in most instances.

The application of the theory of Section 4 has been tentatively included. Any application of such theory would be infinitely advanced by the availability of photometric observations that can suggest values for the shape, orientation

and any relevant spin characteristics of the satellite. In view of the air density results derived from the orbits of Explorer 19, it is fair to assume that this satellite was not rotating during the period of time relevant to this analysis.

Though it may be expected that the diffuse component of reflection from the satellite's surface is generally small, the theory was developed to include the effect as this has not been developed elsewhere. In the case of some satellites it is known that a certain percentage of the surface area involves the use of diffusely reflecting white epoxy paint. If this surface area was known to be significant, then it would be valuable to include this theory.

It was not practicable to give an adequate application of the theory developed for Earth reflected radiation pressure in the example of Explorer 19, as this satellite had a relatively low area to mass ratio for a balloon satellite, 1/3 the A/m value of Dash 2. The height above the Earth of Explorer 19 during the 236 days of the analysis of Section 6, resulted in direct SRP and air drag perturbations that overwhelmed the effects of Earth reflected radiation.

Analysis of the orbit of 1963-53A during the 236 days starting on MJD 42822.0 has yielded values of air density near 803 km. These results have been converted to represent the variations in density at 900 km. The variations in these values due to solar activity and diurnal variations have been removed using Jacchia, 1971. It would appear that the effects of the geomagnetic disturbances have not been totally removed as the

residual variations in density between February and October, represented in the upper half of Figure 42, should show the semi-annual variation. The results appear to be centred on the value of $\rho_B^* = 2 \times 10^{-15}$ kg. m^{-3}, the density at 900 km. and corrected to 800 ^oK. The majority of values lie within the range 1×10^{-15} and 3×10^{-15} kg. m^{-3} with a maximum on the 17th. March, 1976 and a minimum on the 23rd. July, 1976. The range of the extremes is what might be expected for this height as suggested by Jacchia's equations while the actual dates of the maximum and minimum are not clearly distinguished. This might be improved by supplementing values of $\mathring{n}$ with USAF Spacetrack five-card elements. The lower part of Figure 42 shows the air density values for the same period of time standardized to 435 km. and 850 ^oK. Here the semi-annual variation shows a March-April maximum on April 22nd. and the July-August minimum on July 25th.

It is suggested that future work in SRP studies could be aimed at simplifying the expression derived for Earth reflected radiation, so as to reduce the lengthy computational time required to carry out the integrations necessary. It would also be of interest to apply the theory of Section 4 to a satellite that has undergone photometric observation.

REFERENCES

Aksnes, K. (1976)

SHORT-PERIOD AND LONG-PERIOD PERTURBATIONS OF A SPHERICAL SATELLITE DUE TO A DIRECT SOLAR RADIATION. Celestial Mechanics, 13 pp. 89-104. D. Reidel Publishing Company, Dordrecht-Holland.

Brookes, C.J. and Ryland, F.C.E. (1977)

AIR DENSITY AT HEIGHTS NEAR 300 km., FROM ANALYSIS OF THE ORBIT OF CHINA 2 ROCKET (1971-18B). Planetary and Space Science, Vol. 25, No. 11, pp. 1011-1020. Pergamon Press limited.

Brookes, C.J. and Moore, P. (1978)

AIR DENSITY AT HEIGHTS NEAR 435 km. FROM THE ORBIT OF SKYLAB 1 (1973-27A). Planetary and Space Science, Vol. 26, pp. 913-924.

Bryant, R.W. (1961)

THE EFFECT OF SOLAR RADIATION PRESSURE ON THE MOTION OF AN ARTIFICIAL SATELLITE. The Astronomical Journal, Vol. 66, No. 8, pp. 430-432.

Buckingham, R.A. (1962)

NUMERICAL METHODS. Pitman, London.

Cook, G.E. (1965)

SATELLITE DRAG COEFFICIENTS.

Planetary and Space Science, Vol. 13, pp. 929-946.

Pergamon Press Limited.

Cook, G.E. (1972)

BASIC THEORY FOR PROD, A PROGRAM FOR COMPUTING

THE DEVELOPMENT OF SATELLITE ORBITS.

Celestial Mechanics, 7 pp. 301-314.

D. Reidel Publishing Company, Dordrecht-Holland.

Courant, R. (1937)

DIFFERENTIAL AND INTEGRAL CALCULUS, VOL 2.

Blackie and Son Limited.

Fea, K. (1970)

THE ORBITAL ACCELERATIONS OF HIGH BALLOON SATELLITES.

Dynamics of Satellites (1969), ed. by B. Morando,

Springer-Verlag, New York, pp. 295-302.

Fea, K. and Smith, D.E. (1970)

SOME FURTHER STUDIES OF PERTURBATIONS OF SATELLITES

AT GREAT ALTITUDE.

Planetary and Space Science, Vol. 18, pp. 1499-1525.

Pergamon Press Limited.

Gooding, R.H. and Tayler, R.J. (1968)
A PROP 3 USERS' MANUAL.
RAE Technical Report 68299.

GOODING, R.H. (1974)
THE EVOLUTION OF THE PROP 6 ORBIT DETERMINATION PROGRAM, AND RELATED TOPICS.
RAE Technical Report 74164.

Jacchia, L.G. (1971)
REVISED STATIC MODELS OF THE THERMOSPHERE AND EXOSPHERE WITH EMPIRICAL TEMPERATURE PROFILES.
Smithsonian Astrophysical Observatory,
Special Report No. 332.

- CIRA 1972 (COSPAR INTERNATIONAL REFERENCE ATMOSPHERE 1972).
Akademie-Verlag, Berlin.

Keating, M., Mullins, J.A. and Prior, E.J. (1970)
THE POLAR EXOSPHERE NEAR SOLAR MAXIMUM.
Space Research X, pp. 439-449.
North-Holland Publishing Company, Amsterdam.

King-Hele, D. (1964)
THEORY OF SATELLITE ORBITS IN AN ATMOSPHERE.
Butterworths, London.

Kozai, Y. (1959)
THE MOTION OF CLOSE EARTH SATELLITES.
Astronomical Journal, Vol. 64, pp. 367-377.

Kozai, Y. (1961)
EFFECTS OF SOLAR RADIATION PRESSURE ON THE MOTION
OF AN ARTIFICIAL SATELLITE.
Smithsonian Astrophysical Observatory,
Special Report No. 56.

Lala, P. and Sehnal, L. (1969)
THE EARTH'S SHADOWING EFFECTS IN THE SHORT-PERIODIC
PERTURBATIONS OF SATELLITE ORBITS.
Bulletin of the Astronomical Institute of
Czechoslovak Academy of Sciences, Ondrejov.
Vol. 20, No. 6, pp. 327-330.

Lala, P. (1970)
SEMI-ANALYTICAL THEORY OF SOLAR PRESSURE PERTURBATIONS
OF SATELLITE ORBITS DURING SHORT TIME INTERVALS.

Bulletin of the Astronomical Institute of Czechoslovak Academy of Sciences, Ondrejov. Vol. 22, No. 2, pp. 63-72.

Luacs, J.R. (1974)
RADIATION PRESSURE ON A SPHEROIDAL SATELLITE. National Oceanic and Atmospheric Administration, Technical Report No. 61.

Musen, P. (1960)
THE INFLUENCE OF THE SOLAR RADIATION PRESSURE ON THE MOTION OF AN ARTIFICIAL SATELLITE. Journal of Geophysical Research, Vol. 65, No. 5, pp. 1391-1396.

Musen, P., Bryant, R. and Bailie, A. (1960)
PERTURBATIONS IN PERIGEE HEIGHT OF VANGUARD I. Science, Vol. 131, pp. 935-936.

Parkinson, R.W., Jones, H.M. and Shapiro, I.I. (1960)
EFFECTS OF SOLAR RADIATION PRESSURE ON EARTH SATELLITE ORBITS. Science, Vol. 131, pp. 920-921.

Prior, E.J. (1970)
DYNAMICS OF SATELLITES. Springer-Verlag, New York. P. 303.

Shapiro, I.I. and Jones, H.M. (1960)
PERTURBATIONS OF THE ORBIT OF THE ECHO BALLOON.
Science, Vol. 132, pp. 1484-1486.

Smart, W.M. (1953)
CELESTIAL MECHANICS.
Longmans, Green and Company.

Slowey, J.W. (1974i)
RADIATION-PRESSURE AND AIR DRAG EFFECTS ON THE ORBIT OF THE BALLOON SATELLITE 1963-30D.
Smithsonian Astrophysical Observatory,
Special Report No. 356.

Slowey, J.W. (1974ii)
EARTH RADIATION PRESSURE AND THE DETERMINATION OF DENSITY FROM SATELLITE DRAG.
Space Research XIV, pp. 143-149.
Akademie Verlag, Berlin.

BIBLIOGRAPHY

1. ARTIFICIAL SATELLITE OBSERVING, edited by Howard Miles, Faber. (1974)

2. SPHERICAL HARMONICS, T.M. Mac Robert, Methuen and Company Limited, London. (1927)

3. A FIRST COURSE IN NUMERICAL METHODS, A. Ralston, McGraw-Hill, (1965)

4. OPTICS, W.H.A. Fincham and M.H. Freeman, Butterworths, London. (1974)